

AN ADAPTABLE SINGLE-CELL TRAPPING DEVICE FOR A  
WIDE RANGE OF CELL SIZES

A Thesis Submitted to the  
College of Graduate Studies and Research  
in Partial Fulfillment of the Requirements  
for the Degree of Master of Science  
in the Department of Mechanical Engineering  
University of Saskatchewan  
Saskatoon

By

Edgar E. Martinez Soberanes

©Edgar E. Martinez Soberanes, August, 2016. All rights reserved.

## PERMISSION TO USE

In presenting this thesis in partial fulfillment of the requirements for a Postgraduate degree from the University of Saskatchewan, I agree that the Libraries of this University may make it freely available for inspection. I further agree that permission for copying of this thesis in any manner, in whole or in part, for scholarly purposes may be granted by the professor or professors who supervised my thesis work or, in their absence, by the Head of the Department or the Dean of the College in which my thesis work was done. It is understood that any copying or publication or use of this thesis or parts thereof for financial gain shall not be allowed without my written permission. It is also understood that due recognition shall be given to me and to the University of Saskatchewan in any scholarly use which may be made of any material in my thesis.

Requests for permission to copy or to make other use of material in this thesis in whole or part should be addressed to:

Head of the Department of Mechanical Engineering  
University of Saskatchewan  
57 Campus Drive, Saskatoon, SK S7N 5A9, Canada

## ABSTRACT

In the last two decades many microfluidic devices have been developed in order to provide better and more reliable tools for biological assays and analysis. Microfluidic technology has proven its functionality and advantages over conventional cellomics methods such as flow cytometry (FC) and laser scanning cytometry (LSC) in particular for processes that require the analysis of single cells. Different microfluidic platforms capable of capturing, positioning, and sorting single cells have been developed; however, such devices are incapable of working with various sizes of cells. Therefore, once a device has been designed and fabricated it is not possible to modify its dimensions so a new device is required for each different cell size for analysis. In an effort to overcome the limitation of adaptability of microfluidic cell trapping devices, this thesis presents a new microfluidic single cell-trapping device capable of capturing cells of various diameters.

This thesis conducts a review and analysis of several microfluidic cell trapping devices under the FCBPSS (function-context-behavior-principle-state-structure) framework to have a better understanding and classification of the most relevant microfluidic devices, followed by the design of a new device capable of trapping large batches of single cells and modifying its physical features in order to work with multiple sizes of cells. The design process of the new device is based on and guided by the Axiomatic Design Theory. From the thorough review of the literature, it was concluded that the most suitable structure to demonstrate the concept proposed on this thesis an array of single cell trappers, and the best tuning method would be a mechanical stretching to generate a uniform distributed strain on the device.

After designing and modeling the new device, it was imperative for this research to fabricate a device which could be tested in accordance with the literature. The final device consists of two thin layers of polydimethylsiloxane (PDMS), one of which bears trapezoidal microstructures (traps) to physically capture cells. The size of the traps can be modified by

stretching the device via a uniform distributed force, which is applied using a stretching apparatus.

Finally, the performance of the new device was assessed by conducting two main experiments. The first experiment consisted of characterizing the mechanical behavior of the device when different strains were applied. It has been found that all the traps of the device have a uniform deformation when a strain is applied, and the minimum size increment permitted by the stretching apparatus is of  $2\mu\text{m}$ . The second experiment was done in order to characterize the hydrodynamical and trapping behavior of the device. By using water-in-oil microspheres of various sizes the trapping of particles was demonstrated; it was determined that the device can capture particles between  $20\mu\text{m}$  and  $30\mu\text{m}$ . To demonstrate cell viability, the device was tested using melanoma cells. No visible damage onto the cells was observed after the experiments using the device; therefore, it is suitable for biological applications where various sizes of cells are required for analysis.

## ACKNOWLEDGEMENTS

I would like to express my deepest gratitude to my supervisor, Dr. Chris Zhang, who accepted me as his student and encouraged me to study a masters in science. I will always be thankful for his support, patience, advice and instruction during my master's degree.

I also would like to express my gratitude to my co-supervisor, Dr. Ildiko Badea, who provided me with the means and knowledge to conduct experiments with human cells.

Finally, I would like to thank my parents for all their support and love during these long years that I have been away from home. I believe that my achievements are a reflect of their own. Without them nothing would have been possible.

To my parents and family...

# TABLE OF CONTENTS

PERMISSION TO USE .....	i
ABSTRACT .....	ii
ACKNOWLEDGEMENTS .....	iv
TABLE OF CONTENTS.....	v
LIST OF TABLES .....	ix
LIST OF FIGURES.....	x
LIST OF ABBREVIATIONS .....	xvi
CHAPTER 1: INTRODUCTION .....	1
1.1 Background and Motivation .....	1
1.2 Microfluidic Cell-trapping Devices.....	2
1.3 Tunable Devices.....	4
1.4 Hypothesis of the Research.....	6
1.5 Objectives and Scope of Thesis .....	6
1.6 Thesis Organization.....	7
CHAPTER 2: LITERATURE REVIEW AND DEVICE CLASSIFICATION .....	8
2.1 Introduction.....	8
2.2 FCBPSS Framework.....	8
2.3 Hydrodynamic Cell-trapping Devices .....	9
2.3.1 Function .....	11
2.3.2 Context.....	11
2.3.3 Behavior.....	12
2.3.4 Principle .....	14
2.3.5 Structure .....	16
i. Comb Arrays .....	16
ii. Bypass Channels .....	18

iii.    Microwell Arrays .....	25
iv.    Trap Arrays .....	27
2.4 Adaptable Devices .....	33
2.5 Concluding remarks .....	37
CHAPTER 3: CONCEPTUAL DESIGN .....	39
3.1 Introduction.....	39
3.2 Axiomatic design for a new cell-trapping chip .....	39
3.3 Proposed conceptual design of the adaptable microfluidic single-cell trapping device.....	43
3.3.1 Large and uniform deformability: DP3.....	43
3.3.2 Trapping arrays: DP1.....	49
3.3.3 Traps for a single cell: DP2 .....	51
3.4 Summary.....	57
CHAPTER 4: MODELING AND OPTIMAL DESIGN.....	59
4.1 Introduction.....	59
4.2 Mechanical Simulation .....	59
4.3 Hydrodynamic Simulation .....	62
4.4 Conclusion.....	66
CHAPTER 5: FRABRICATION.....	67
5.1 Introduction.....	67
5.2 Soft Lithography .....	67
5.3 Replica Molding.....	68
5.4 Stretching Apparatus .....	72
5.5 Cleaning of the Microfluidic Cell-trapping Device.....	73
5.6 Summary.....	74

CHAPTER 6: MEASUREMENTS AND EXPERIMENTS .....	75
6.1 Introduction.....	75
6.2 Experiment 1: Stretching and deformability.....	75
6.3 Experimental Procedure (Experiment 1) .....	76
6.4 Experimental Results (Experiment 1).....	81
6.4.1 Measuring in ImageJ .....	81
6.4.2 Maximum Deformation and Strain.....	83
6.4.3 Uniform Deformation .....	87
6.4.4 Minimum Deformation .....	91
6.5 Discussion (Experiment 1).....	91
6.6 Experiment 2: Trapping of Particles .....	93
6.7 Experiment 2: Part I .....	94
6.8 Experimental Procedure (Experiment 2: Part I).....	94
6.9 Experimental Results (Experiment 2: Part I) .....	98
6.9.1 Trapping of single microspheres.....	98
6.9.2 Trapping of single microspheres of different sizes .....	101
6.10 Discussion (Experiment 2: Part I) .....	109
6.11 Experiment 2: Part II .....	111
6.12 Experimental Procedure (Experiment 2: Part II) .....	111
6.13 Experimental Results (Experiment 2: Part II) .....	114
6.14 Discussion (Experiment 2: Part II) .....	116
6.15 Conclusion.....	116
CHAPTER 7: CONCLUSION AND RECOMMENDATIONS .....	118
7.1 Overview .....	118
7.2 Outcomes .....	119
7.3 Discussion on the Limitations of Using Microspheres instead of Cells.....	121



7.4 Conclusions.....	121
7.5 Future Research Recommendations.....	123
7.5.1 Design Modifications .....	123
7.5.2 Rescale and Optimization .....	124
7.5.3 Air bubbles and Filters .....	124
7.5.4 Assess the device on a biological assay.....	125
7.5.5 Single-cell retrieving system.....	125
LIST OF REFERENCES.....	126
APPENDIX A: CAD DRAWINGS OF THE NEW MICROFLUIDIC SINGLE CELL TRAPPING DEVICE .....	130
APPENDIX B: CHARTS OF THE SIZE INCRMENT OF THE TRAPS .....	137

## LIST OF TABLES

Table 3.1 Young’s Modulus of PDMS with different mixing ratios of base and curing agent (Khanfer, Duprey, Schlicht, & Berguer 2009, p. 506) .....	45
Table 3.2 Young’s Modulus of PDMS determined when varying the curing temperature (Johnston, McCluskey, Tan, & Tracey, 2014, p. 5) .....	45
Table 3.3 Number of traps that captured a single cell, no cells, and multiple cells .....	52
Table 3.4 Probability of trapping a single, zero, and multiple cells for each device .....	53
Table 3.5 Reliability (R) and failure (Q) for the different trap shapes .....	54
Table 4.1 Material properties used for simulation .....	60
Table 6.1 Average dimensions of the traps in the array one (A1) .....	84
Table 6.2 Average dimensions of the traps in the array two (A2) .....	84
Table 6.3 Coefficients of variance of the measured traps in array one (A1). .....	85
Table 6.4 Coefficients of variance of the measured traps in array two (A2). .....	85
Table 6.5 Size increments of the traps on each zone of array A1 .....	87
Table 6.6 Size increments of the traps on each zone of array A2 .....	87
Table 6.7 Size increments of the traps on each zone of array A2 .....	92

## LIST OF FIGURES

Fig. 1.1 Different geometries and shapes of microstructures used as cell traps. (A) Cup-shape microwells (Di Carlo et al., 2006, p. 1447). (B) Rectangular trap (Wu et al., 2007, p. 199). (C) U opened-shape trap (Huebner et al., 2008, p. 694). (D) Triangular trap (Xu et al., 2013, p. 5). (E) Rectangular and cup shape traps with a rear opening (Benavente-Babace et al., 2014, p. 300) ..... 3

Fig. 2.1 Classification of trapping techniques.  $D$  is the particle diameter,  $\rho$  is the density of the particle,  $\beta$  is the compressibility of the particle,  $\epsilon$  is the dielectric constant,  $\sigma$  is the Conductivity of the medium,  $X$  is the permittivity of the particle, and  $n$  is the index of refraction of the particle (Nilsson et al., 2009, p.156) ..... 10

Fig. 2.2 Symbols used to represent a function diagram (Pahl et al., 2007, p. 32) ..... 12

Fig. 2.3 General functions (behaviors) of the systematic design theory (Pahl et al., 2007, p. 35) ..... 13

Fig. 2.4 Generalized systematic design diagram of the behavior of microfluidics particle-trapping devices based on hydrodynamic principles ..... 14

Fig. 2.5 Comb array of microposts to immobilize single particles. When flowing along the channels, single particles are captured in the multiple gaps formed by the parallel microposts. The immobilized particles can be latter released by reversing the flow (Sochol et al., 2012, p.5052) ..... 17

Fig. 2.6 Traps formed by to microposts joint by a small bridge at the bottom, which is shorter in deep than the posts creating a small opening to allow the flow of carrier fluid through the trap towards the delivery channel (Chung et al., 2011, p.7047) ..... 18

Fig. 2.7 (A) Trapping mode. If a trap is empty, the flow resistance of path 1 is lower than that of path 2. Otherwise, the particles will bypass the occupied trap taking the path 2. (B) Retrieving mode. Using laser focusing, the aluminum plates are heated to produce a bubble in the trapping channel, which will push the bead out of the trap into the main flow (Tan et al., 2006, p.1147) . 19

Fig. 2.8 Kobel et al. device features. (A) Diagram of the traps and channels, as well as, the flows. (B) A micrograph of a section of the cell-trapping device (Kobel et al., 2010, p.859) ..... 20

Fig. 2.9 SEM (Scanning electron microscope) micrographs of the device showing the double trap feature. (A) Zoom focusing in a single pair of traps. (B) Six trap pair in series. (C) Entire trapping chip (Frimat et al., 2011, p.232) ..... 22

Fig. 2.10 Schematic of the main trapping device, and trap configurations (squared, triangular, conical, and elliptical) used in three device generations (Lawrenz et al., 2013, p.8) ..... 23

Fig. 2.11 T junction device (A) Schematic diagram of the trapping principle showing both paths, trapping and bypassing. (B) Drawing of PDMS device (Jin et al., 2015, p.4) ..... 24

Fig. 2.12 Suspended cells being trapped individually in microwells (Rettig et al., 2005, p.5629) ..... 25

Fig. 2.13 Trapping process for a pair of cells. (i) Device at the slack position, none strain applied. (ii) Device stretched on the x direction to increase the size of the vertical L-branch and capture a single cell. (iii) Change the stretching direction to y-axis to increase the size of the horizontal L-branch and capture a second single cell. (iv) Stretching on both direction, x and y axes, to allow cell interaction between the two trapped cells. (Lee et al., 2015, p.2) ..... 27

Fig. 2.14 Trapping mechanisms of microfluidics trap array devices. (A) Diagram taken from Di Carlo et al. (2006) which shows how the cells are trapped in an empty microstructure and diverted when the microstructure is already filled (p.4928). (B) Schematic flow retrieved from Huebner et al. (2009) which depicts the stream lines when cells approach the traps (p.694) .... 28

Fig. 2.15 Array of single water-in-oil microspheres (Huebner et al., 2009, p.694) ..... 30

Fig. 2.16 Array of traps uniformly distributed on a triangular surface. Traps are shaped by four no-joined microstructures with a middle rear gap, which allow the pass of flow through the trap to direct cells into it (Wlodkowic et al., 2009, p.5518) ..... 30

Fig. 2.17 (A) Triangular trap composed of two inverted trapezoids to capture single microspheres. (B) Picture of the optimized device during a trapping experiment to show the high density array of traps capturing single microspheres (Xu et al., 2013, p.5) ..... 32

Fig. 2.18 Tunable particle-sorting device (Beech, 2008)..... 34

Fig. 2.19 The cell trapping principle. (A) Plan view and cross-sectional views along lines (B) a-a and (C) b-b of cell trapping approach. Dimensions are given in micrometers (Zhu et al., 2013, p.2)..... 35

Fig. 2.20 Schematic diagram of the tunable principle via modification of trap dimensions. (A) Original position (none strain applied) to capture single cells on each trap. (B) Strain is applied to capture multiple cells on each trap (Zhu et al., 2013, p.2) ..... 36

Fig. 3.1 Picture diagram of the lateral contraction effect of a material due to the application of a normal force, which is determined by the Poisson’s ratio..... 46

Fig. 3.2 The final design of the microfluidic device (note that in Appendix A a complete drawing with the specific dimension of the design is provided). ..... 47

Fig. 3.3 3D drawing of the stretching apparatus. The apparatus comprises a long board (base) with holes spread out every 5mm and two clamps (on blue) to hold the microfluidic device (on dark gray). Detail dimensions are specified on Appendix A..... 48

Fig. 3.4 3D drawing of the arrays of traps designed for the new single-cell trapping device ..... 49

Fig. 3.5 Design and dimensions of the array of traps defined for the new device. The final design encompasses two identical arrays ..... 51

Fig. 3.6 Trap designed for the new cell-trapping device. (A) 3D drawing of a single trap. (B) Dimensions of the trap ..... 56

Fig. 3.7 Direction of the strain applied to the device via a mechanical induced force to produce a size increment of the traps. (A) The diagram shows the whole device, and the blue arrows represent the direction of the tensile force to produce deformation. (B) Only depicts a single trap and the blue arrows represent the direction on which the deformation or size increment will be produced. Such size increment is experienced by all the traps in the arrays ..... 57

Fig. 4.1 ANSYS model. In the image it can be seen the input conditions of the system to be solved by the simulation..... 60

Fig. 4.2 FEA simulation results. (A) Horizontal deformation of the device and maximum strain. (B) von Mises equivalent stress distribution in the trapping device ..... 61

Fig. 4.3 Fluent model. An enclosure has been added in order to define the fluid domain, and only a small section of 5 traps were modeled ..... 63

Fig. 4.4 Fluent simulation results. The picture depicts the flow profile predicted for the arrays of traps..... 64

Fig. 4.5 Fluent simulation results of a single trap. (A) Shows the maximum shear stress produced on a cell when it is docked in the trap. (B) Close-up of the cell in picture A, where it can be seen that the higher stress is on the wall side touching the trap’s walls. On (C) the flow velocity profile of a cell coming to the trap is depicted. The shear stress induced by the flow itself is very low, of approximately  $7.5e^{-4}$  [Pa]..... 65

Fig. 5.1 Photolithographic process diagram showing the developing process differences between positive and negative tone resists. In general, for the fabrication of molds for microfluidic devices, silicon (Si) substrates and negative tone resist SU-8 are used..... 70

Fig.5.2 Picture of the final microfluidic single-cell trapping device fabricated on PDMS ..... 71

Fig. 5.3 General flow diagram of the replica molding method followed to fabricate the microfluidic single-particle trapper device proposed in this thesis ..... 72

Fig. 5.4 Stretching apparatus fabricated on Acrylic. On the picture all the components of the stretching apparatus used to apply a uniformly distributed force onto the trapping device can be observed, which include two clamps with screws and a base board ..... 73

Fig. 6.1 Example of a micrograph taken by the Olympus IX70 microscope at a 10X magnification ..... 76

Fig. 6.2 Micrograph showing the three linear dimensions (exit, entrance, and gap between traps) that were examined on 80 traps for experiment 1 ..... 77

Fig. 6.3 Schematic diagram showing the selection of traps. The device was divided on two arrays A1 and A2, later each array was divided in 5 regions denoted by the letters A to E. From each zone 8 different traps were selected to be examined on three linear dimensions, exit, entrance, and gap between traps ..... 78

Fig.6.4 Components required for the assembling of the new microfluidic single cell trapping device onto the stretching apparatus ..... 80

Fig. 6.5 Procedure to mount the new cell trapping device onto the stretching apparatus. (A) Put the PDMS chip on top of the bottom sections of the clamps. (B) In a sandwich manner locate and align the top sections of the clamps on top of the PDMS chip, and secure the device on the clamps using the short screws. (C) Fix the left clamp to the main board by using two large screws, the position could be arbitrary. (D) Determine the strain or size increment you want to apply to the traps and fix the right clamp in the corresponding hole. Remember that the stretching direction is to the right side and you can choose from 6 holes (6 positions); hole 0 means no deformation and hole 5 means maximum deformation ..... 80

Fig. 6.6 Example of measuring the traps using Image J. (A) Shows an original size micrograph with a size of 720x480 pixels. (B) Shows the same image in (A), but enlarged 300%. The red arrow in (A) and (B) is pointing at a measuring line to exemplify that it is easier to select the edges of a trap by zooming in the image. (C) Depicts the real vertical length of a pixel in image (A), which is of 1 micron; the image has a zoom of 3200%. (D) Shows that Image J is capable of measuring lengths smaller than the pixel size of the image being analysed. The resolution of the measuring tool was empirically determined to be approximately of 1/30 pixels for the image size used ..... 83

Fig. 6.7 Charts in this figure displays the average magnitudes recorded for the exit (blue dots), the entrance (orange dots), and the gap between traps (grey dots) at all the stretching position tested (hole 0 to 5) for the traps in all the regions, such that the x-axis is the stretching position and the y-axis is the trap dimension expressed in microns. In addition to the scattered dots, a trend line has been included with its corresponding equation for each series in order to show that the deformation of the traps follows a linear and constant tendency, which can be represented by a linear equation of first order ..... 89

Fig. 6.8 Micrographs taken at array one section B. (A) Image taken when the device was not stretched. (B) Micrograph obtained when the device was expanded to position hole 1. (C)-(F) Pictures taken when the device was stretched from hole 1 to hole 5 progressively. By looking at all the micrographs one can observe the increase on size of the traps as they go from A to F, but a small deformation of the microstructures..... 90

Fig. 6.9 Picture of the equipment used to conduct Part I of experiment 2. In the picture (A), one of the two syringe pumps used is showed loaded with three plastic syringes (BD) of 3ml which are connected to the modified T-junction device for the microsphere production by Teflon tubing (two syringes were actually used during the experiments, this setup is just proposed as an example). The microsphere generator device and the trapping devices are located at all times under the optical microscope for visualization. A computer which is connected to the output of the video camera displays the image obtained by the microscope. Picture (B) shows in a close up, the modified T-junction device and the trapping chip, as well as, how these two are connected by a Teflon tubing to allow the direct flow of microspheres..... 97

Fig. 6.10 Micrographs showing the trapping of single 20 $\mu$ m particles at various zones of the trap arrays. In (A) most of the traps are filled with a single microsphere, while in (C) several traps captured multiple particles. (E) and (C) shows that undesired particles larger than 20 $\mu$ m were captured. However, among all the images single trapped microspheres predominate..... 99

Fig. 6.11 Micrographs showing the release of previously trapped microspheres at various zones of the trap arrays. In all the micrograph here presented it can be seen than all the traps are empty due to the reversed flow; however, many microspheres are retained at the rear of the traps..... 100

Fig. 6.12 Micrographs showing the capturing of single particles at different zones of the trap arrays. The red circles highlight particles with a diameter of 20 $\mu$ m or close ..... 102

Fig. 6.13 Micrographs showing the capturing of single particles at different zones of the trap arrays. The red circles highlight particles with a diameter of 22 $\mu$ m or close. Among the three images showed it can be seen that some traps have two microspheres; however, they are highlighted because one of the microspheres has the ideal size..... 103

Fig. 6.14 Micrographs showing the capturing of single particles at different zones of the trap arrays. The red circles highlight particles with a diameter of 24 $\mu$ m or close ..... 104

Fig. 6.15 Micrographs showing the capturing of single particles at different zones of the trap arrays. The red circles highlight particles with a diameter of 26 $\mu$ m or close ..... 105

Fig. 6.16 Micrographs showing the capturing of single particles at different zones of the trap arrays. The red circles highlight particles with a diameter of 28 $\mu$ m or close ..... 106

Fig. 6.17 Micrographs showing the capturing of single particles at different zones of the trap arrays. The red circles highlight the particles with a diameter of 30 $\mu$ m or close ..... 107

Fig. 6.18 Traps filled with multiple particles, particles escaping traps, and clogged channels are common issues that occur when an improper size of particle is used. Image (A) shows several traps filled with two or more microspheres. In (B) it can be seen how some small microspheres are flowing out the traps thru the trap's exit. (C) depicts some channels blocked by large microspheres trying to go thru the same channel. Although the big particles are captured within the trap, half of its body protrudes out of the trap narrowing the microfluidic channel ..... 109

Fig. 6.19 Micrographs showing massive clogs of microspheres at the first row of the arrays. Image (A) was taken at array A2 when microspheres of 24 $\mu$ m were introduced into the device. The clog depicted on (B) was developed when microspheres of 26 $\mu$ m were used; here it can be seen that larger microspheres help on building up such huge obstructions ..... 110

Fig. 6.20 Micrograph of a sample of melanoma cells. The cells were placed on a microscope slide flowed by the addition of a drop of trypan blue. The black circles highlight two cells stained on blue which are actually death ..... 114

Fig. 6.21 In pictures A and B very few single cells were captured by the traps. (B) shows couple traps with multiple cells and only one trap with a large cell properly captured (black circles). Only couple cells were found death and they are highlighted by the red circles ..... 115



## LIST OF ABBREVIATIONS

ADT	Axiomatic Design Theory
BSC	Biosafety cabinet
CCD	Charge-coupled device
CV	Coefficient of variation
DP	Design parameter
EAM	Electrical-adaptive method
FBS	Fetal bovine serum
FC	Flow cytometry
FCBPSS	Function-context-behavior-principle-state-structure
FEA	Finite element analysis
FR	Function requirement
LSC	Laser scanning cytometry
MCF-7	Michigan Cancer Foundation-7
PDMS	Poly(dimethylsiloxane)
SD	Systematic Design

## CHAPTER 1: INTRODUCTION

### 1.1 Background and Motivation.

There are various assays or analyses which are required to be conducted on a single cell or group of cells, with multiple samples in order to be able to make a relevant inference. Cells separation, isolation, positioning, trapping, and sorting are various kinds of cell manipulation processes that are of great importance in basic biological research and clinical diagnostics (Zhu et al., 2013). However, conventional methods such as flow cytometry (FC) and laser scanning cytometry (LSC) for cell analysis do not permit effective and efficient cell trapping and cell positioning, which may be offered by the microfluidic technology (Lindström & Andersson-Svahn, 2010). Different microfluidic technologies capable of capturing single cells have been developed in the past decades, for instance, microwells arrays, U-shaped weirs, and micro-trap arrays.

Although cell trapping of different numbers and sizes of cells can be accomplished using micro-traps with different geometries and dimensions (Lawrenz, Nason, & Cooper-White, 2012; Di Carlo, Aghdam, & Lee, 2006), microfluidic devices lack flexibility in processing different cell diameters. Therefore, once a device has been designed and fabricated it is not possible to modify its dimensions and a new device is required for each different cell diameter (Zhu et al., 2013; Di Carlo, Wu, & Lee, 2006). This becomes inconvenient since among different kinds of cells, sizes can range from 2  $\mu\text{m}$  to 100  $\mu\text{m}$ , for example, chlorella algae cells (average diameter of 2 $\mu\text{m}$ -5 $\mu\text{m}$ ), MS cells (average diameter of 14 $\mu\text{m}$ ), and MCF-7 cells (average diameter of 20 $\mu\text{m}$ -24 $\mu\text{m}$ ) (Lawrenz et al., 2012; Zhu et al., 2013).

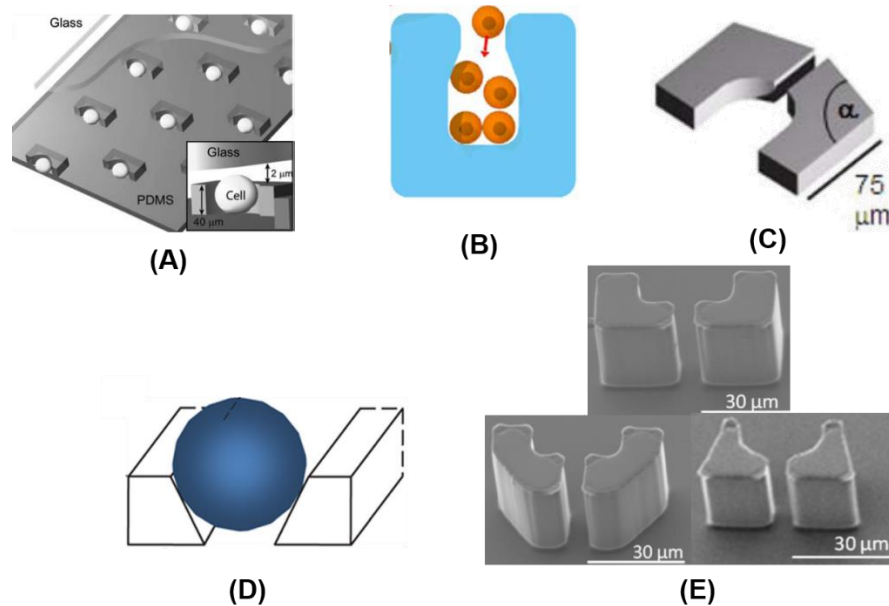
The approach of requiring a microfluidic device (tool) for each size of cell for analysis (operation) could be considered, from an engineering point of view, as an inefficient method, which motivated us to think of how to design a more “universal” device capable of working with multiple cell sizes.

## 1.2 Microfluidic Cell-trapping Devices

Microarray technology has been implemented in various biological fields. Such technology allows the screening of biomolecules in array formats, which presents at a specific position and time a single library element of a known structure. For instance, using specific methods, small numbers of cells, or even single cells, can be observed as library elements (Seliger, 2007). With the birth of microarray technology new tools were required in order to fulfill the needs of such techniques. This is how micro-devices and microfabrication techniques, first seen in microelectronics, entered into biological sciences; in particular, microfluidic devices. Microfluidics is a technology for the manipulation of fluids through microchannels, with small dimensions in the order of hundred microns and flow speeds characterized by low Reynolds numbers, resulting in laminar flows. Moreover, regardless of the small dimensions of the channels the fluid behaves like a continuum, and the Navier-Stokes equations are still valid to describe the flow behaviour.

In general, a microfluidic device is composed of two bonded thin sheets of either polymer or silicon to glass or polymer to polymer. The bottom layer usually bears the geometry features and channels while the top layer represents the lid to seal the device; as a result, the two bonded layers form an enclosure for the fluids. Many microfluidics cell-trapping devices that use hydrodynamic trapping principles have been reported. In this section only those using arrays of physical traps are considered for further explanation. Other cell-trapping devices are discussed in Chapter 2 to give a broader context. Microfluidics cell-trapping arrays have an arrangement of microstructures protruded on the surface of the bottom sheet to physically capture cells. Such microstructures work as traps for the traveling cells and they could have different geometrical shapes as evidenced by various array devices reported in literature. For example, Di Carlo et al. (2006) reported a microfluidic cell-trapping device in which high-density arrays of single cells were captured using a cup-shape microwells; another platform using rectangular-shape traps for the analysis of multicellular tumor spheroids (cancer) was developed by Wu et al. (2007). Huebner et al. (2008) presented a device capable of isolating microdroplets for drug applications

utilizing U opened-shape microstructures, while Xu et al. (2013) reported a more efficient device using triangular traps. More recently another microfluidic chip incorporating different sieve-like microstructures for studying the effects of novel drugs was divulged by Benavente-Babace et al. (2014). Figure 1.1 shows the microstructures utilized on the foregoing studies.



**Fig. 1.1** Different geometries and shapes of microstructures used as cell traps. (A) Cup-shaped microwells (Di Carlo et al., 2006, p. 1447). (B) Rectangular trap (Wu et al., 2007, p. 199). (C) U opened-shape trap (Huebner et al., 2008, p. 694). (D) Triangular trap (Xu et al., 2013, p. 5). (E) Rectangular and cup shape traps with a rear opening (Benavente-Babace et al., 2014, p.

300)

Microfluidic cell-trapping array devices accomplish their goal of trapping cells by combining two working principles. Note that trapping here means to corraling the cells at predetermined position in the array of traps. The first principle is based on the probability that cells suspended in a carrier fluid will collide against the traps and therefore they will remain in the trap, and the second principle is a hydrodynamic principle based on the difference of flow resistance of two

paths (Lawrenz et al., 2012; Di Carlo et al., 2006; Huebner et al., 2008; Xu et al., 2013; Zhu et al., 2013).

On regards of the fabrication materials, it was mentioned before in this section that microfluidic devices can be fabricated from different materials such as glass or polymers; however, polydimethylsiloxane (PDMS) is the most popular material among polymers used in microfluidics technology. PDMS is a silicone-bases organic polymer, which is characterized by its optical transparency and inert properties. It is ideal for bioassays because it is compatible with optical methods for detection and does not react with biological agents such as living cells. Also, PDMS devices are easy and fast to fabricate (Sia & Whitesides, 2003; Wang, 2011). Moreover, PDMS behaves mechanically as an elastomer, it is very flexible and elastic, which makes it suitable for adaptable applications. In particular, its elastic properties are of high interest in this thesis as it will be discussed further later on Chapter 3.

### **1.3 Tunable Devices**

As mentioned in section 1.1 although microfluidic cell-trapping devices are very efficient on capturing cells, they present some limitations when they are required to work with various sizes of cells. Microfluidic devices are designed and fabricated considering a fixed size of particle, so a single device is limited to only work with a specific particle size. Complications thus arise due to the considerable variation in sizes of cells, not only when considering different types of cells but also within the same type. For instance, the diameter of Mesenchymal Stem cells can vary from 15 to 50  $\mu\text{m}$  (Ge et al., 2014). Thus, cell trapping devices are required to have flexibility to accommodate various particle diameters. However, this represents a challenge to produce devices capable of changing or adapting its properties in order to work with particles of different sizes. Some efforts on addressing the lack of flexibility in microfluidics devices (not necessarily focused on cell trappers) have been made by some researchers. Although a more detailed review of the literature and classification of devices and tuning methods will be presented in

Chapter 2, three significant devices are summarized in this section. First, Huh et al. (2007) developed a nanofluidic device made of PDMS, which consists of a parallel array of nanochannels capable of modulating their size in response of an external compressive force. Such modulation is performed in order to reduce the cross-section of the channels and thus to limit the size of nanoparticles flowing through them. The second device is a tunable particle separator, which uses PDMS's high-elasticity property to achieve a relative large displacement between its features when the entire device is stretched across its width. The device is based on a previous Deterministic Lateral Displacement (DLD) device which uses an array of micro-pillars as obstacles to sort particles. By increasing the gap between such micro-pillars, Beech and Tegenfeldt were able to use the same device to target particles of different sizes without reducing the separation accuracy (Beech & Tegenfeldt, 2007). The third device is a PDMS cell-trapping array. Zhu et al. (2013) presented a device that can be mechanically modulated to tune the characteristics of cell trapping in order to capture a predetermined number of cells from single cells to multiple cells. The mechanical modulation is achieved by inducing an uniformly distributed strain through the application of an external force on the chip to modify its geometry. It is important to notice that the cells fed into the device are of a fixed size at all times.

Among the three works above briefly discussed, there are two main similarities: the material selection and the tuning method, regardless their different applications. The three devices were all fabricated from Polydimethylsiloxane (PDMS) and they used a mechanical induced force to produce the desire modulation of the device. On regard of their adapting objectives, the first two devices aim for controlling the size of their channels in order to accommodate different sizes of particles, while the goal of the third one is to change the size of its microstructures in order to fit more particles (cells) of a fixed size in each trap. Thus, the following question arose: if it is possible to modify the shape and dimensions of geometrical features in microfluidic devices in order to target various sizes of particles, and such methods have been incorporated into microfluidics cell-trapper, as presented by Zhu et al., would it be

possible to produce a microfluidic single cell-trapping device capable of accommodating cells of various diameters while using a single device as Beech and Tegenfeldt did with their particle separator?

#### **1.4 Hypothesis of the Research**

Inspired by the studies above, the following idea came out. It is possible to design and produce an adaptable single cell-trapping device capable of modifying its geometric features to target cells of different sizes rather than working only with a fixed cell size.

#### **1.5 Objectives and Scope of Thesis**

The general objective of my research is to design a new microfluidic cell-trapping device capable of modifying its features in order to capture multiple single-cells of different sizes without compromising its capture efficiency. The general methodology is to apply a uniform distributed strain on the device via a mechanical stretching. Therefore, the key attributes of such a device include: (A) the deformation of the elastomeric polymer (PDMS) feasible to stretch, (B) compliance of the traps, and (C) uniformity of the deformation of the traps. Therefore; the specific objectives are as follows:

Objective 1: Analysis of the existing principles of single cell trappers to lead to the classification of the principles with their pros and cons.

Objective 2: Development of a simulation system for the device, as well as its deformation process, and to guide the design optimization.

Objective 3: Design of the device to achieve a large deformation as possible (which is at least a size increment of 60% on the traps) and a uniform deformation of all the traps.

Objective 4: Fabrication of the device in accordance with the design specifications resulting from the research in objective 2 to test the hypothesis of the research.

## **1.6 Thesis Organization**

Chapter 2 covers a comprehensive literature review focused on microfluidic devices based on hydrodynamic principles for the capturing and isolation of particles. The review is presented in a classification fashion, where several particle trappers pertinent to this research are discussed under the FCBPSS (Function-Context-Behaviour-Principle-Structure-State) framework. Devices with adaptive properties are also considered in the classification analysis.

Chapter 3 presents the conceptual design of a new device. The design process is based on and guided by the Axiomatic Design Theory, and this theory is briefly introduced first.

Chapter 4 presents a model of the device that was created in the commercial software ANSYS Release 14.5 (ANSYS Inc., PA.) to simulate the deformation of the traps when the device is stretched, and to determine the maximum strain possible before plastic deformation. The chapter also presents a second model created in Fluent to simulate the flow profile developed within the micro-channels, and to determine numerically the maximum stress induced in a particle (living cell) when captured by a trap.

Chapter 5 provides a brief introduction to soft lithography and explains the replica molding technique used to fabricate the device. It is also presented a detailed description of the process followed to make the new trapping device designed in Chapter 3.

Chapter 6 presents the experiments conducted to test the attributes of the device fabricated in Chapter 5, as well as the results obtained. Two main experiments were carried out. The first experiment is proposed to evaluate the deformation of the device, and the second to assess the capturing performance.

Chapter 7 provides the conclusion and future work.



## CHAPTER 2: LITERATURE REVIEW AND DEVICE CLASSIFICATION

### 2.1 Introduction

In the introductory chapter the main characteristics of the hydrodynamic cell-trappers based on microfluidics were briefly presented; as well as, some outstanding adaptable devices. In this chapter, a literature review focused on microfluidic devices dealing with particle processes, in particular capturing and isolation, is conducted. Note that the term “particle” is here used to refer to any kind of cells or microspheres. Various published reviews on microfluidic systems for particle trapping provide indeed a thorough overview of the methods available to manipulate particles, including but not limited to the followings: magnetic, optical, mechanical, and electrical (Andersson & van den Berg, 2003; Yi, Li, Ji & Yang, 2006; Nilsson, Evander, Hammarström & Laurell, 2009; and Lindström et al., 2010). In contrast to these works, the scope of this chapter of the thesis is limited to hydrodynamic trapping, a branch of mechanical manipulation. The following review is presented in a classification fashion, where several particle trappers pertinent to this research are discussed under the FCBPSS (Function-Context-Behaviour-Principle-Structure-State) framework. Devices with adaptive properties are also considered in the classification analysis.

### 2.2 FCBPSS Framework

A thorough understanding of a system is essential to produce a proper classification. The goal is to unravel all the functions and relationships of all its components. In order to unravel the “nature” of a system different design theories could be useful such as the Axiomatic Design Theory (Suh, 1990), the Systematic Design Methodology (Pahl, Beitz, Feldhusen, & Grote, 2007), and the FBS model (Umenda et al., 1990). However, since this analysis is not a design process, it should rather be called ontological process, which by definition is to show the relations between the concepts and categories in a subject or domain. Ontologies provide uniform frameworks to identify differences and similarities among systems; moreover, they can

be used to record the evolutionary steps of a technology (Gero et al., 2007). In particular, the FCBPSS framework proposed by Lin and Zhang (2004) is adopted in this thesis to produce an ontology of hydrodynamic cell-trapping devices.

Under the FCBPSS framework an entity is defined as a system, and a process is defined as a set of operations of the system. A system can be decomposed or analysed upon its function (F), context (C), behavior (B), principle (P), structure (S), and state (S). The function of a system answers to the question “what is the system for?” and can be accomplished by the system’s structure through the provision of certain behaviors. In addition, the function or usefulness of a system is context-sensitive, which means that the same system can be used for fulfilling different tasks in different contexts without mayor changes on the system. The context is the precondition, post condition, and environment where the system performs its function. The behavior is about the response of the system when it receives stimuli, and it is represented by the relation between the input and output variables of the system. Unfortunately, the behaviour and function can be easily mixed up due to colloquial language. Therefore, behavior must be considered only as the observable effects on the structure of the system when a stimulus is induced. The principle is the fundamental law that governs the behavior of the system, so it defines the relationships and constraints among state variables. The principle is usually represented or modeled as a set of mathematical equations. The structure is a set of elements linked in a meaningful way. These elements are represented by their properties, which are called states. States thus can be represented as variables since they are quantities of either physical or chemical domains that can change in time (Lin et al., 2004; Zhang, Lin, & Sinha, 2005).

### **2.3 Hydrodynamic Cell-trapping Devices**

Hydrodynamic trapping techniques are the most common in microfluidic devices for particle trapping functions (Nilsson et al., 2009). The main reason is that hydrodynamic techniques do not require the addition or use of a concurrent principle to achieve their goal.

Devices based on hydrodynamic principles use their geometrical features, such as channel dimensions, channel contractions or expansions, and physical barriers to define and control the characteristics of the induced flows. As a result of the small dimensions of the channel, the flows are predominantly laminar, which can precisely transport and manipulate cells throughout the channels (Kim, Lee, & Suh, 2008). In figure 2.1, a table presented by Nilsson et al. (2009) summarizes the characteristics of different trapping methods, which the advantages of hydrodynamic methods over others like optical, dielectrophoretic, and magnetic, can also be observed.

Trapping technique	Discriminating parameters	Buffer demands	System complexity (non-contact mode)		System complexity (contact mode)
Hydrodynamic	$D$	Transparent pH, ion, clean surfaces	Low		Low
Optical	$D, n$		Medium/high		Scarcely operated in contact mode
Dielectrophoretic	$D, \epsilon, \sigma$		Medium		Low
Magnetic	$D, \chi$		High		Low
Acoustic	$D, \rho, \beta$		Low		Scarcely operated in contact mode
Trapping technique	Trapping resolution	Singe cell trapping	Cell cluster trapping	Trapping force (pN)	References
Hydrodynamic	Low ( $\sim 10 \mu\text{m}$ )	Low	Medium	NA	
Optical	High ( $\sim 50 \text{nm}$ )	High	Low	100–2000 <sup>a</sup>	[45,46,53]
Dielectrophoretic	Medium ( $\sim 1 \mu\text{m}$ )	Medium	Medium	200–400	[63,67]
Magnetic	Medium ( $\sim 1 \mu\text{m}$ )	Medium	High	2–1000 <sup>b</sup>	[67,71,73–78,80,81]
Acoustic	Low ( $\sim 100 \mu\text{m}$ )	Low	High	100–400	[95,117,118,127]

**Fig. 2.1** Classification of trapping techniques.  $D$  is the particle diameter,  $\rho$  is the density of the particle,  $\beta$  is the compressibility of the particle,  $\epsilon$  is the dielectric constant,  $\sigma$  is the Conductivity of the medium,  $X$  is the permittivity of the particle, and  $n$  is the index of refraction of the particle (Nilsson et al., 2009, p.156).

Being the most common method to trap particles, in the literature there are endless numbers of hydrodynamic particle trappers reported. Consequently, a classification of these many devices is proposed next to have a thorough understating of such technology. The domain for this classification has been already limited to hydrodynamic microfluidic devices. Whilst most of the devices that are here reviewed share the same function, context, behavior, and principle, they differ on their structure. Since a classification of the structure only makes sense when the function, behavior, context, and principle have been determined, these concepts of the FCBPSS

framework are first discussed as group for the many hydrodynamic trapping devices reviewed, followed by the classification of their structures.

### **2.3.1 Function**

The function of particle-trappers is coincidentally stated on their own name, so the function of any microfluidic particle-trapper is to capture particles in predetermined positions for different biological assays. Here one can observe how the function of a system is indeed context-sensitive because the same system can be used for different purposes such as, measuring cell response to different stimuli (Chung, Rivet, Kemp, & Lu, 2011), cell co-culture (Frimat et al., 2011; Lee et al., 2014), screening methods (Tan & Takeuchi, 2006), drugs development (Wu, Di Carlo, & Lee, 2007; Wlodkowic, Faley, Zagnoni, Wikswo, & Cooper, 2009), and others.

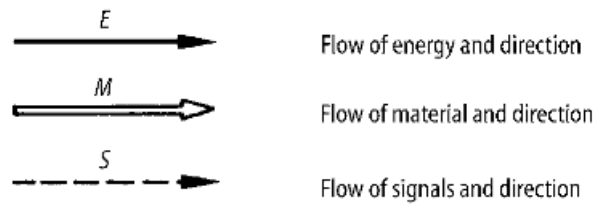
### **2.3.2 Context**

The microfluidic particle-trappers work with microparticles usually smaller than  $100\mu\text{m}$ , and in order to feed the microparticles into the device they must be suspended on a fluid which is called carrier fluid. As a result, the working environment or context of the devices is mainly determined by the target particles; in other words, on the input to the trapper device. For instance, water-in-oil microspheres are suspended on an oil solution, while living cells are suspended on culture media. Also, living cells are very sensitive to changes of their environment, and depending on the cell type they might require special environment conditions, which the devices must provide. In addition, when using cells, it is important to observe the forces exerted on them to guarantee cell viability. The main concern on this regard is the wall-shear stress induced on the membrane, which must be lower than  $4.5 \text{ [Pa]}$  (Dimmeler, Haendeler, Rippmann, Nehls, & Zeiher, 1996, p. 71). Among the literature reviewed, the devices encountered mainly work with either microspheres or living cells, so the devices can be classified regarding their context on these two: microsphere context or cell context.

### 2.3.3 Behavior

The behavior and the function of these devices could be easily confused due to their similitude. Therefore, in order to clarify the behaviour of hydrodynamic particle-trappers a Systematic Design (SD) approach (Pahl et al., 2007) of decomposing the system function is used. It is important to mention that unfortunately SD uses the term function as the relationship between the input and output of a system; however, we know that for FCBPSS this is the definition of behavior. Nevertheless, the approach proposed by the SD methodology is still valid to determine the behavior of hydrodynamic particle-trapping platforms. Since an overall system can have many sub-elements (structures), it would be helpful to state the behavior of these in a diagram, which will allow one to clarify the overall behavior of the system. The SD theory proposes the following “universal” schematic representation of a function (behavior) (Fig. 2.2).

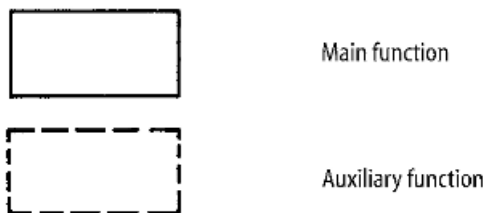
#### Types of flow:



#### System:

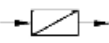

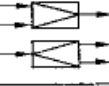
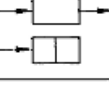



#### Function:



**Fig. 2.2** Symbols used to represent a function diagram (Pahl et al., 2007, p. 32).

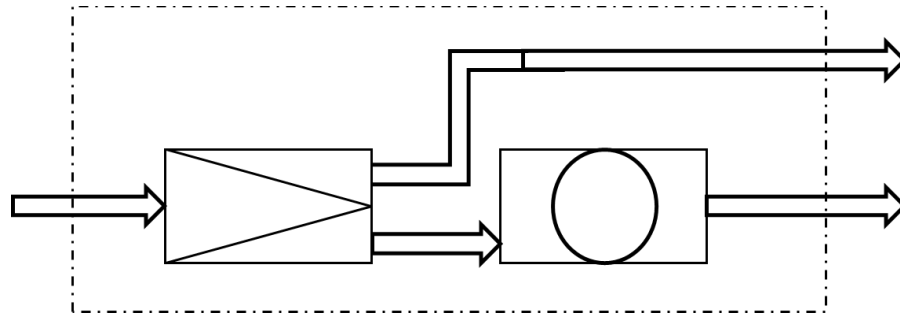
Establish the input and output of the system. The input of the particle-trapping devices is a fluid with a determined number of particles. The output is the same fluid with a reduced number of cells in comparison to the input. Also, the docked particles are stored and retained for a certain time at their trapped position to be driven out the device later. Once the general behavior of the device has been stated, one can proceed to generalize it in order to recognize the natural relationship of the input-output without context. This process requires a high level of abstraction of the system, and the elimination of the context, so that the general behavior resulting from the process would be very general. With a general function (behavior) one would be able to look for other possible solutions, regardless of the context they are coming from. The SD approach holds that any general function (behavior) should fit on the next five categories showed in figure 2.3:

Characteristic Input (I)/Output (O)	Generally valid functions	Symbols	Explanations
Type	Change		Type and outward form of I and O differ
Magnitude	Vary		$I < O$ $I > O$
Number	Connect		Number of $I > O$ Number of $I < O$
Place	Channel		Place of $I \neq O$ Place of $I = O$
Time	Store		Time of $I \neq O$

**Fig. 2.3** General functions (behaviors) of the systematic design theory (Pahl et al., 2007, p. 35).

It has been stated that the microfluidic cell-trapping device has behavior without the context of capturing particles and retaining them for a certain period of time at their trapped position, later the trapped particles are expelled from the device. Thus, following the notation

proposed by the SD approach, one can come up with the general function diagram depicted in figure 2.4.



**Fig. 2.4** Generalized systematic design diagram of the behavior of microfluidics particle-trapping devices based on hydrodynamic principles.

### 2.3.4 Principle

The principle is related to the behavior by the question “how and why?”. Therefore, to determine the principle of the particle-trapping devices one should answer the question: how does such devices capture particles and retain them for a certain period of time at their trapped position? The answer is: using hydrodynamic principles, in particular the “paths of the least flow resistance”. When a flow is induced into the device the flow will take the path with the least flow resistance. Thus, if one of the paths goes through the trap, the flow will go through it unless that path is blocked. In a case where the path is blocked by a cell, the flow resistance of that path will be higher than any alternative flow path thereby making the main flow to take another path with less resistance. Once the traps are occupied by particles, the flow of the carrier fluid is kept in the same direction in order to hold the trapped particles within the traps.

Mathematically, the above principle can be modeled by determining the pressure drop in a microchannel using the Darcy-Weisbach equation and solving the Hagen-Poiseuille flow problem for continuity and momentum. If one assumes a fully established fluid inside the

trapping area, which in practice can be done by placing the trapping area far enough from the inlet (Xu et al., 2013) the pressure difference in a channel is given by,

$$\Delta P = \frac{fL\rho V^2}{2D}, \quad (2.1)$$

where:

*f* is the Darcy friction.

*L* is the length of the channel.

$\rho$  is the fluid density.

*V* is the average velocity of the fluid.

*D* is the hydraulic diameter of the channel.

Considering a rectangular channel because it is the most common cross section in micro-channels one has that,

$$D = \frac{4A}{P}, \quad (2.2)$$

and

$$V = \frac{Q}{A}, \quad (2.3)$$

where:

*A* is the cross section area of the channel.

*P* is the cross section perimeter of the channel.

*Q* is the volumetric flow rate.

The Darcy friction factor *f* is related to the aspect ratio of the channel and the Reynolds number *Re* as,

$$Re = \frac{\rho V D}{\mu}, \quad (2.4)$$

where:

$\mu$  is the fluid viscosity.

Substituting equations 2.2, 2.3, and 2.4 to 2.1, yields,



$$\Delta P = \frac{f Re \mu L Q P^2}{32 A^3}, \quad (2.5)$$

where,  $f$  times  $Re$  can be determine by the following function (Xu et al., 2013, p. 6),

$$f(\alpha) = 96(1 - 1.3553\alpha + 1.9467\alpha^2 - 1.7012\alpha^3 + 0.9564\alpha^4 - 0.2537\alpha^5), \quad (2.6)$$

Since the trapping principle is based on a flow in two paths (trapping path and bypass path), one should apply the obtained difference pressure  $\Delta P$  on both paths. As these paths are connected, the pressure drop is the same for both. Therefore, one can equate both expressions and obtain,

$$\frac{Q_1}{Q_2} = \left( \frac{f_2(\alpha_2)}{f_1(\alpha_1)} \right) \left( \frac{L_2}{L_1} \right) \left( \frac{P_2}{P_1} \right)^2 \left( \frac{A_1}{A_2} \right)^3, \quad (2.7)$$

Finally, to guarantee the trapping of particles, the volumetric flow that goes through the trap ( $Q_1$ ) must to be greater than that of the bypass path around the trap ( $Q_2$ ) (Tan et al., 2006; Xu et al., 2013).

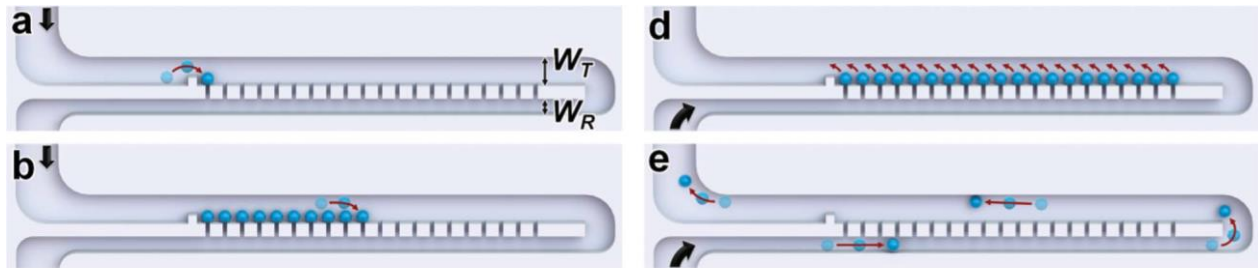
### 2.3.5 Structure

In a review of the literature several particle-trapping platforms based on hydrodynamic principles were found. Most of them fall into three categories considering their structure, which are comb arrays, bypass channels, and trap arrays. In addition, microwell arrays are also reviewed. As it is not the scope of this review to produce a compilation of devices, only the most relevant for this research are now considered.

#### *i. Comb Arrays.*

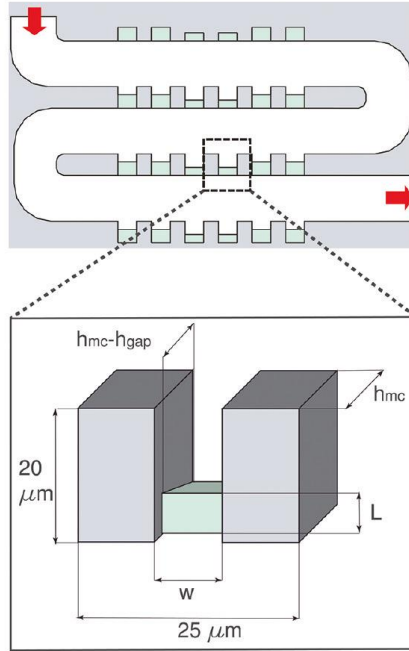
A PDMS device which includes an array of rectangular microposts resembling a comb, as illustrated in figure 2.5, was presented by Sochol, Dueck, Li, Lee, and Lin (2012). The gaps between the microposts that connect the main flow channels serve as traps to immobilize single particles. The device is characterized by the dimensions of the two main channels designated as the trapping (top) and resetting (bottom) channels, respectively. In order to trap the particles

suspended in the carrier fluid, a flow from trapping channel towards the resetting channel is induced. When the suspended particles are immobilized in a trapping location, the channel between posts is blocked diverting the flow to the next empty gap. Once a comb segment is filled, the particles can freely flow to the next array connected in series and repeat the process.



**Fig. 2.5** Comb array of microposts to immobilize single particles. (a) When flowing along the channels, single particles are captured in the multiple gaps formed by the parallel microposts. (b) The ideal trapping process is done in sequence. (d) and (e) Show the release process when the flow is reversed (Sochol et al., 2012, p.5052).

Chung, Rivet, Kemp, and Lu (2011) presented a similar comb array trapping device to that of Sochol et al. (2012). However, they did not use two but only one main serpentine channel called cell-delivery channel. Each comb array has 24 single cell-traps and 8 dummy traps at both ends of the row. The traps used and illustrated by figure 2.6 are more complex structures than the simple parallel microposts used on the foregoing device. The device captures single cells of a fixed size by diverting the cells flowing into the delivery channel. Using the dummy traps located at the beginning of each comb a sort of suction force is produced to attract the cells closer to the traps. Once the cells are near to the traps, they experience two streams: the main delivery channel flow and a cross-flow which passes through the trap's gap forcing the cells into the traps. Then, if a cell is docked in a trap, it will clog the flow across the gap and divert the coming cells to the next vacant trap. Thus, single cell-trapping is controlled by the delivery flow, and the size of the traps.



**Fig. 2.6** Traps formed by two microposts joined by a small bridge at the bottom, which is shorter in depth than the posts creating a small opening to allow the flow of carrier fluid through the trap towards the delivery channel (Chung et al., 2011, p.7047).

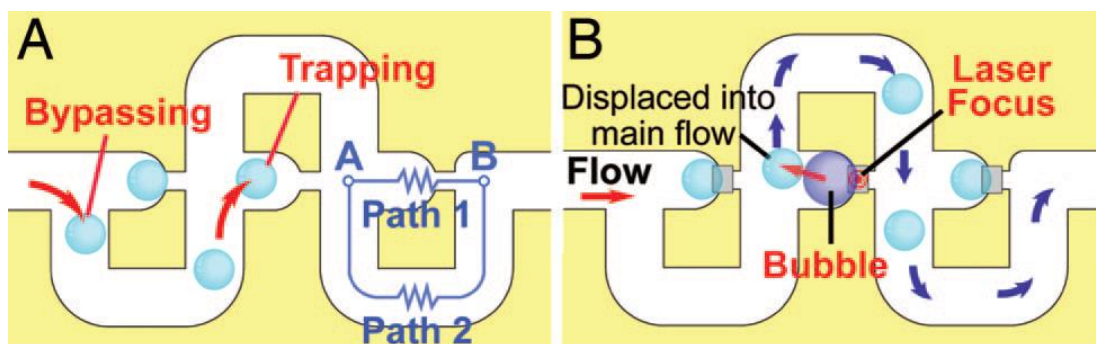
In contrast to the comb structure, for which few devices are reported, many more devices with a bypass structure were found in the literature.

*ii. Bypass Channels.*

Another kind of single particle trapping devices that use serpentine channels can be found in the literature. Such devices, rather than to incorporate arrays of traps along the channels, only have one trap in each loop. Most of the devices reported are likely inspired from a device reported in 2006 by Tan and Takeuchi, which will be illustrated in this section.

A dynamic trap-and-release system capable of trapping single particles and later retrieving specific particles at will was reported by Tan and Takeuchi (2006). The device fabricated on PDMS consists of a main square-wave shaped channel connected to the vertical sections by a

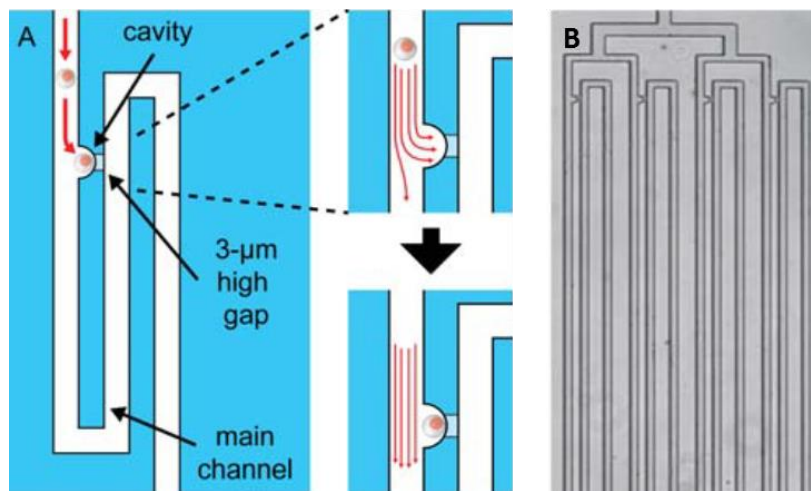
straight channel with narrowed zones that function as traps. The device presented here has been designed to trap particles of a specific size and it poses 100 traps, yet the authors claim to have fabricated a high-density device with  $1 \times 10^4$  traps (Tan et al., 2006, p.1148). The device function and geometry is schematized in figure 2.7. Although the trapping approach employed by Tan and Takeuchi is similar to previous works, they were able to control and use in a more reliable manner the hydrodynamic forces produced in their device to achieve single particle trapping. Their channels are designed such that the straight channel bearing the traps always has a lower flow resistance than that of the square-wave loops. As a result, particles will flow directly to the traps as this stream presents the lowest flow resistance. The trapped particle acts as a plug to the straight channel increasing rapidly the channel flow resistance, and diverting the up coming particle to the next path; i.e., the bypass channel. Thus, once a trap is occupied the following particles will bypass the trap to fill up the next one along the straight channel. Furthermore, the device posses the unique function of retrieving a determined particle in any trap by using bubbles, which are produced by an optical method. To do so, aluminum plates are located near to the traps, on which a IR laser is focused to produce localized heat. Such heat results in the formation of a bubble that forces the particle out of the trap into the main flow which will carry the particle out of the device (Tan et al., 2006, p.1147).



**Fig. 2.7** (A) Trapping mode. If a trap is empty, the flow resistance of path 1 is lower than that of path 2. Otherwise, the particles will bypass the occupied trap taking the path 2. (B) Retrieving mode. Using laser focusing, the aluminum plates are heated to produce a bubble in

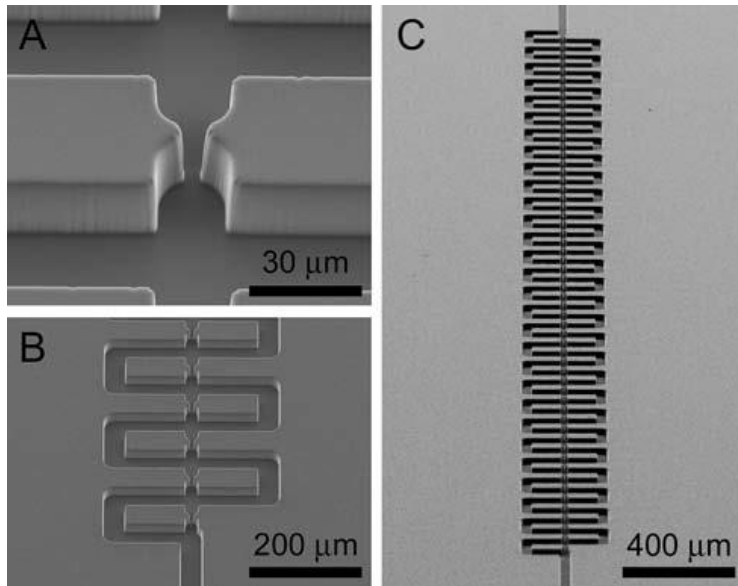
the trapping channel, which will push the bead out of the trap into the main flow (Tan et al., 2006, p.1147).

Tan and Takeuchi tested their device using polymer beads; afterwards, another group of Kobel, Valero, Latt, Renaud, and Lutolf (2010) came up with the idea of optimizing Tan and Takeuchi's device in order to capture single cells. Consequently, they did some modification to the previous device mainly on the traps. Kobel et al. (2010) changed the narrowed regions in the straight channel for smaller gaps, resulting in larger loop channels to still complying with the bypass trapping principle. By reducing the dimensions of the channel across the traps, the flow resistance of this path increases, and remember that in order to direct the particles into the trap the trap's cross flow resistance has to be lower than that of the loop or bypass channels. The resulting device shown in figure 2.8 has 64 parallel channels with 9 to 3 traps in series yielding a trap density, of more 700 to 175 *traps/cm*<sup>2</sup>. Finally, the group tested the device using non-adherent T-cells, a lymphoma cell line, achieving a trapping efficiency of nearly 100%.



**Fig. 2.8** Kobel et al. device features. (A) Diagram of the traps and channels, as well as, the flows. (B) A micrograph of a section of the cell-trapping device (Kobel et al., 2010, p.859).

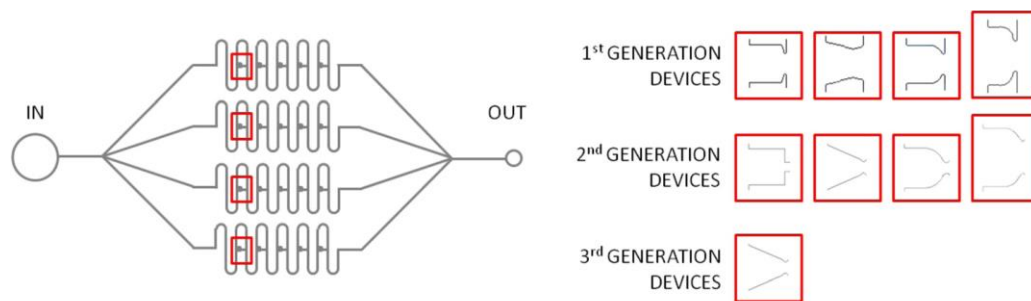
Unlike the ordinary trapping devices already presented, Frimat et al. (2011) introduced a new device, also inspired by Tan and Takeuchi's system but incorporating a novel cellular valving principle for single cell co-culture. Using the same trapping principle and material, PDMS, as the previous devices discussed above, Frimat et al. (2011) adapted Tan and Takeuchi's device by adding mirrored traps linked by the trap's cross channel, as it can be observed in figure 2.9. With such design, they were capable of not only capturing single cells but also capturing pairs of cells separated only by the inter traps aperture; still, the communication and contact between captured cells is possible. The final device fabricated possess 8 parallel lines of analysis each containing 25 trap pairs (200 in total), and the dimensions of the channels were defined by the size of cells to be used (Frimat et al., 2011). The system has two loading sequences. The first sequence is done exactly as Tan and Takeuchi did, where the trapping process is achieved using the bypass method, which obeys the principle of a flow going through the path of less resistance. Being all the traps on the "right side" filled, a new stream carrying new cells is induced in opposite direction to fill the "left side" traps. In the experiments feeding cells into the device, Frimat et al. (2011) observed a trap occupancy of 99% for trap diameters between 15 $\mu$ m to 37 $\mu$ m. However, when using the larger traps single cell occupancy decreased to 68.6%. Although the reason for this reduction was unknown, the authors assumed that it was due to the greater freedom of the cell within the trap, which might allow the cell to fall back into the main stream (p.235).



**Fig. 2.9** SEM (Scanning electron microscope) micrographs of the device showing the double trap feature. (A) Zoom focusing in a single pair of traps. (B) Six trap pair in series. (C) Entire trapping chip (Frimat et al., 2011, p.232).

Lawrenz et al., (2013) did an investigation on the bypass platform, with the objectives of optimizing, testing different trap shapes, and producing a device with larger trap density. Again the main structure of the devices fabricated was based on the Tan and Takeuchi's model. For the optimization part, numerical simulations were conducted in order to assess the hydrodynamic conditions, determine geometrical dimensions, and define the best velocity input flow. More importantly, they tested four different trap shapes (square, triangular, conical, and elliptical), all with the same dimensions in depth, across trap channel, and main channel. All the trap shapes were tested in order to determine the characteristics of channels flow and shear stress induced in the cell due to the geometric features of each trap. On this regard, the triangular shape turned out to be the most efficient on capturing single cells because of the flow entering the trap has a more focused stream line, while the others produce larger distortion of the flow passing through the trap (Lawrenz et al., 2013). In addition, it was also observed that bigger traps in relation to particle size, as well as larger trap exits (or across channel), increase

the probability of capturing multiple cells per trap in a 75% (Lawrenz et al., 2013). On the other hand, accordingly to Lawrenz et al. (2013) in order to induce the lowest shear stress on a captured cell, this has to be completely sheltered inside the trap. After three iterations as shown in figure 2.10, the group produced a high trap density and optimized device to trap single cells, of more 2 to 15 $\mu$ m. The final device composes a total of 1056 traps divided in 4 parallel microfluidic circuits, and its channel dimensions had to be scaled down to work with the smaller cells used, which demonstrates that a new device is required for each different size of cells.

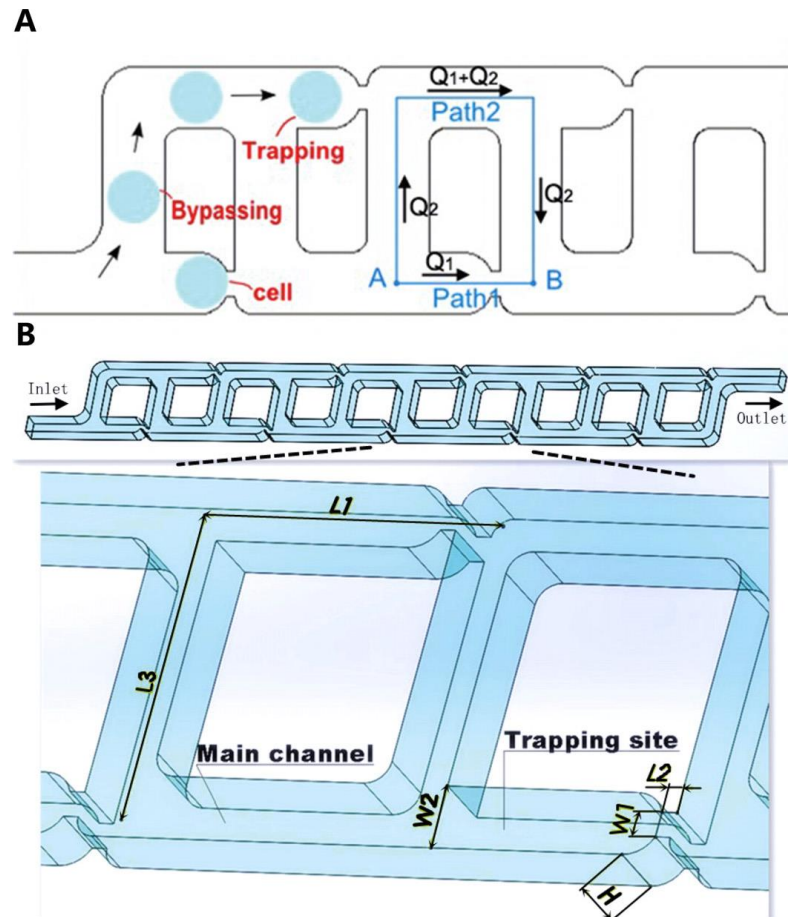


**Fig. 2.10** Schematic of the main trapping device, and trap configurations (squared, triangular, conical, and elliptical) used in three device generations (Lawrenz et al., 2013, p.8).

The results obtained on this investigation are very valuable, in particular those made on the trap shapes, because no other authors had tried another trap configuration. In fact, all of them had used the same cup shape for the traps developed by Tan and Takeuchi (2006).

To further improve the single cell trapping efficiency a more recent bypass chip was presented by Jin et al. (2015). They designed a PDMS device concatenating T-shaped channels with bypassing stream and trapping regions to reduce the area comprised by long loop channels, the amount of cells required to fill all the traps, and the filling time (Jin et al., 2015). The device presented in figure 2.11 also adopted the least flow path resistance principle to trapping cells. However, it is evident at sight that the loop channels have been reduced to a minimum.



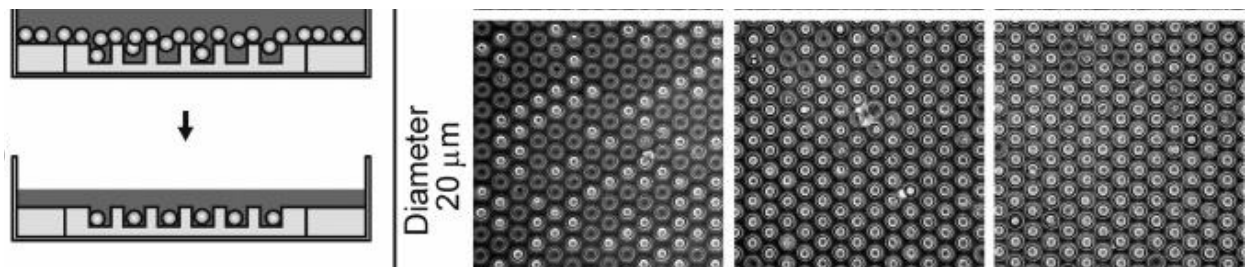


**Fig. 2.11** T junction device (A) Schematic diagram of the trapping principle showing both paths, trapping and bypassing. (B) Drawing of PDMS device (Jin et al., 2015, p.4).

Jin et al. (2015) also achieved an orderly trapping, where the queue of cells in the main channel were trapped consecutively without skipping a cell, thus saving cell samples. Nevertheless, when conducting experiments with 2 cell lines, they observed a reduction in trapping efficiency using HEK293T cells (average diameter of  $13\mu\text{m}$ ), which are smaller than HeLa cells (average diameter of  $15\mu\text{m}$ ). They concluded that the size variance of cells is the main factor which affects trapping efficiency because the channel dimensions are predetermined to house a specific cell size. As a result, large cells could clog the channels, and small cells might be captured in multiple form by the traps (Jin et al., 2015).

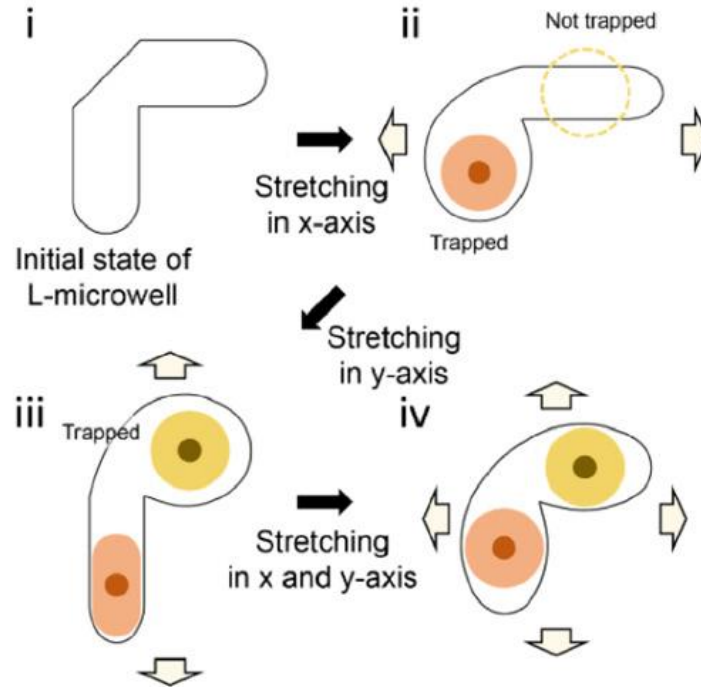
### iii. Microwell Arrays.

Another technology widely used to capture single particles is the microwell arrays. Many examples of applications and fabrication methods can be found in the literature (Rettig & Folch, 2005; Zheng et al., 2007; Charnley, Textor, Khademhosseini & Lutolf, 2009; Wood, Weingeist, Bhatia, & Engelward, 2010; Liu, Liu, Gao, Ding, & Lin, 2010; Lee, Rigante, Pisano, & Kuypers, 2010; Kim, Lee, & Park, 2013). Such a technology uses a simple system's structure and trapping principle. A microwell array is a chip composed of a substrate with an array of hundreds to thousands of micro cavities of a certain geometry. Thus, the main difference to hydrodynamic microfluidic devices is their lack of channels; in other words, microwell arrays are solely arrays of niches (traps) to hold cells using a gravity principle. In order to fill the wells, a high-density solution of cells is poured on top of the array, and the cells are randomly retained at the bottom of the wells by sedimentation (Fig. 2.12). After few minutes the excessive cell solution on top of the substrate is carefully rinsed off, leaving the cavities filled with single cells for further biological studies (Charnley et al., 2009). To optimally hold single cells, the microwells must be designed to only fit a single cell, and must be deep enough to protect the cell to be washed out in the rinse steps (Rettig et al., 2005; Wang et al., 2011). Therefore, microwell systems also are particle-size sensible; i.e., the microwells have to be designed and fabricated considering the size of the particles to be used in the experiments.



**Fig. 2.12** Suspended cells being trapped individually in microwells (Rettig et al., 2005, p.5629).

Regardless of their advantageous structure and principle simplicity, microwell array devices are limited to static analysis or screening. They are not suited platforms for active manipulation such as medium change, staining, and exposure of cells to certain substances for drugs studies because such processes would sweep the trapped cells out of the microwells. As a consequence, to address this issue, Wang et al. (2011) proposed a device capable of holding the cells within the microcavities by using the large deformability of PDMS. They fabricated a microwell device that can be mechanically stretched to increase the size of the niches. Therefore, when stretching the device, cells can fit widely in the microwells, and then by releasing the applied force, the cells remain secured inside the microwells due to the pressure produced by the recovered walls. As a result, further analysis as the ones previously mentioned involving rinsing methods are possible on this chip. In addition, more recently an enhanced microwell array device for cell-to-cell interaction was presented by Lee et al. (2015). Such a device presents an array of L-shape microwells on a PDMS substrate. In order to load a pair of cells, Lee et al. (2015) followed the stretching approach of Wang et al. (2011). First, they stretch the device in x-direction to increase one branch of the L-shape and to fit a single cell. Second, after loading the first cell the device is returned to its original form and stretched again but orthogonally (y-direction) to increase the size of the another L-branch; the process is depicted in figure 2.13. Once the cell loading is done, the cells can interact to each other with the advantage that all the possible interactions can be observed at specific and controlled locations (Lee et al., 2015). These last two devices are very interesting in particular for this research because they prove that the microfluidic technology can be enhanced by incorporating external methods to make the static devices more flexible and perform more complex processes.

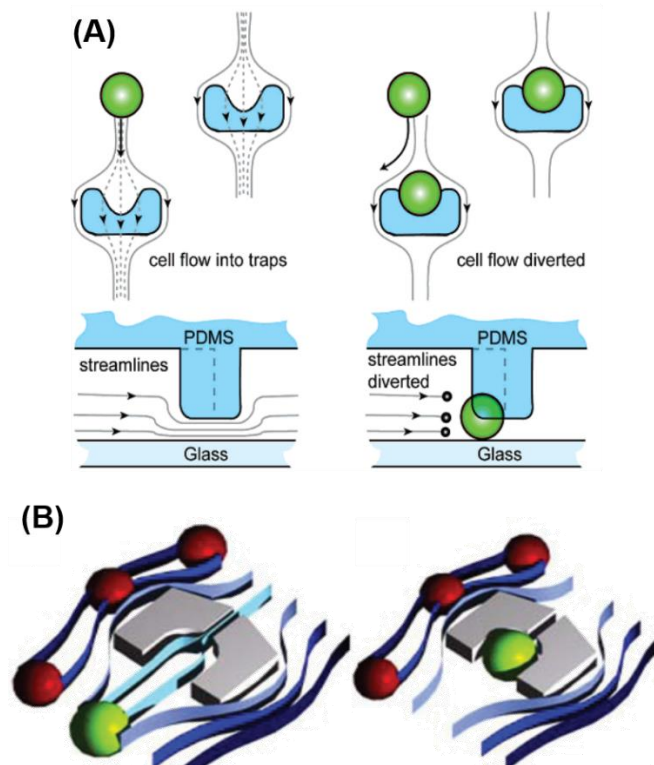


**Fig. 2.13** Trapping process for a pair of cells. (i) Device at the slack position, none strain applied. (ii) Device stretched on the x direction to increase the size of the vertical L-branch and capture a single cell. (iii) Change the stretching direction to y-axis to increase the size of the horizontal L-branch and capture a second single cell. (iv) Stretching on both direction, x and y axes, to allow cell interaction between the two trapped cells. (Lee et al., 2015, p.2).

#### *iv. Trap Arrays.*

Almost parallel to the bypass device presented by Tan and Takeuchi (2006), another technology for large batches of single cells analysis was produced by Di Carlo, Aghdam, and Lee (2006). Although both technologies use hydrodynamic principles to capture single particles, their structure are very different. Trap array devices, like the one here presented by Di Carlo et al. (2006) composes a thin sheet of elastomer PDMS bonded to another thin sheet of glass, the PDMS layer has an array of microstructures protruded on the surface to physically capture cells, and each microstructure has a dam-like cup-shaped geometry with a 2  $\mu\text{m}$  gap between the trap and the glass sheet. The device accomplishes its goal of trapping cells by combining two

principles, which are collisions of cells with physical barriers and “paths of least flow resistance”. The first principle is based on the probability that cells suspended in a fluid will crash against the traps and therefore they will remain in the traps while the main fluid flows across the rear aperture or dam opening of the trap (Lawrenz et al., 2012). The second principle is based on the different resistance of two flow paths, the same principle used by the bypass devices. When a flow is induced into the device the flow will take the path with the least flow resistance. Thus, if one of the paths goes through the trap, the flow will go through it unless that path is blocked. In a case where the path is blocked by a cell, the flow resistance of that path will be higher than any alternative flow path thereby making the main flow to take another path with less resistance (Di Carlo et al., 2006; Lawrenz et al., 2012; Zhu et al., 2013). Figure 2.14 represent visually these two trapping principles.

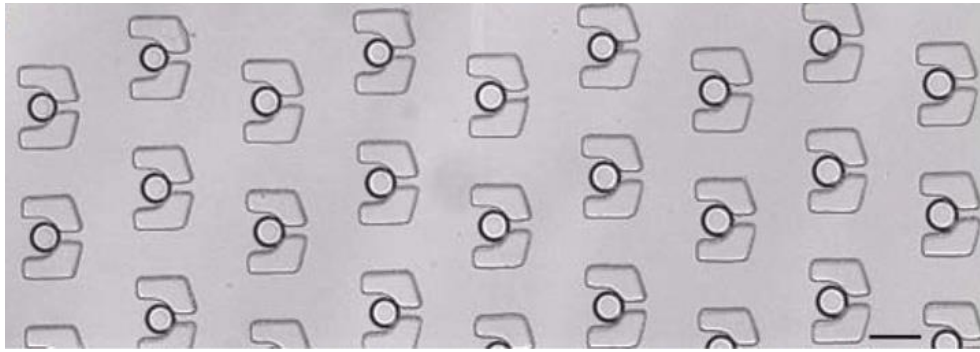


**Fig. 2.14** Trapping mechanisms of microfluidics trap array devices. (A) Diagram taken from Di Carlo et al. (2006) which shows how the cells are trapped in an empty microstructure

and diverted when the microstructure is already filled (p.4928). (B) Schematic flow retrieved from Huebner et al. (2009) which depicts the stream lines when cells approach the traps (p.694).

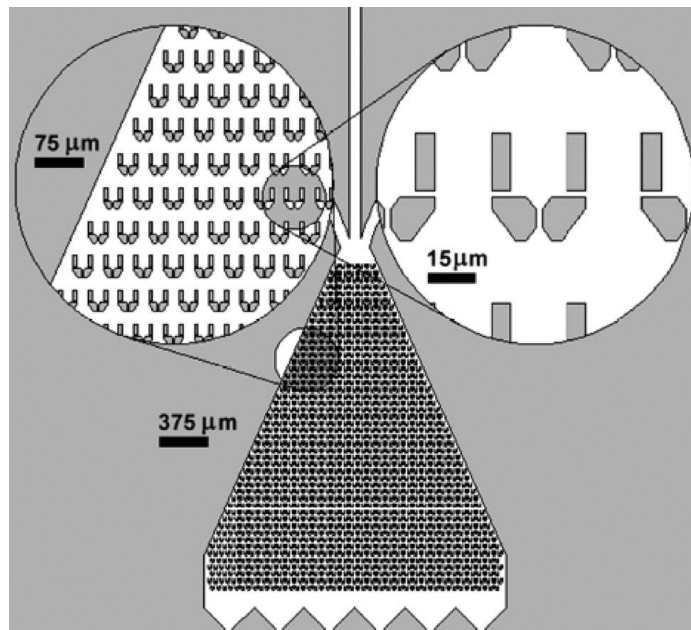
Similarly, to what happened with Tan and Takeuchi's device, plus the promising capabilities of this trapping method for cell assays shown by Di Carlo et al., many systems clearly inspired from such devices were later reported. For instance, the same group of Wu, Di Carlo, and Lee (2007), made another device to capture multiple cancer cells on each trap allowing the formation of tumor spheroids for anticancer drug discovery. Therefore, they had to increase the size of the microstructures in order to fit about 10 MCF-7 cells per trap. The group also concluded that the dimensions of the traps are directly related to the size of the cells targeted, so for different cell types with different sizes, the optimum trap size should vary in relation of the cell size (Di Carlo et al., 2006).

Huebner et al. (2009) reported a device for droplet trapping using the same approach reported by Di Carlo et al. (2006); however, instead of capturing single cells, they trapped single water-in-oil microspheres. In contrast to Di Carlo et al. (2006), they designed a different trap microstructure, as it can be seen in figure 2.15. Instead of having a one-piece structure they created a trap with two mirrored structures separated by a small gap, which serves as a cross flow channel to attract the microspheres into the trap. To retrieve the microspheres, Huebner et al. (2009) simply reversed the flow, and observed that a 110° angle on the rear of the trap allow a smoother flow of the freed microspheres throughout the array. Their final device composes four arrays, each one with 96 traps, and it was designed to capture 50 μm microspheres.



**Fig. 2.15** Array of single water-in-oil microspheres (Huebner et al., 2009, p.694).

Similar to the device presented by Wu et al. (2007) for the investigation of new drugs for cancer treatment, another study but focused on the response of single cells to anticancer drugs was reported by Wlodkovic et al., (2009). Aiming to address the limitations of conventional methods for cell analyses, such as flow cytometry or microplate imaging, they proposed a new platform with an array of traps to capture single cells. Again, based on the already discussed trapping principle and structure. Their device differs from the others only on the arrangement of the traps and the microstructures employed as traps. Such differences can be observed on the figure 2.16.

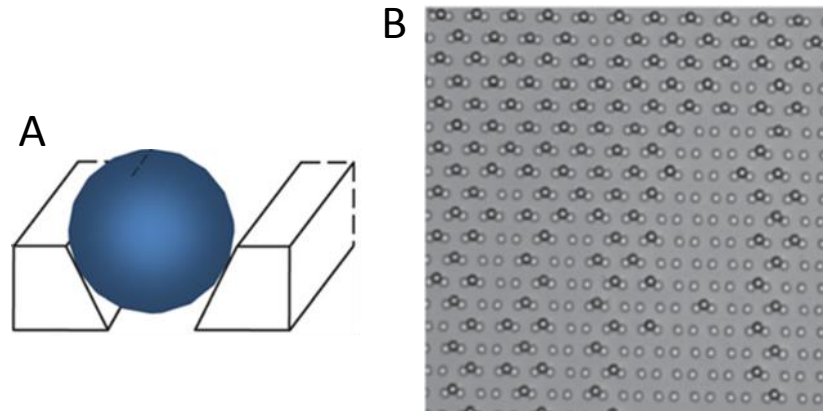


**Fig. 2.16** Array of traps uniformly distributed on a triangular surface. Traps are shaped by four no-joined microstructures with a middle rear gap, which allow the pass of flow through the trap to direct cells into it (Wlodkowic et al., 2009, p.5518).

It is important to mention that the trapping efficiencies (10% to 20%) reported for the above device (Wlodkowic et al., 2009, p.5519) are very low in comparison to those obtained by Di Carlo et al. (2006) of 50% to 70% (Di Carlo et al., 2006, p.1447). However, the authors did not provide any comment on the reason for such a drop on trapping efficiency.

In order to provide robustness to the trap array technology, Xu et al. (2013) proposed a work to optimize microfluidic microspheres-trap arrays. The optimization is focused on the geometric parameters to improve packing density, trapping efficiency of single particles, particle retrieving and avoid channel clogging. In order to present an optimized device, the group proposed a function with several constraints such as, compliance with the trapping principle of the least path resistance, size of traps to fit no more than one microsphere and retain it from being swept by the main flow, inter-trap space large enough to avoid clogging, and fabrication feasibility. In order to solve the equation to optimize, Xu et al. (2013) used the interior-point optimization algorithm and considered a microsphere with a radius of  $5\mu\text{m}$  (Xu et al., 2013, p.7). Therefore, the problem solved or the device optimized is a single device that can only work with particles of a fixed size of  $5\mu\text{m}$ . Regardless of this fact, their final results are very impressive achieving a considerable improvement in comparison to previous systems presented. Their final optimized device resulted in a trap density of  $1438\text{ traps}/\text{mm}^2$ , a single-particle trapping efficiency of 99%, while multiple trapping and clogged channels were 0.38% and 0% respectively. In addition, it is worth to mention that the trap shape used by Xu et al., depicted on figure 2.17, is not a U or cup shape used on previous trapping platforms, but a triangular shape as recommended by Lawrenz et al. (2012) in the previous section.





**Fig. 2.17** (A) Triangular trap composed of two inverted trapezoids to capture single microspheres. (B) Picture of the optimized device during a trapping experiment to show the high density array of traps capturing single microspheres (Xu et al., 2013, p.5).

Several particle-trapping platforms have been reviewed and classified under the FCBPSS framework. On the previous classification some remarks were observed. First, all the reviewed devices share the same function, which is to capture single particles. Second, they perform their function under two main contexts, microspheres and cells. It has also been observed that all the devices could work with either input source by changing some preconditions like the carrier fluid. Third, there are three main structures found among the literature: comb arrays, bypass channels, and trap arrays. In addition, microwell arrays were also reviewed. While all the devices behave in the same manner, not all of them employ the same trapping principle. For instance, the comb structure uses the “least flow path resistance” to divert the particles flowing on the main stream into the traps. Bypass channel devices solely rely on this principle (least flow path resistance) and must comply with it in order to capture particles. Trap array platforms combines two principles, the “least flow path resistance” and the probability of particles encountering a trap. In this last type of devices, the particles are not fed in a queue fashion as on the bypass channel devices, so the random interaction among particles play an important role besides the hydrodynamic principle to achieve their function.

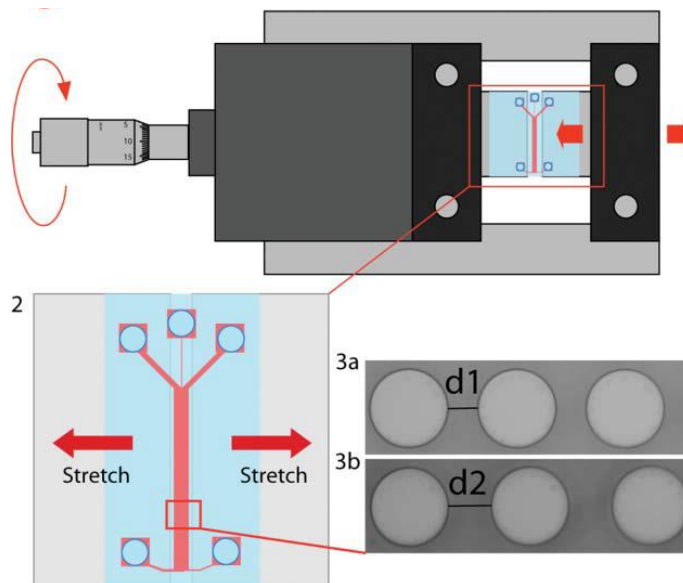
Regarding the performance of the different structures analysed, at first sight it seems that the bypass devices have a higher trapping efficiency. However, Xu et al. (2013) achieved an equally comparable trapping efficiency of 99% with their optimized array of triangular traps device. Furthermore, trap arrays platforms have the advantage over other structures of allowing higher trap densities. Also, although many issues have been solved and optimizations have been attempted during the evolution of the hydrodynamic particle-trapping technology, a common issue to all the platforms is still not addressed. On all the devices reviewed it was noticed a restriction on the particle size than can be used, so all the devices are particle-size sensible. As a consequence, if different size particles want to be captured or analysed using such devices, a whole new device has to be designed and fabricated. In the next section, few attempts to address this lack of flexibility on targeting particles of a wide range of sizes are presented.

## **2.4 Adaptable Devices**

On the contrary of the many investigations conducted and already reviewed in order to achieve an optimized and more efficient cell-trapping device, there are very few works focused on enhancing such devices by making them more flexible or universal. Which should be a very important line of research since regardless of the microfluidic chip's application all of them lack of the ability of processing particle with multiple sizes.

In the literature one can find that Huh et al. (2007) proposed a method using very small forces in order to actively control and modulate the cross-section of nanochannels to adjust the transport characteristics of their device. They observed the need of a device capable of dynamically adjusting its geometry according to the manipulation needs of different molecules and nanoparticles. In order to achieve such a device, they use PDMS for the fabrication of an array of nanochannels that can change their cross-section size by applying a compression force perpendicularly to the nanochannels. Thus, by adjusting the applied compressive force the nanochannels reduce their size allowing only the passage of the desired sizes of molecules.

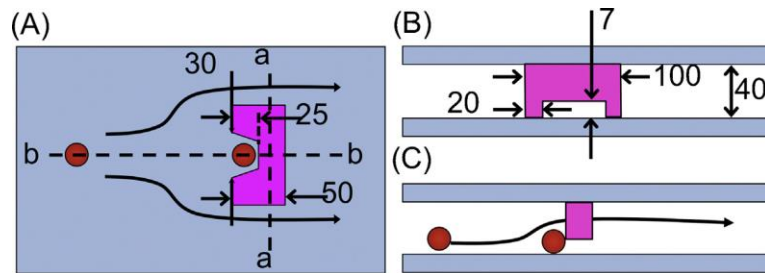
Another example of a tunable device is the device achieved by Beech et al. (2008), a device for particle separation in Deterministic Lateral Displacement (DLD). The microfluidic chip composes an array of micropillars which allow the device to accomplish its objective of sorting particles. Moreover, by mounting the device onto a chuck, a mechanical and controlled lateral strain can be applied to it resulting on an increase of the distance between micropillars. The device is enough elastic to stand an extension of 50% its original size. Thus, by stretching the device it was provided with more versatility since more particles were able to be sorted using a single chip. The device just described is depicted on figure 2.18 below.



**Fig. 2.18** Tunable particle-sorting device (Beech, 2008).

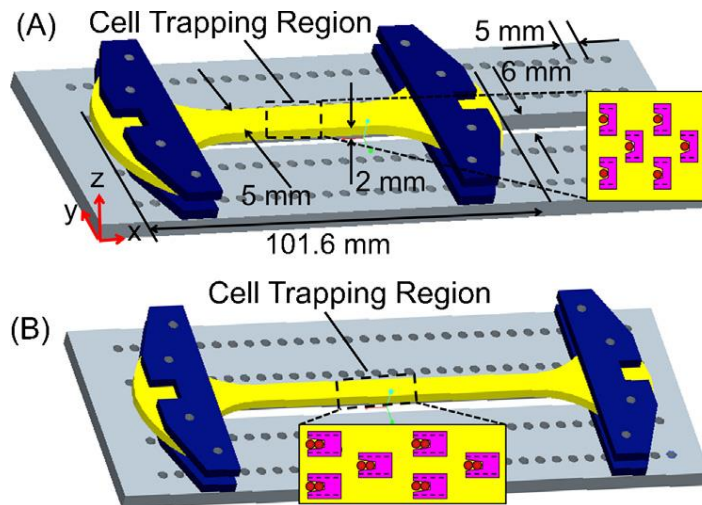
Unlike the ordinary cell trapping devices, Zhu et al. (2013) presented a tunable microfluidic device manufactured on PDMS that can be mechanically modulated to tune the characteristics of cell-trapping to capture a predetermined number of cells from single cells to multiple cells. The mechanical modulation is achieved by inducing a uniformly distributed strain through the application of an external force on the chip to modify its geometry. Zhu et al., (2013) tunable cell trapping microchip composes two thin sheets of elastomer PDMS, the bottom one has an array

of microstructures protruded on the surface to physically capture cells, and each microstructure has a dam-like, cup-shaped geometry with supporting pillars on both sides (Fig. 2.19).



**Fig. 2.19** The cell trapping principle. (A) Plan view and cross-sectional views along lines (B) a-a and (C) b-b of cell trapping approach. Dimensions are given in micrometers (Zhu et al., 2013, p.2).

The microstructures geometry can be tuned via the application of strain to the chip and this is achieved through stretching the device by mounting it onto a motherboard shown in figure 2.20. The motherboard has different mounting pin locations which allow the variation of the strain applied on the device. As a result of this mechanical modulation the geometry of the microstructures is changed as well as the main flow channel. This process allows the device to vary its function from trapping one single cell per trap to capturing more than one cell per trap; however, the target cells for both cases are always of a determined size (Zhu et al., 2013). It is important to notice that the capability of tuning is due to the mechanical properties of the manufacturing material.



**Fig. 2.20** Schematic diagram of the tunable principle via modification of trap dimensions.

(A) Original position (none strain applied) to capture single cells on each trap. (B) Strain is applied to capture multiple cells on each trap (Zhu et al., 2013, p.2).

With this device Zhu et al. (2013) not only addressed effectively the lack of flexibility of microfluidic cell trapping devices on controlling the number of cells captured, but also they demonstrated the functionality of this mechanical tuning method, opening new possibilities to further adaptable microfluidic devices, in particular those based on hydrodynamic trapping principles.

The mechanical tuning method above presented is a simple offline method that is passively and feedforward controlled. The method is considered offline because the tuning or modification of the channel features is done before or after the process but not while the device is performing its function; otherwise, it will be an online method. In addition, although to produce such deformation an external force is required, the system that controls the modification on the device is a material property, and in fact it is the elasticity property. Therefore, the control of the method is passive since there is no need of an external intervention or system other than the material property to control the deformation (strain) resulted from the applied force. Finally, the control is also feedforward because there is not a feedback in the device that can account for

discrepancies and correct the input force. The force is induced and held previous to the feeding of particles into the device. If the device is not working properly under the pre-set strain, then the force has to be readjusted and the whole process has to be restarted.

Examples of other tunable techniques are (i) electrical-adaptive method (EAM) which utilize dielectric polymers in order to produce a deformation when applying an electric charge (Murray et al., 2013), (ii) Pneumatic actuation has been used in cell-trapping devices to control the size of microstructures (Liu et al., 2012), and (iii) piezoelectric actuation in which piezoelectric actuators are used to apply an external stimulus to modify a microfluidic device (Graf & Bowser, 2008). The mayor drawbacks of all the three techniques are more complicated fabrication methods, either electrical or pneumatic extra connections, need of additional equipment other than purely microfluidics means, and more difficult devices to operate. Therefore, a simple mechanical stretching approach as presented by Zhu et al. (2013) and Beech et al. (2008), seems to be more suitable for a new cell-trapping device capable of processing more than a single cell size.

## **2.5 Concluding remarks**

The review of the literature has shown that there are several microfluidic devices dedicated to trap single particles. Upon a classification of hydrodynamic particle-trapping devices under the FCBPSS framework a thorough understanding of the function, behaviour, and principle of such technology was achieved. Also the literature has shown that in contrast to the many studies and efforts conducted to produce an optimal single cell-trapping device, very little has been published on adaptable devices to address the lack of flexibility of such devices. Moreover, no research (to my knowledge) has been conducted on designing and fabricating a hydrodynamic single cell-trapping device capable of handling a large number of different cell sizes. From the knowledge gained after the literature review, the following conclusion for a new device is forwarded. The geometry and dimensions of the traps play the main role on the

function and performance of a microfluidic cell trapping device. Since the traps catch cells from a carrying fluid, their dimensions determine not only the number, but also the size of cell captured. Therefore, if a flexible device capable of targeting a wide range of sizes of cells is intended, it must be able to modify somehow its trap dimensions without interfering with its trapping function. While there are various active methods to achieve such modification in the traps, a mechanical force is the most suitable for this application as it is simpler and more austere than using other more complex systems. Thus, details on the design, fabrication, and test results of a new tunable single cell-trapping device capable of capturing large batches of single-cells of various diameters (not a fixed size) after being tuned will be presented in Chapters 3, 4 and 5.

## CHAPTER 3: CONCEPTUAL DESIGN

### 3.1 Introduction

To achieve the objectives of this research, the design, fabrication, and testing of a new microfluidic single cell-trapping device capable of tuning to target various cell sizes is conducted.

In Chapter 2 after a thorough analysis of several platforms based on hydrodynamic principles to isolate single particles, it has been concluded that the most suitable structure to demonstrate the concept proposed in this thesis is the array of traps, and the best tuning method would be a mechanical stretching to generate a uniform distributed strain on the device. Thus, in this chapter the conceptual design of the new device is presented. The design process is based on and guided by the Axiomatic Design Theory, which is briefly introduced. The function requirements and the design parameters that could comply with such requirements are firstly defined, followed by the determination of the actual material and parameters that would characterize the new device. Finally, a new device is presented.

### 3.2 Axiomatic design for a new cell-trapping chip

A design process begins with the establishment of function requirements (FRs) that represent a number of needs. The second step is the conception of a physical entity which will be characterized in terms of design parameters (DPs) that satisfy the FRs independently. The axiomatic design theory (ADT) was proposed by Nam P. Suh in 1990's; he states that in the design process there are two axioms that must be met for every good design. The two axioms are the independence axiom also called axiom one, and the information axiom also called axiom two (Suh, 1990). Axiom one states that the FRs must be independent of each other, so when a DP is modified this will affect only one FR. This axiom can be mathematically represented by:

$$[FR] = [A][DP] \quad (3.1)$$



where  $[FR]$  is the function requirement vector,  $[DP]$  is the design parameters vector, and  $[A]$  is the design matrix (Suh, 1990). This matrix representation allows one to evaluate the compliment of the axiom one in any design. One may face three different kinds of design on this context; they are uncoupled design, coupled design, and decoupled design. Uncoupled design refers to a design that has an independent relationship between FRs and DPs; that is its matrix representation will be a matrix with all its non-diagonal elements equal to zero:

$$\begin{bmatrix} FR_1 \\ FR_2 \\ FR_3 \end{bmatrix} = \begin{bmatrix} A_{11} & 0 & 0 \\ 0 & A_{22} & 0 \\ 0 & 0 & A_{33} \end{bmatrix} \begin{bmatrix} DP_1 \\ DP_2 \\ DP_3 \end{bmatrix} \quad (3.2)$$

Coupled design is the opposite of an uncoupled design. This means that if a DP is modified all the FRs will be affected. Then, this design will not comply with axiom one. Its matrix representation will be a design matrix with no element equal to zero:

$$\begin{bmatrix} FR_1 \\ FR_2 \\ FR_3 \end{bmatrix} = \begin{bmatrix} A_{11} & A_{12} & A_{13} \\ A_{21} & A_{22} & A_{23} \\ A_{31} & A_{32} & A_{33} \end{bmatrix} \begin{bmatrix} DP_1 \\ DP_2 \\ DP_3 \end{bmatrix} \quad (3.3)$$

Finally, a decoupled design is a design where the FRs and DPs relationship is not completely independent. This means that there may be some DPs which are related to more than one FR. However, this design is still being considered as a good design when a proper order to set the value of DPs is achieved. The matrix representation of this design is a triangular design matrix (Suh, 1990, p. 55):

$$\begin{bmatrix} FR_1 \\ FR_2 \\ FR_3 \end{bmatrix} = \begin{bmatrix} A_{11} & 0 & 0 \\ A_{21} & A_{22} & 0 \\ A_{31} & A_{32} & A_{33} \end{bmatrix} \begin{bmatrix} DP_1 \\ DP_2 \\ DP_3 \end{bmatrix} \quad (3.4)$$

Therefore, in order to propose a new device that can comply with the objective of capturing large batches of single-cells and after being tuned perform the same trapping task but with cells of larger sizes, it is necessary, as the ADT states, to define the FRs of such a device. The FRs for the new device can be obtained from the systematic design analysis that has earlier been executed when determining the behaviour of cell-trappers (Section 2.3.3). Thus, the general function requirements (FRs) of the new device include:

- **FR<sub>1</sub>**: The device must capture large batches of single-cells;
- **FR<sub>2</sub>**: Each device's trapper must capture a single cell; and
- **FR<sub>3</sub>**: The trappers must be capable of adapting its size to capture cells of various diameters.

In addition to the FRs, one must recognize if the design has any constraints. In ADT, constraints are “the bounds on an acceptable solution” (Suh, 1990), and they are divided into two kinds, input and system. Input constraints are found in the design specifications while the system constraints are imposed by environment within which the design solution must operate (Suh, 1990). In the case of this device, the model is not exempted of constraints. In particular, the model presents input constraints imposed mainly by the working material; which are the carrier fluids and the cells. Therefore, it is important to explore these constraints deeper by analyzing the characteristics of cells that may be influenced by the design. In general, cells vary on sizes and shapes. Therefore, the size of the cell will represent a constraint since many dimensions of the pursued device will depend directly on the cell's diameter. Moreover, the cells are very delicate and sensitive to external stimuli, which may cause changes on their natural behaviour or even the death of the cell. Thus, as reported by Lawrenz et al. (2013) on in-vitro experiments, where cells are exposed to artificial flows such as those used in microfluidics, the mechanical forces applied to cells by fluids are an important aspect to consider. For instance, it has been determined that a shear stress up to 4.5 Pa interferes with the common cell death and may affect the endothelial cell integrity (Dimmeler et al., 1996). Also, Griffith and Swartz reported that vascular endothelial cells experience a physiological shear stress of ~ 1 Pa (as cited in Di Carlo et al, 2006, p. 1447). Thereby, these shear stress values could represent the maximum shear stress that can be exerted to the cells when captured into the new device. Hence, it can be said that another constraint is to ensure shear stress lower than 4.5 Pa applied to the cells. Finally, the last input constraint can be stated as the non-chemical alteration on the carrier fluid properties, which represents the cell's environment within the chip.

Once the FRs and the constraints for the design have been determined, it is time to derive the design parameters (DPs) in the physical domain in order to satisfy the FRs and the constraints resulted from the previous discussion. At this point it would be important to recall that one is looking for DPs that can achieve the one-to-one correspondence between DPs and FRs in order to comply with the definition of an uncouple design stated by the axiomatic design theory. Thus, the respective DPs that can fulfill independently each FRs are as follows:

- **DP<sub>1</sub>**: Arrays comprised of a large number of single-cell trappers;
- **DP<sub>2</sub>**: Traps capable of corralling and isolating only one cell from a large group of cells suspended in a fluid; and
- **DP<sub>3</sub>**: Large and uniform deformability of the traps.

Mapping the FRs to the DPs is as follows:

$$\begin{array}{lll}
 \mathbf{FR}_1: \text{Capture cells} & \longleftarrow & \mathbf{DP}_1: \text{Array of traps} \\
 \mathbf{FR}_2: \text{One cell per trap} & \longleftarrow & \mathbf{DP}_2: \text{Trap for a single cell} \\
 \mathbf{FR}_3: \text{Increase trap's size} & \longleftarrow & \mathbf{DP}_3: \text{Large deformability}
 \end{array}$$

One can observe that DPs introduced satisfy independently each FR. This means that if  $DP_1$  is varied, this will solely affect  $FR_1$ , and it is the same for  $DP_2 - FR_2$  and  $DP_3 - FR_3$ . For example, if the arrangement or the number of traps specified in the array ( $DP_1$ ) is modified it will only affect the number of total single-cells captured ( $FR_1$ ), but not the other FRs. Using a matrix representation of FRs and DPs one can observe that the design solution proposed complies with axiom one, and it is an uncoupled design:

$$\begin{bmatrix} FR_1 \\ FR_2 \\ FR_3 \end{bmatrix} = \begin{bmatrix} A_{11} & 0 & 0 \\ 0 & A_{22} & 0 \\ 0 & 0 & A_{33} \end{bmatrix} \begin{bmatrix} DP_1 \\ DP_2 \\ DP_3 \end{bmatrix} \quad (3.5)$$

### **3.3 Proposed conceptual design of the adaptable microfluidic single-cell trapping device.**

Having determined the DPs for the new device, now it is possible to proceed to the embodiment of a physical entity characterized by the above DPs. The conceptualization along with the decision making process that resulted in the final microfluidic chip is briefly discussed. First, a thorough exploration of the DPs is made in order to understand all the factors and possible constraints surrounding each of them. Next, a concrete object or method that complies with the DP in consideration is presented. Lastly, the geometry and dimensions of the object or method are shown. Note that although the DPs have been stated in a certain order in the previous discussion, in the following section this sequence will not be taken into account, and the DPs might change in order when explaining each one. This is done in order to understand better the conceptualization process. Also, remember that all the DPs are independent and they do not have any hierarchy relationship, so changing the order does not affect anything.

#### **3.3.1 Large and uniform deformability: DP3**

DP3 was proposed as “large and uniform deformability” of the traps. The deformability is determined by the material that will be used in the fabrication of such a device. However, a method is also required to produce such deformation. In particular, the method selected to tune the device or to increase the size of the traps is a mechanical stretching. Some researchers have reported a stretching approach to modify the function of a microfluidic device. For instance, Zhu et al. (2013) have shown that by modifying longitudinally the geometrical shape of the microstructures the number of cells captured per trap increases. In addition, Beech and Tegenfeldt (2008) have also used the elastomer’s high-elasticity property to create a tunable particle separation device, which is capable of increasing the gap between micro-pillars resulting in the sorting of different particle sizes. Other potential tunable techniques, which were

discussed earlier are: electrical-adaptive method (EAM), pneumatic actuation, and piezoelectric actuation. These later methods would result in a more complex device because they require a more complicated fabrication processes and additional components difficult to operate and control. Therefore, the application of a uniformly distributed strain on the device via a mechanical stretching seems to be a more suitable method to increase the trap size of the new pursued device. However, such a method is not exempted of issues to be concern about. For instance, all the traps within the device must experience the same strain in order to increase their size in the same proportion. Hence, the uniform distribution of the deformation along the device is a major concern in the design of the new device.

On the other hand, the material to fabricate the device should have very specific properties to comply not only with the device constraints, but also with the mechanical tuning method. As it was introduced before, Polydimethylsiloxane (PDMS) is a silicone-based polymer which is biologically compatible, optically transparent, suitable for microfabrication processes and it is one of the most used materials for the microfluidics application. However, nothing has been said about its mechanical properties. Two mechanical properties of great interest for this design are, the Young's modulus and the Poisson ratio. First, the Young's modulus or elastic modulus provides information of the stiffness of a material. In engineering materials, the Young's modulus ( $E$ ) is represented by Hooke's law as,

$$E = \frac{\sigma}{\varepsilon} \quad (3.6)$$

where,  $\sigma$  represent the stress and  $\varepsilon$  the strain. Stress ( $\sigma$ ) is force per unit area and strain ( $\varepsilon$ ) is length change per unit length, which is  $\varepsilon = (L - L_0)/L_0$ . Thus, the lower the value of the Young's modulus, the more elastic the material is, or conversely the higher the value of the Young's modulus, the stiffer the material is. For example, steel has a Young's modulus of about 210 GPa while the Young's modulus of aluminum is of about 70 GPa, and PDMS has a Young's

modulus of about 1.82 MPa. As a consequence, aluminum is easier to deform than steel and at the same time PDMS is much easier to deform than aluminum. Unfortunately, the value of the elastic modulus of PDMS depends on the mixing ratio of polymer base and curing agent, and the curing temperature. For instance, table 3.1 shows different values of PDMS Young's modulus resulting from varying the mixing ratio, and table 3.2 presents more values of PDMS Young's modulus, but in this case, they correspond to different curing temperatures.

**Table 3.1** Young's Modulus of PDMS with different mixing ratios of base and curing agent (Khanafer, Duprey, Schlicht, & Berguer 2009, p. 506).

Mixing ratio (base to curing agent)	Young's modulus (MPa)
6:1	1.35
7:1	1.9
8:1	2.05
9:1	2.2
10:1	2.1

**Table 3.2** Young's Modulus of PDMS determined when varying the curing temperature (Johnston, McCluskey, Tan, & Tracey, 2014, p. 5).

Temperature (°C)	Young's modulus (MPa)
25	1.32 ± 0.07
100	2.05 ± 0.12
125	2.46 ± 0.16
150	2.59 ± 0.08
200	2.97 ± 0.04

In this design a large deformation on the chip is desired, so the PDMS must have a low Young's modulus, and the desired deformation must be achieved within the elastic region. Thus, it must be ensured that the force induced on the device will not result in a stress greater than the yield strength limit. Second, the Poisson's ratio gives information on the lateral deformation of a

material. The Poisson's ratio ( $\nu$ ) is known as the negative coefficient of the lateral strain to the longitudinal strain. For example, the elongation of a sample under a tensile stress is usually accompanied by a contraction of its lateral dimensions, as exemplified in figure 3.1.



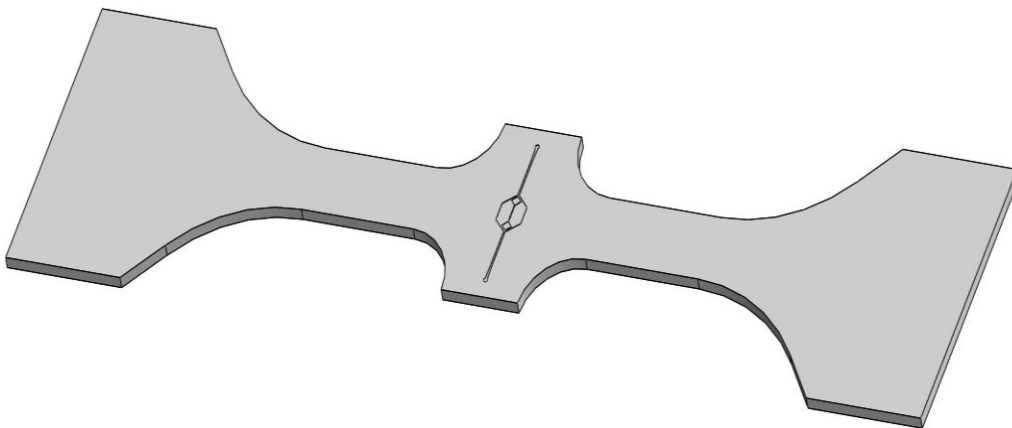
**Fig. 3.1** Schematic diagram of the lateral contraction effect of a material due to the application of a normal force, which is determined by the Poisson's ratio.

The Poisson ratio of PDMS is close to 0.5 meaning that the strain perpendicular to the direction of stress is half that in the parallel direction. For the new device, it is very important to consider such a lateral reduction predicted by the Poisson's ratio because when the device is stretched to a certain strain the lateral dimensions of the channels will be reduced considerably.

Besides the Young's modulus and Poisson's ratio of PDMS there are more parameters that have to be assumed in order to present an object that could be characterized by DP3. For instance, the actual deformation or strain that will result in the desired increased size of the traps has to be specified; in other words, a limit or maximum trap size increment must be defined. In this regard, to prove that the device is capable of adapting its trap's size to capture cells of larger diameters, a range of cell sizes, which goes from 20 microns to 30 microns, is proposed. Thus, the device must be able to capture cells of 20 microns without applying any strain to the chip, and cells of 30 microns when the maximum strain is exerted. Although the geometry of the traps has not been determined, it can be inferred that such traps will require a minimum opening size equal to the target cell's diameter. Hence, if one assumes that the opening space to the trap should be of about 25 microns and 35 microns to fit a cell of 20 microns and 30 microns respectively. Then the original size of the trap must be increased in 10 microns, which

represents a strain of 0.4. However, considering the actual dimensions of the traps, which are later on this section presented, the final strain determined was of 0.5. As a safety consideration for the design a maximum strain of 0.6 is finally established.

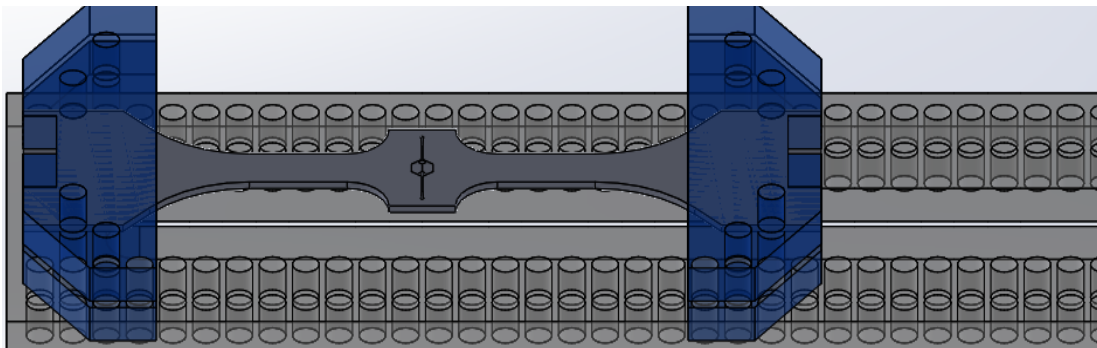
Figure 3.2 depicts the final design. In this isometric view of the microfluidic device, the height of the channels is shown. All the dimensions of the channels in particular the height of the device and the space between rows were carefully chosen considering the lateral reduction established by the Poisson's ratio of PDMS. For instance, the original height of the channels is of 43 microns (zero strain applied), which represents a large margin to fit cells of 20 microns (minimum cell size) in the device; however, when the chip is stretched up to the maximum strain permitted of 0.5, the height of the channels is expected to be reduced down to 34.4 microns, as calculated with a Poisson's ratio of 0.5. Even with such expected reduction in the dimensions of the channels, it will be possible for cells of 30 microns (maximum cell size) to freely flow through the device.



**Fig. 3.2** The final design of the microfluidic device (note that in Appendix A a complete drawing with the specific dimension of the design is provided).



In addition to DP3 (large and uniform deformability), an apparatus or equipment is required to apply a uniform stretching force on the PDMS device. Such stretching apparatus must be capable of (i) holding steadily and firmly the PDMS chip, (ii) standing the elastic force exerted by the PDMS device when stretched, (iii) producing a uniform displacement increment on the direction of the PDMS chip's stretching axis, and (iv) being easy to operate. As a consequence, a simple device inspired on the motherboard proposed by Zhu et al. is proposed for this work. Such stretching apparatus (Fig. 3.3) consist of a 30cm long and 5mm thick acrylic board, bearing many holes spread along the board every 5mm. The gap between the holes determines the displacement increment and position of the two clamps that hold the PDMS chip in position. Each clamp has two acrylic pieces that are screwed together to hold the PDMS chip like a sandwich. Once the PDMS device is held in between the clamps from both ends, the further outside screws on the clamps are secured to the main board at the desire position. To stretch the PDMS device, one clamp can be easily detached from the motherboard and moved to the next holes.

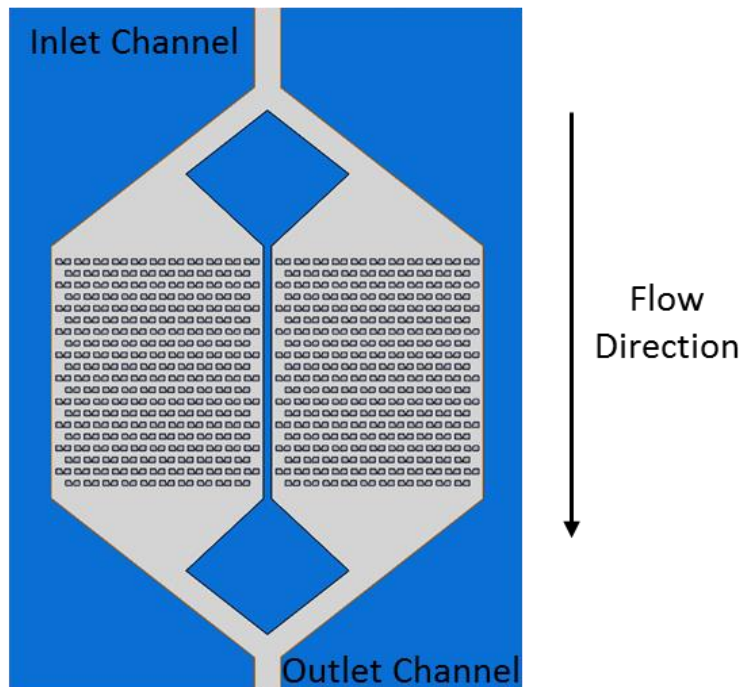


**Fig. 3.3** 3D drawing of the stretching apparatus. The apparatus comprises a long board (base) with holes spread out every 5mm and two clamps (on blue) to hold the microfluidic device (on dark gray). Detail dimensions are specified on Appendix A.

### 3.3.2 Trapping arrays: DP1

$DP_1$  was defined as “an array comprised of a large number of single-cell trappers”.

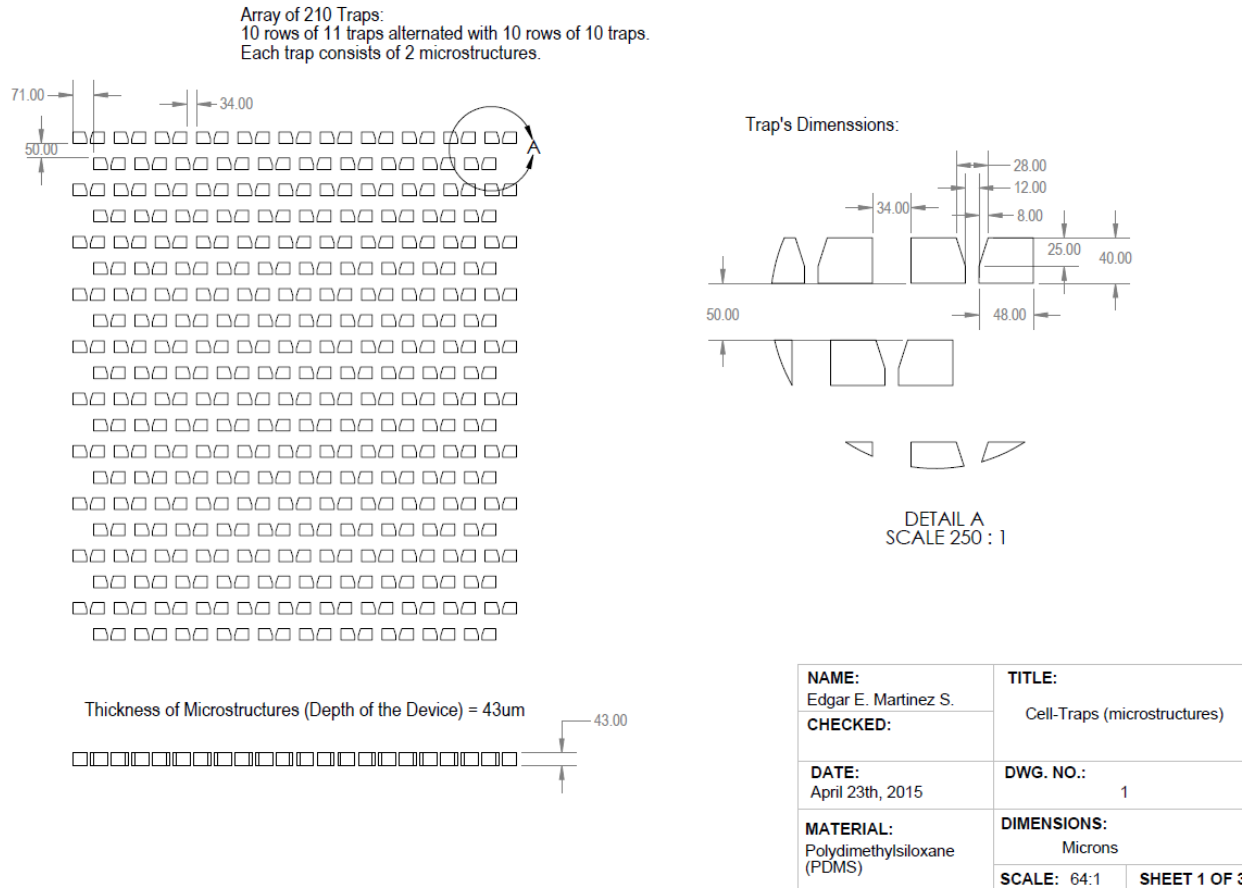
However, an array could have different amounts of traps and these could be distributed in a distinct manner at the same time. Also, regardless of the number and distribution of traps it is very important to consider the deformation that the chip will experience when a strain is induced. The distribution of the traps in this design has been inspired on previous microfluidic cell-trapping devices like those reported by Di Carlo et al., Zhu et al., and Xu et al. In the array each row of traps is offset horizontally from the previous row; thereby, there is an alternation of trap and “open gap” every other row along the channel (Fig 3.4). Following this approach, the capturing probability increases because if a cell is not captured in the first row of traps it might be trapped on the next row. This array distribution also requires the open gaps between neighbor traps and vertical spaces between rows to be large enough not only to ensure the free flow of cells, but also to avoid any possible clogging of the channels.



**Fig. 3.4** 3D drawing of the arrays of traps designed for the new single-cell trapping device.

In order to present a fully defined array it is necessary to define the number of traps to be used in the device. The number of traps was decided in a random manner, considering that the objective is just to demonstrate the functionality and the method proposed on this research. There are 210 traps distributed in two arrays, which are located in two separated channels. The channels are connected by a common inlet and a common outlet, as depicted in figure 3.4.

Finally, figure 3.5 shows some of the main dimensions of the actual new device, which fully define the proposed array to meet FR1. It is important to notice that the space between rows is larger than the gap between adjacent traps. This was done considering the deformation to which the microfluidic chip will be submitted. In fact, when the device is stretched normal to the travelling direction of the carrier fluid, the chip will present a size reduction on all the vertical features, as predicted by the Poisson ratio. A complete blue print where all the dimensions and geometries are specified for the new design is provided in **Appendix A**.



**Fig. 3.5** Design and dimensions of the array of traps defined for the new device. The final design encompasses two identical arrays.

### 3.3.3 Traps for a single cell: DP2

In order to fulfill FR2 a trapper capable of capturing only single-cells has been proposed as DP2. In general, a cell trap under the context of this work is a microstructure protruded onto the surface of the bottom layer that will immobilize a cell at a predetermined location. To fill the traps a liquid or carrier fluid loaded with cells flows through the channels. Once a cell encounters a microstructure it should be retained in the microstructure until the feeding of new cells into the device is finished. As it was previously stated, the geometrical characteristics of the trap and its dimensions determine not only the number of cells, but also the size of cell captured. Thus,

when designing a trap, the geometric shape of the trap and its dimensions must be carefully considered.

Many researchers have presented similar microfluidic cell-trapping devices, but with different trap shapes. For example, Di Carlo et al. (2006) reported a device with U-shaped PDMS structures as a trap for their device; while Xu et al. (2013) presented a microsphere-trapping device in which they utilized two trapezoidal grooves forming a triangular trap. Also, Zhu et al. (2013) designed a cell-trapping device with dam-like traps very similar to those presented by Di Carlo et al. (2006). With different geometrical options the most efficient geometry on capturing single cells should be selected for the new design. Therefore, a reliability assessment is conducted next considering different traps in order to determine the trap shape to be used. Similarly, Lawrenz et al. (2012) have studied the performance of different devices using four different trap configurations, which are square, triangular, conical, and elliptical. As the scope of this research is not the assessment of different traps, the following evaluation is conducted using data reported by others. The data collected is presented in table 3.3, which displays loading time, trap shape, total number of traps in the device, and number of microstructures that corral zero, one, and multiple cells. Also, the devices are sorted by author.

**Table 3.3** Number of traps that captured a single cell, no cells, and multiple cells.

Trap Shape	# of Traps	Single-cell	No cells	Multiple cells
<i>Lawrenz et al. (2012)</i>				
Triangular	400	124	272	4
Conical	400	44	344	12
Square	400	22	312	66
Elliptical	400	44	352	4
Triangular	1056	910	127	19
Conical	1056	474	540	42
Square	1056	229	824	3
Elliptical	1056	114	919	23
Triangular	1056	951	11	94
<i>Xu et al. (2013)</i>				
Triangular	1390	1380	5	5
Triangular	762	446	0	316
<i>Di Carlo et al. (2006)</i>				
Conical	199	107	44	48

<i>Zhu et al. (2013)</i>				
Conical	246	101	16	129

From table 3.3, the probability of the three possible outcomes: capture one, zero, or multiple cells are calculated for each device, see table 3.4.

**Table 3.4** Probability of trapping a single, zero, and multiple cells for each device.

Trap shape	P (single)	P(zero)	P(multiple)
<i>Lawrenz et al. (2012)</i>			
Triangular	0.31	0.68	0.01
Conical	0.11	0.86	0.03
Square	0.06	0.78	0.17
Elliptical	0.11	0.88	0.01
Triangular	0.86	0.12	0.02
Conical	0.45	0.51	0.04
Square	0.22	0.78	0.00
Elliptical	0.11	0.87	0.02
Triangular	0.90	0.01	0.09
<i>Xu et al. (2013)</i>			
Triangular	0.99	0.00	0.00
Triangular	0.59	0.00	0.41
<i>Di Carlo et al. (2006)</i>			
Conical	0.54	0.22	0.24
<i>Zhu et al. (2013)</i>			
Conical	0.41	0.07	0.52

In order to perform the reliability evaluation of the trap geometries a specific criterion must be defined. It has been said that function requirement of the traps is to capture a single cell; therefore, the criterion that the trap must achieve is to capture one cell, which is translated into the reliability context of this thesis. The success output of a trap in this thesis is to capture one cell, while no capturing any cell or capturing more than one are failure outputs. As such, for a single microstructure or trap one has:

$$R_{(Reliability)} = Probability\ of\ capturing\ one\ cell_{(success\ probability)} \quad (3.7)$$

$$Q_{(1-R)} = Probability\ of\ capturing\ multiple\ cells\ and\ zero\ cells_{(failure\ probability)} \quad (3.8)$$

To be able to compare the results, the reliability values are exposed in table 3.5, which displays the reliability (R) of each trap shape as well as the failure (Q). From this table one can observe that the reliability value coincides with the probability of capturing a single cell, which happens because capturing a single cell has been defined as the success output of the component. While Q is the sum of the two undesired outcomes.

**Table 3.5** Reliability (R) and failure (Q) for the different trap shapes.

Trap shape	R	Q
<i>Lawrenz et al. (2012)</i>		
Triangular	0.31	0.69
Conical	0.11	0.89
Square	0.06	0.95
Elliptical	0.11	0.89
Triangular	0.86	0.14
Conical	0.45	0.55
Square	0.22	0.78
Elliptical	0.11	0.89
Triangular	0.90	0.10
<i>Xu et al. (2013)</i>		
Triangular	0.99	0.01
Triangular	0.59	0.41
<i>Di Carlo et al. (2006)</i>		
Conical	0.54	0.46
<i>Zhu et al. (2013)</i>		
Conical	0.41	0.59

From the above analysis one can observe that the triangular shape is the most reliable one on capturing a single cell whilst the elliptical geometry presents the lowest reliability, as it is shown in table 3.5. It is important to highlight that the differences between the probabilities from devices with 400 traps and 1056 traps are not proportional because not only the trap number was increased, but also their dimension was modified. Regardless of these changes, the

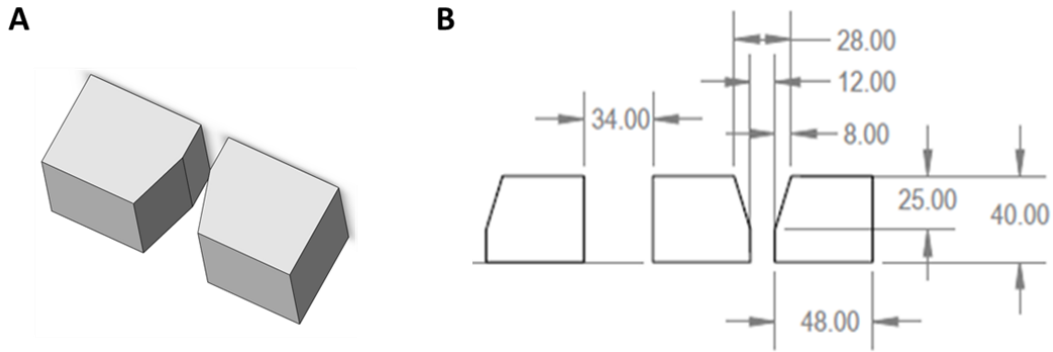
triangular shape still presents the highest probability on capturing single cells. This fact proves, as it was assumed previously, that although judicious dimensioning of the traps can improve the trapping probability, the trap geometry is also very important. In addition, in table 3.5 the data of three more microfluidic cell trapping devices are also included to support the behaviour observed in Lawrenz et al. (2012) devices. For instance, while Di Carlo et al. (2006) and Zhu et al. (2013) used a conical trap configuration, Xu et al. used a triangular shape obtaining a higher percent of traps filled with only one cell. Consequently, for the new design a triangular geometry for the traps will be chosen.

Figure 3.6 depicts the designed trap that fulfills FR2 and shows the corresponding dimensions to ensure the trapping of a single cell, in particular a cell of 20 microns. The trap consists of two trapezoidal microstructures separated by a small gap which are properly positioned to generate a triangular trap. The trap has an opening of 28 $\mu\text{m}$  which only allows the entrance of a single cell of 20 microns and avoids the possibility of two cells entering at the same time. The rear channel in the trap functions as the carrier fluid exits and its dimensions of 12 $\mu\text{m}$  prevents the captured cell to squish out of the trap. Lastly, in order to prevent the transient flow motion around the trap to sweep the cell out of the trap, the trapezoid has an angle of 35.5° which is much greater than the minimum angle of 5° recommended by Xu et al. (2013). Such angle is described by:

$$\alpha = 2 \tan^{-1} \left( \frac{0.5(u-b)}{l} \right) = 2 \tan^{-1} \left( \frac{0.5(28-12)}{25} \right) = 35.48^\circ \quad (3.9)$$

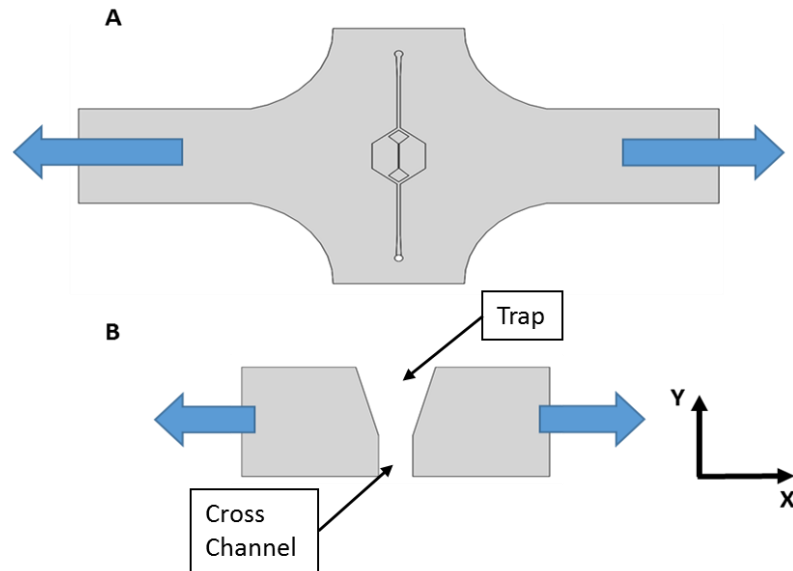
In addition, the trap has a depth of 25 $\mu\text{m}$  to completely fit a 20 $\mu\text{m}$  cell into the trap.





**Fig. 3.6** Trap designed for the new cell-trapping device. (A) 3D drawing of a single trap. (B) Dimensions of the trap.

As mentioned previously the device must be able to capture cells of 20 microns without applying any strain to the chip, and cells of 30 microns when the maximum strain is exerted. Although the dimensions presented above are those when the trap is not deformed due to the stretching force, the dimensions were defined taking into account the maximum possible strain, as follows. At the zero strain applied, the opening rear aperture of the trap measures  $12\mu\text{m}$ . Once a strain is induced the opening must increase its size up to a maximum of  $22\mu\text{m}$ , limited by the maximum strain permitted. Since the strain is applied uniformly along the device and perpendicular to the traps opening orientation, as shown in figure 3.7, all trap's dimensions will increase in the same proportion. Note that while all the lateral dimensions (X-axis) increase proportionally to the exerted strain the vertical dimensions (Y and Z axis) will present a reduction.



**Fig. 3.7** Direction of the strain applied to the device via a mechanical induced force to produce a size increment of the traps. (A) The diagram shows the whole device, and the blue arrows represent the direction of the tensile force to produce deformation. (B) Only depicts a single trap and the blue arrows represent the direction on which the deformation or size increment will be produced. Such size increment is experienced by all the traps in the arrays.

### 3.4 Summary

The conceptual design of the novel microfluidic single-cell trapping device was conducted following the Axiomatic Design Theory. The function requirements (FRs) of such a device were first defined. It was concluded based on a previous behaviour analysis (Section 2.3.3) that the function requirements were three, (i)  $FR_1$ : the device must capture large batches of single-cells; (ii)  $FR_2$ : each trap must capture a single cell; and (iii)  $FR_3$ : the traps must be capable of adapting its size to capture cells of various diameters. In addition, some constraints intrinsic to the design were revealed, such as the context on which the device must operate and the maximum shear stress that must not be exceeded to achieve cell viability.

In order to present a physical entity capable of meeting the function requirements, three design parameters (DPs) were proposed, (i)  $DP_1$ : array comprised of a large number of single-cell trappers; (ii)  $DP_2$ : trap capable of corralling and isolating only one cell from a large group of cells suspended in a fluid; and (iii)  $DP_3$ : large and uniform deformability of the traps. After mapping the FRs and DPs one to one, it was found that the design complies with axiom one (independence axiom), since any modification of a DPs would only have effects on its related function requirement.

Finally, the design was obtained considering the above DPs. As a result, PDMS was chosen as a final material due to its high elasticity property; two arrays of 210 triangular traps were proposed; and dimensions of the final microstructures and channels were defined. In contrast to the many devices previously discussed in the literature review (Chapter 2), the new device resulted from the design process has the capability of adaptation to various sizes of cells. Even though the tuning method and the stretching apparatus were inspired from those proposed by Zhu et al. (2013), the new device here presented differs in two specific aspects. First, the adaptation is made with the objective of increasing the size of the traps, so the traps could capture bigger cells in size, while Zhu et al. (2013) device adapts its traps to capture a larger number of cell but with a fixed size. Second, not only the function and objective of both devices are different, but also the traps. Zhu et al. (2013) used a dam like U-cup geometry similar to the one proposed by Di Carlo et al. (2006), while we designed a new triangular trap with a cross channel (Fig. 3.7).

## CHAPTER 4: MODELING AND OPTIMAL DESIGN

### 4.1 Introduction

Before proceeding to the fabrication, it is important, from the design point of view, to create a virtual model of the device in order to predict the mechanical and hydrodynamic performance of the device.

This chapter presents the simulation of the deformation using ANSYS Release 14.5 (ANSYS Inc., PA.) to show the deformation of the traps when the device is stretched, and to determine the maximum strain possible before plastic deformation.

The chapter also presents a second model using Fluent to simulate the flow profile developed within the micro-channels, and to determine numerically the maximum stress induced in a particle (living cell) when captured by a trap.

### 4.2 Mechanical Simulation

It was mentioned previously in Chapter 3 that the PDMS does not have a specific Young Modulus, and its value depends upon various factors such as, curing temperature, mixing ratio, and concentration. As a consequence of these variations, a finite element analysis (FEA) was proposed to determine the maximum stress that the device could experience when stretched up to the maximum desired length. The model of the device was developed on ANSYS, but only the middle section and the bottom layer, where microfluidic channels are, was considered for the analysis, as shown in figure 4.1. In the simulation, three conditions were considered, a fixed side, gravity, and applied force to produce the desired deformation. The fixed side represents the left side clamp of the stretching apparatus which is fixed in the motherboard. The applied force is exerted by displacing the right clamp of the stretching apparatus to any available hole. In the design section it was mentioned that a size increment of the trap's exit of 60% would be

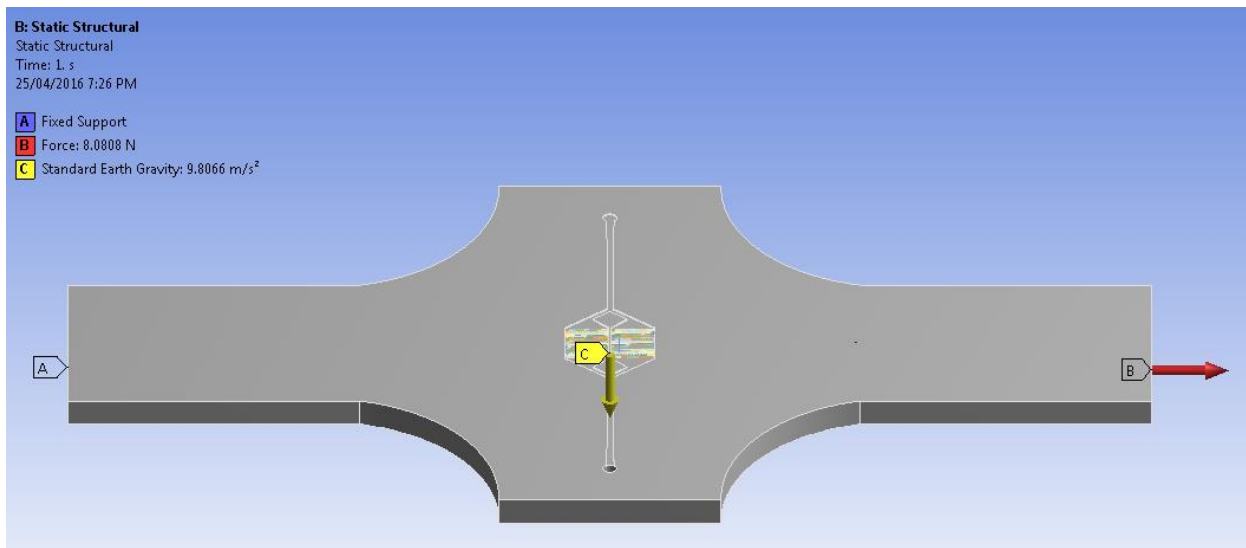
enough for the device function requirements, so the force required to produce such deformation was determined as follows considering a Young's Modulus of 1.82 MPa,

If the maximum strain desired is of 0.6, then from  $\varepsilon = \frac{\sigma}{E}$  one has that,

$$\sigma = \varepsilon E = (0.6)(1.82 [MPa]) = 1.092 [MPa] \quad (4.1)$$

Then the needed force to produce a strain of 0.6 on the PDMS is,

$$F = \sigma A = (1.92 [MPa])(7.4 [mm^2]) = 8.0808 [N] \quad (4.2)$$



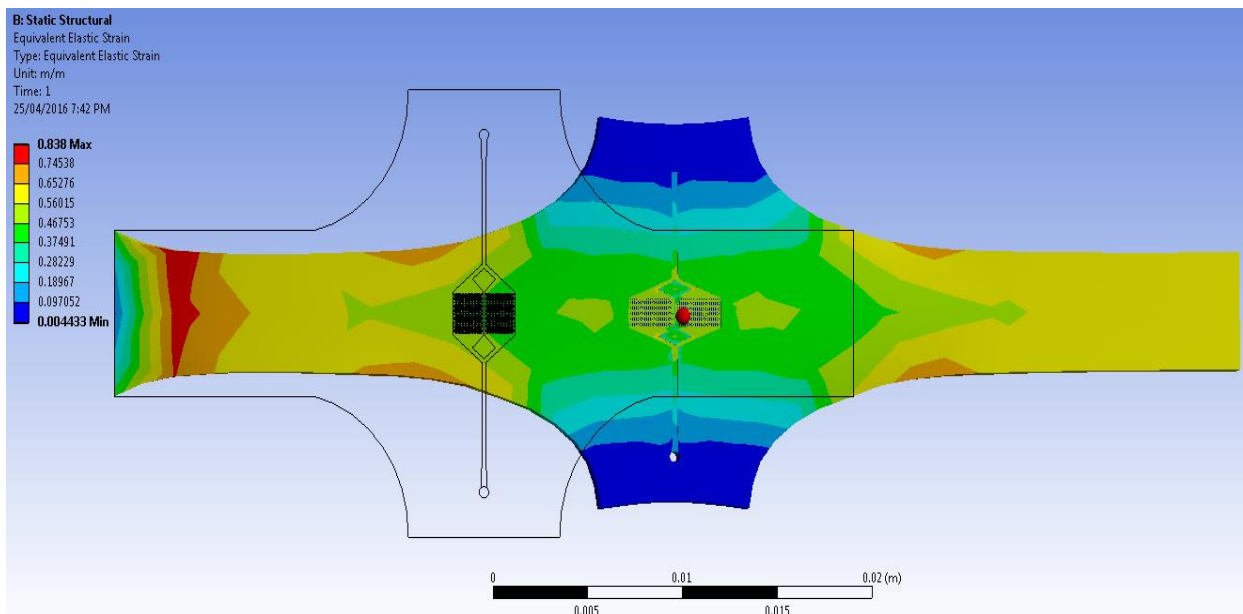
**Fig. 4.1** ANSYS model. In the image it can be seen the input conditions of the system to be solved by the simulation.

**Table 4.1** Material properties used for simulation.

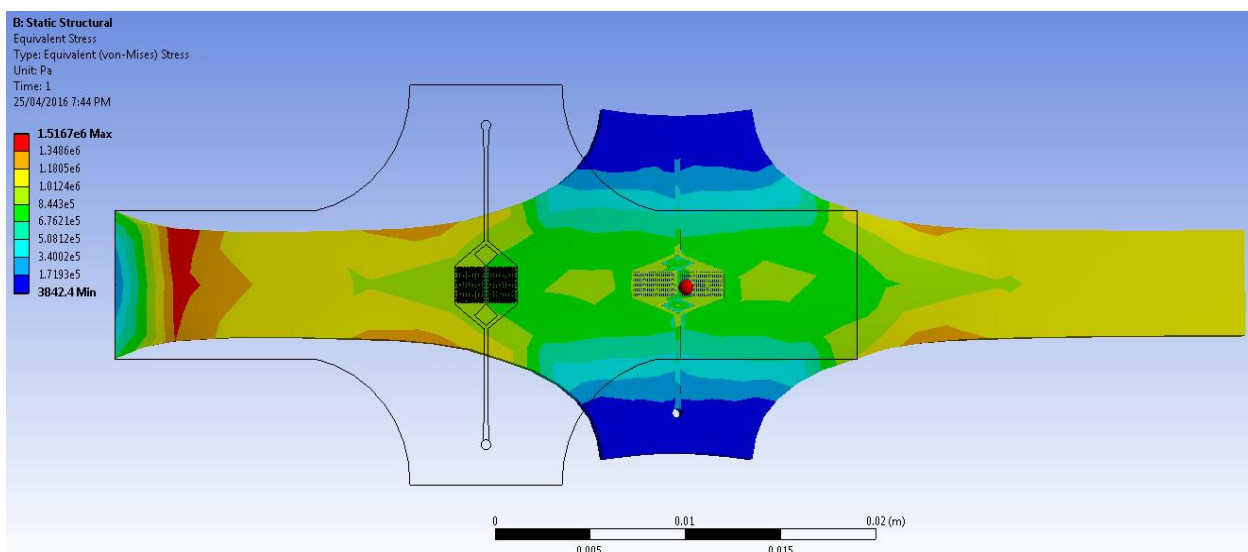
	<b>PDMS</b>
<b>Density</b>	0.97 [kg/m <sup>3</sup> ]
<b>Young's Modulus</b>	1.82 [MPa]
<b>Poisson's Ratio</b>	0.48

Table 4.1 shows the PDMS properties used for the simulation. The results of the FEA are shown in figure 4.2. The simulation depicts that the device experiences a large deformation, but its geometries such as inlet/outlet holes, microchannels, and microstructures still holding their

shapes; remember that the simulation only considers the worse scenery at the maximum deformation. Additionally, the simulation indicates that the maximum stress incurred with the applied force was of 1.5 [MPa] and the maximum strain was of 0.83. Note that the maximum strain obtained in the simulation is 20% higher than the one considered when calculating the force; nevertheless, the maximum stress is lower than the yield strength point which allows safely assume that the PDMS device will not present plastic deformation, if a strain of 0.6 is applied.



(A)

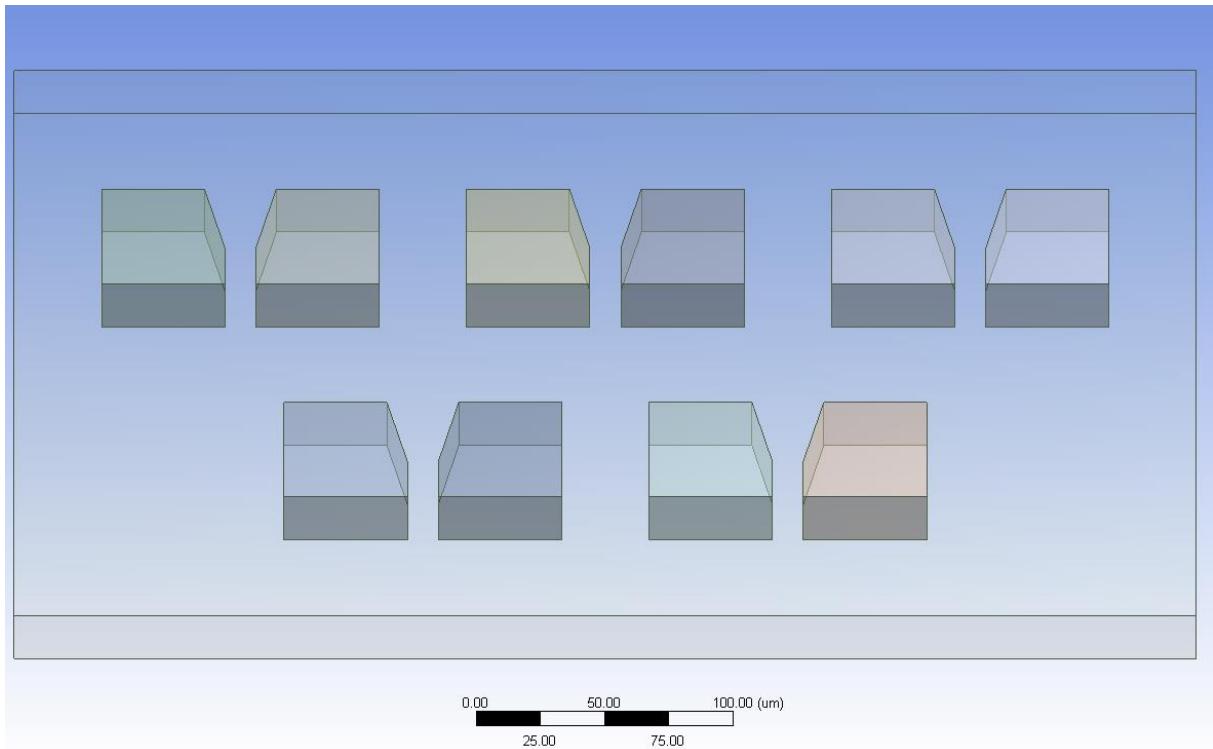


(B)

**Fig. 4.2** FEA simulation results. (A) Horizontal deformation of the device and maximum strain. (B) von Mises equivalent stress distribution in the trapping device.

### 4.3 Hydrodynamic Simulation

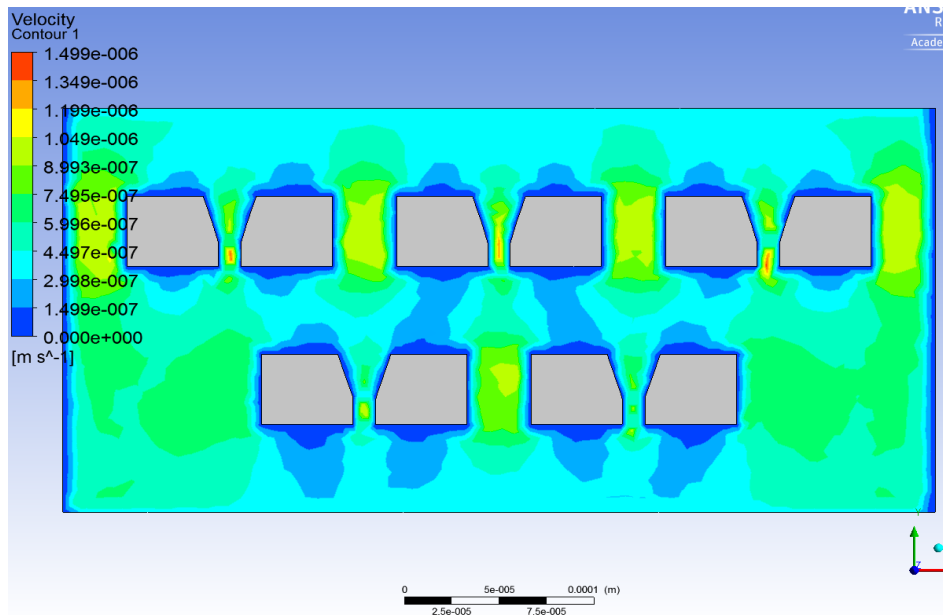
An hydrodynamic simulation was conducted in order to observe and predict the flow profile developed in the micro-channels and to determine the maximum stress exerted in the cells when captured in the traps. The model was developed using Fluent, and only a small section of the device was modeled. Since the traps are the same and they are arranged in the same fashion throughout the device, a small section of the array should be sufficient to exemplify the flow profile on all the traps. Thus, figure 4.3 shows the model used; some constraints of the model were input flow velocity and output pressure, which were  $4.047e^{-7}$  [m/s] and 0 [Pa] respectively. The flow velocity corresponds to an input flowrate equal to 100 [ $\mu\text{m/hr}$ ], which is much larger than the used in experiments, of 30 [ $\mu\text{m/hr}$ ]. Also, water properties were used instead of the cell media's physical characteristics.



**Fig. 4.3** Fluent model. An enclosure has been added in order to define the fluid domain, and only a small section of 5 traps were modeled.

The results of the simulation are shown in figure 4.4. The flow profile simulation reveals that there is liquid flowing through the traps, which is compulsory in order to direct cells into them. Also, the flow velocity is higher within the traps as expected due to the channel's narrowing.



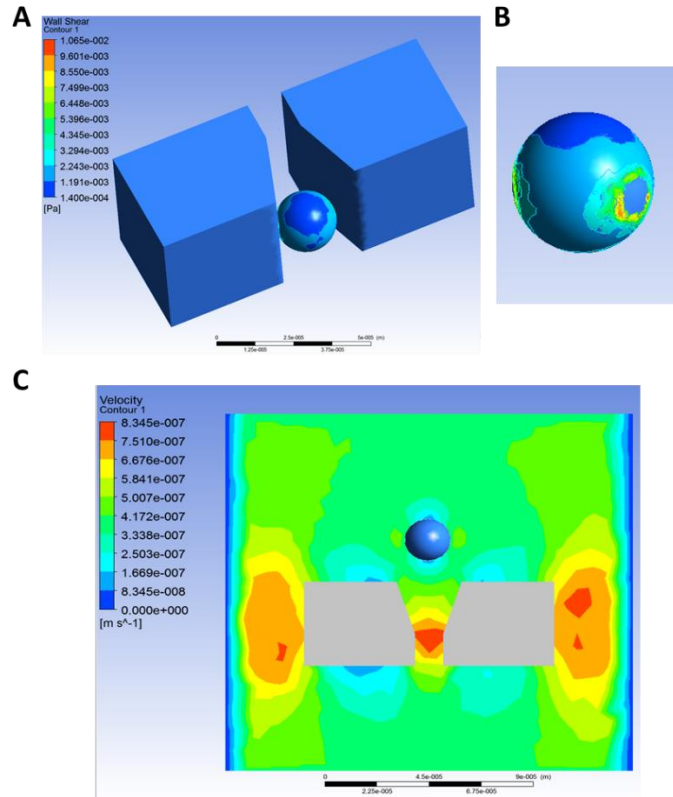


**Fig. 4.4** Fluent simulation results. The picture depicts the flow profile predicted for the arrays of traps.

The maximum flow velocity encountered in the simulation was, of  $1.5e^{-6}$  [m/s]. This value does not mean anything by itself; therefore, another simulation is needed in order to determine if such a flow velocity would produce damage onto the cells.

To determine the shear stress induced onto a cell in the device, a model of a single cell was made using again Fluent. The inlet and outlet conditions were kept as before, and the cell was modeled as a perfect sphere. For the simulation, it is not important to define the material and properties of the cell because the stress calculated depends upon the flow velocity and the interaction of the flowing cells with the walls of the traps. The goal of the simulation is to obtain the maximum shear stress induced in the cell and compare it to the maximum shear stress permitted on a cell to not produce damage, which is of 4.5 [Pa] (Dimmeler et al., 1996).

The results are presented in figure 4.5. From the results it can be seen that for a trapped cell, the maximum shear stress produced on its wall is of  $1.065e^{-2}$  [Pa], which is much lower than 4.5 [Pa]. Therefore, the viability of cells should not be compromised by the device.



**Fig. 4.5** Fluent simulation results of a single trap. (A) Shows the maximum shear stress produced on a cell when it is docked in the trap. (B) Close-up of the cell in picture A, where it can be seen that the higher stress is on the wall side touching the trap's walls. On (C) the flow velocity profile of a cell coming to the trap is depicted. The shear stress induced by the flow itself is very low, of approximately  $7.5e^{-4}$  [Pa].

Considering both simulations conducted, the mechanical and the hydrodynamical, the device should work properly if it is fabricated and no change in the design is needed. Although, it might be possible to create a dynamic model where one could simulate the trapping behaviour of the device, it was decided to proceed with the fabrication in order to test all the rest of the properties via experiments. Thus, the following chapters 5 and 6 provide details on both, the fabrication process and the results obtained from the experiments conducted.

#### **4.4 Conclusion**

The mechanical simulation of the new design was conducted using ANSYS to predict the deformation of the traps, and to determine numerically the maximum strain possible to applying before exceeding the elastic region. This point was very important and represents a keystone for the design because if the material (PDMS) results not to be adequate for the large deformability desired, the whole design or tuning method would have to be rethought. On the other hand, Fluent was employed simulate the flow profile in order to characterize the flow of the cells within the micro-channels, and to determine the wall shear stress exerted on the cells, which has to be lower than 4.5 [Pa] as determined by Dimmeler et al. (1996) to guarantee their viability. By the results obtained from the simulations it was concluded that both mechanically and hydrodynamically, the design proposed in Chapter 3 complies with all requirements originally established. Therefore, the device could be fabricated in order to conduct more tests to define its behaviour in a real situation. Chapter 5 and 6 will cover the fabrication process and the results obtained during the experiments, respectively.

## CHAPTER 5: FRABRICATION

### 5.1 Introduction

In order to achieve all the objectives of this research, a physical device is required to conduct experiments and tests. In Chapter 3 a new microfluidic trapping device was proposed, and this chapter states the fabrication process of this device. A brief introduction to soft lithography is given first, in which its advantages and disadvantages in comparison to other microfabrication processes are discussed. The replica molding technique used to fabricate the device is presented and explained in detail, followed by the real procedure conducted to make the PDMS chip. Finally, the chapter ends with the description of the fabrication process to obtain the stretching apparatus.

### 5.2 Soft Lithography

There are many different micro-manufacturing methods that have their foundations on photolithography, a technique developed in microelectronics for the fabrication of microelectronic components. For instance, UV lithography, soft X-ray lithography, electron-beam writing, focused ion beam writing, and proximal-probe lithography are very effective and capable of generating very small features in nanometer scale, but they have the following disadvantages when used for micrometer scale features: they are very expensive; they cannot be easily adapted for patterning on non-planar surfaces; they are largely ineffective in generating 3D structures; they are restricted to a limited set of photoresist materials; and they do not integrate well with glass, plastics, ceramics or carbon (Xia & Whitesides, 1998). Thus, other techniques need to be developed to overcome these problems, and fulfill the requirements of other areas outside of microelectronics. Examples of non-photolithographic methods that have been proposed are injection molding, embossing, cast molding, laser ablation, soft lithography, and many others. Soft lithography is a set of microfabrication methods such as micro-contact

printing, replica molding, micro-transfer molding, and rapid prototyping that use elastomeric molds to transfer patterns (Xia et al., 1998). Soft lithographic techniques have characteristics that allow to overcome the problems present by the lithographic techniques: the processes are rapid; they do not require the use of expensive equipment; they do not require expensive cleanrooms; they can be used on non-planar surfaces, and they are suitable for polymers and organic materials.

Soft lithography is a micro-manufacturing methodology that encompasses different techniques such as contact printing, replica molding, and rapid prototyping, and so on. These techniques are very useful to transfer patterns from a hard master or mold to a soft material such as silicone. In particular replica molding and rapid prototyping have been extensively used in the fabrication of microfluidics. Indeed, all the devices reviewed in Chapter 2 were manufactured by one of these two methods. One of the main reasons for this selection is that replica molding and rapid prototyping have become arguably standard procedures for the fabrication of PDMS devices. In addition, these methods are very fast (one could obtain a complete device in 24 hours), procedurally simple, and inexpensive, which make them optimal processes for the fabrication of microfluidic devices (Wolfe & Whitesides, 2005; Xia et al., 1998; McDonald et al., 2000). Thus, in this research the replica molding method was employed as the manufacturing technique to produce the new mechanically tunable microfluidic cell-trapping device resulted from the design presented in Chapter 3.

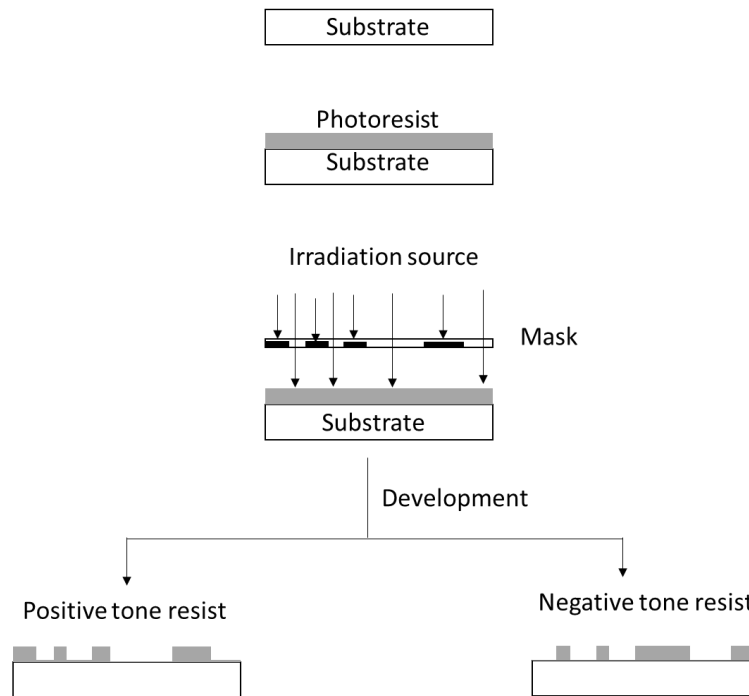
### **5.3 Replica Molding**

Replica molding is a simple casting method, where the features of a mold are negatively replicated on a soft polymer (PDMS); so that, the extruded microstructures on the master mold result in microchannels on PDMS. This method allows the replication of highly complex features with nanometer resolutions, which mainly depends on van der Waals interactions, wetting, and kinetic factors such as filling of the mold (Xia et al., 1998). After molding, a PDMS device will

have three walls out of four needed to have enclosed channels. Therefore, a sealing or bonding process is required to add the lid of the microfluidic device. Different materials can be used to produce the fourth wall such as glass, PDMS, Si, SiO<sub>2</sub>, quartz, silicon nitrate, polyethylene, polystyrene, and glass carbon; and the bonding can be irreversible or reversible. The main difference between a reversible and irreversible bonding is the pressure they can stand before breaking the seal. Reversible sealing is achieved thanks to the van der Waals interaction between the surfaces of the PDMS device with other materials, while irreversible sealing requires the exposure of both material surfaces to air plasma (McDonald et al., 2000). Molds can be made out of many different materials such as silicon, metal, and various hard polymers, and they can be fabricated using the most suitable procedure to achieve the desired features. For example, etching, photolithography, electroforming, x-ray lithography, 3D printing, and conventional machining could be used. Therefore, the selection of the method to create a mold will depend on the resolution required by the application and the resources available for its production.

Most microfluidic devices among the literature have employed SU-8 molds. SU-8 is a negative photoresist epoxy that becomes very rigid ( $E = 4.02 \text{ GPa}$ ) after baking at  $95^\circ$ , so it is capable of producing high-aspect-ratio structures mechanically stable (Del Campo & Greiner, 2007). SU-8 molds can be fabricated using photolithography. Photolithography, a micro-manufacturing process taken from microelectronics, allows the generation of a pattern on a substrate through the use of an optical image and a photosensitive polymer. The substrate can be silicon or another material. In the fabrication process the photoresist (SU-8) was first coated on the surface of the substrate. The substrate with the photoresist material is then exposed to an irradiation source such as UV light, through a transparent mask with the desired 2D pattern. When the photoresist is exposed to the light radiation, those areas exposed (not covered by the mask) change their solubility so that they can be differentiated on the subsequent developing process. Hence, the retained photoresist material creates the imprinted patterns after the

development. A material is said to be a negative tone photoresist when the portions that were not exposed to light dissolve in solution development, and positive tone when the exposed areas remain intact after the developing step (Hsu, 2002; Del Campo et al., 2007). The photolithography process is illustrated in figure 5.1.



**Fig. 5.1** Photolithographic process diagram showing the developing process differences between positive and negative tone resists. In general, for the fabrication of molds for microfluidic devices, silicon (Si) substrates and negative tone resist SU-8 are used.

The replica molding process carried out for the fabrication of the new single particle trapper consisted of the fabrication of a SU-8 mold using photolithography techniques to later proceed with the casting of PDMS and bonding. The process begins with preparing a silicon wafer by cleaning and prebaking it. Vitriol, ethyl alcohol and acetone were used to wash the silicon chip in sequence, and an electric hot plate was used to bake the cleaned silicon chip for 15 min. Before coating the Si wafer with SU-8 the surface was modified to produce a better adhesion with HMDS (Hexamethyldisilazane) in a volatile cylinder for 3 minutes. The photoresist

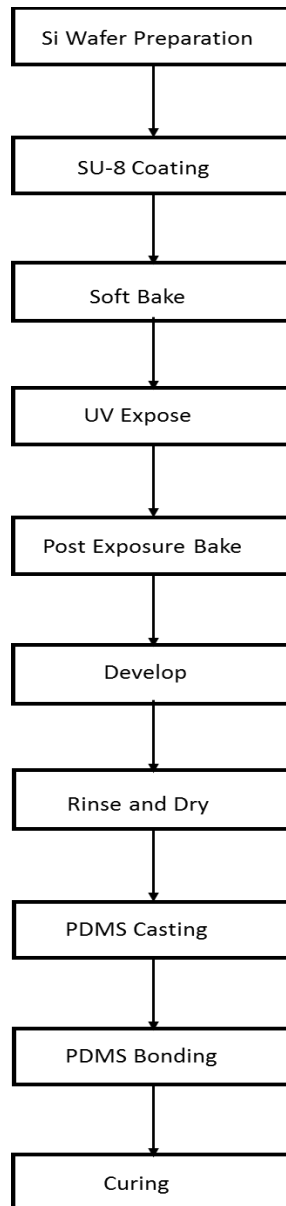
(SU-8-2050) was poured on the treated silicon chip and spin coated at 3000 rpms for 30 seconds. Before exposing the coated wafer was soft baked at 65°C for 3 minutes. The photolithography process was performed exposing the coated wafer through the mask bearing the desired pattern to UV (350-400nm) radiation for 6 seconds. After exposure, the chip was post baked at 95°C for 6 minutes. In order to develop the SU-8, the wafer was immersed in the developing solution for 5 minutes under constant agitation. After a drying process with nitrogen the mold is finished and ready to be used. To produce the PDMS (RTV-615 PDMS) devices a mixing base-to-curing agent ratio of 10:1 was mixed and degasified to remove air bubbles using a vacuum drying oven. The PDMS was poured onto the mold and the thickness was controlled at 1mm. The PDMS was dried up using a drying oven at 85°C. Upon solidification, the PDMS chip was carefully stripped from the mold and 0.75mm inlet/outlet holes were punched. After an optical assessment of the microstructures and microchannels under microscope the device was exposed to air plasma and bonded to a 1mm layer of PDMS. Finally, the bonded PDMS device shown in figure 5.2 was cured overnight at constant temperature of 65°C.



**Fig.5.2** Picture of the final microfluidic single-cell trapping device fabricated on PDMS.

For each of the devices fabricated for testing and experiments, the process flow is as depicted in figure 5.3.



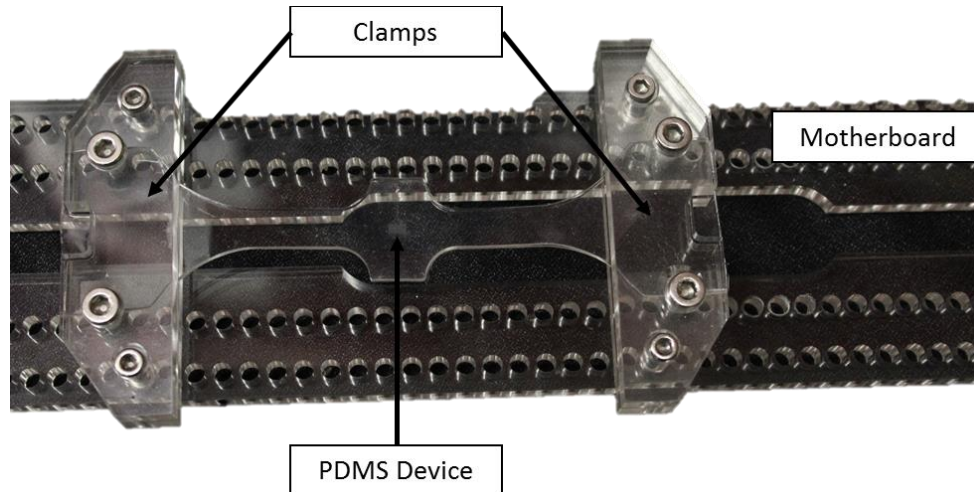


**Fig. 5.3** General flow diagram of the replica molding method followed to fabricate the microfluidic single-particle trapper device proposed in this thesis.

#### **5.4 Stretching Apparatus**

To produce the Acrylic stretching device a regular CNC machining procedure was conducted. First, as all parts comprising the device are 5mm thick a single acrylic layer was used for the fabrication of all the parts. After introducing the program code into the CNC

machine, the acrylic layer was set in position and the process was started. The process began drilling all the holes on the motherboard and clamps followed by cut of the parts. Figure 5.4 shows the finished stretching apparatus and its components.



**Fig. 5.4** Stretching apparatus fabricated on Acrylic. On the picture all the components of the stretching apparatus used to apply a uniformly distributed force onto the trapping device can be observed, which include two clamps with screws and a motherboard.

### 5.5 Cleaning of the Microfluidic Cell-trapping Device

The fabricated device must be reusable; indeed, this is a consequence of its function requirements. Since the device was designed in order to work with different batches of cells, the device should have a method to be cleaned and reused with either the same batch of cells or another batch with another average cell size. Most microfluidic devices are reusable, so this is not a novelty of this new device. In the literature, PDMS devices are usually cleaned before used for experiments by injecting 70% ethanol into the microfluidic channels, followed by the injection of culture media for several minutes in order to remove the ethanol and to prepare the channels for the cells (Benavente-Babace et al., 2014; Wang et al., 2014; Liu et al., 2012; Wu et al., 2007). The former cleaning-method is recommended for when the device is used constantly. If the device is left unused for several days or channels get clogged, a cleaning method proposed

by McKenna (2016) can be conducted. The method is based on ultrasonic bathing which is a technique commonly used in laboratories to clean small devices that cannot be mechanically brushed. Briefly, to clean the microfluidic device: place the PDMS device in a disposable plastic bag. Add a mild detergent solution or solvent (about 10 - 50 mL) to the bag. Hang the bag inside the ultrasonic bath machine and start the machine. Once the ultrasonic cleaning is over, remove the device from the bag and dry it either in an oven or with a nitrogen gun. Finally, analyze optically under the microscope if the channels are clean. It is also recommended to always carry out the first cleaning method with 70% ethanol before conducting any experiment in the device.

## **5.6 Summary**

In this chapter, the steps followed to fabricate the new PDMS single-particle trapper device were described in detail. In general, the process requires the fabrication of a hard master or mold on which the PDMS is later casted to generate the 3D microstructures and channels followed by an irreversible bonding of the PDMS device to another PDMS sheet. The microfabrication method chosen for the single-particle trapping device, namely replica molding belongs to a set of microfabrication techniques called soft lithography which has become a standard method to produce microfluidic devices on PDMS. The fabrication process to make the stretching apparatus was described, and the cleaning method to be able to reuse the trapping device was described as well.

## CHAPTER 6: MEASUREMENTS AND EXPERIMENTS

### 6.1 Introduction.

In the introductory chapter it was stated that the main attributes which a new adaptable single-cell trapping device should have are: (A) deformation of the elastomeric polymer (PDMS) feasible to stretch, (B) compliance of the traps, and (C) uniformity of the deformation of the traps. Therefore, in order to address, assess, and characterize these attributes on the new fabricated device, a set of experiments and tests are required. This chapter reports and presents the experiments conducted and the results obtained. The chapter initially introduces the methodology followed to conduct the experiments along with a brief explanation on how the foreseen outcomes would help to prove the fulfilment of the objectives proposed for the device. Also, the equipment, apparatuses, and devices used during the experiments are briefly described.

Two main experiments, as well as the difficulties encountered during these and their respective results are presented in this chapter. The first experiment is related to the deformation of the device and the elasticity property of PDMS, so it is intended to assess attributes: (A) and (C). The second, which was divided in two parts, is related to the capturing performance of the device, and they are focused on evaluating attribute: (B). It should be noted that in this chapter, the emphasis is on verification and evaluation of the properties and performance of the new device.

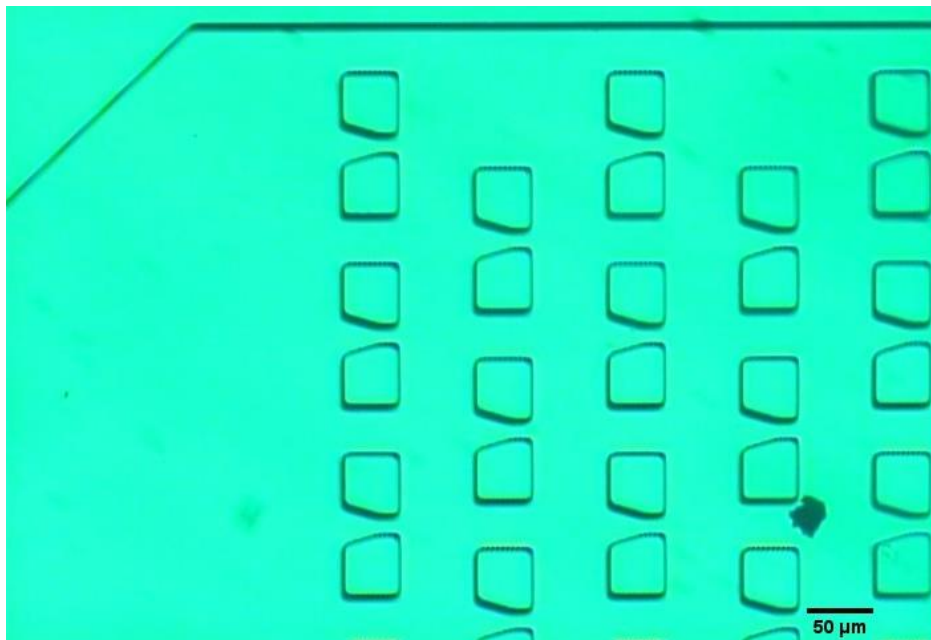
### 6.2 Experiment 1: Stretching and deformability.

The new device must be capable of adapting or modifying its trap dimensions in order to capture different sizes of particles every time it is tuned. However, the deformation must be controllable, repeatable, and uniform along the entire device. Also, it has been stated in the design that the size increment of the traps must be enough to capture at maximum deformation

particles 10  $\mu\text{m}$  in diameter larger than the particles captured at no-deformation (from 20  $\mu\text{m}$  to 30  $\mu\text{m}$ ). To assess and characterize the deformation behaviour of the device, several mechanical tests were carried out. These mechanical tests attempt to determine: (i) the strain at which the maximum deformation of the traps is achieved, (ii) the deformation of the traps at the maximum strain applied, (iii) the minimum trap-size increment possible with the stretching apparatus, and (iv) the distribution of deformations through all the traps, which should be uniform; i.e., the same for all of traps. In order to test the device in terms of these requirements the following procedure was followed.

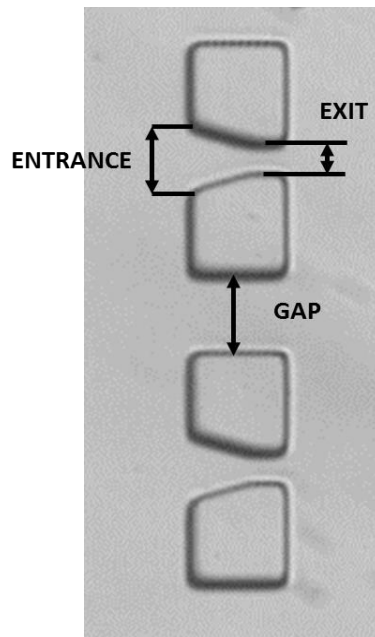
### 6.3 Experimental Procedure (Experiment 1)

In order to measure the deformation of the traps, several micrographs of the PDMS single-particle trapping device were taken using an optical microscope (Olympus IX70) with a 10X objective; an example of the micrographs obtained is depicted in figure 6.1 below.

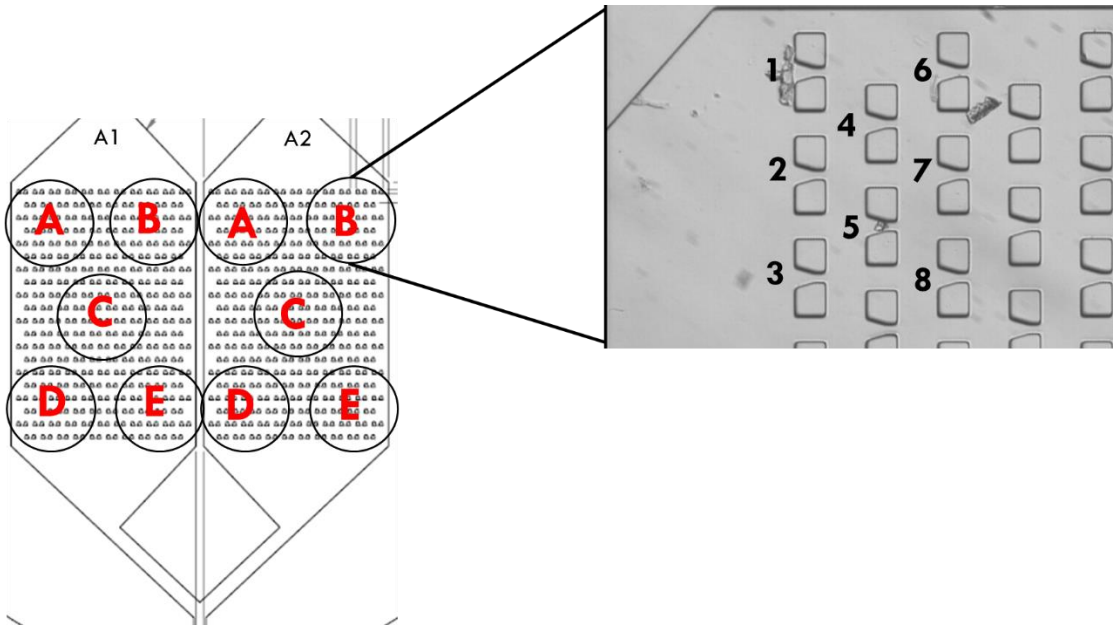


**Fig. 6.1** Example of a micrograph taken by the Olympus IX70 microscope at a 10X magnification.

After obtaining all the micrographs with a RGB video camera (JVC TK-1270 U) plugged to the microscope, they were post-processed on a computer software, called Image J, in order to do the required measurements. Three linear dimensions on the traps were measured, the exit, the entrance, and the gap between traps (Fig. 6.2). It is important to mention that instead of examining all the 420 traps (which would be ideal), only an strategically representative sample of traps was considered, 80 in total. To do the selection of traps, the device was divided as its structure on two arrays of traps. Each array was then segmented in 5 zones A, B, C, D, and E, and from each zone 8 traps were selected as shown in figure 6.3. Only 8 traps were chosen on each region because they fit within the scope of the microscope when the device is stretched to the maximum strain. The selection of 5 zones was based on the assumption that all the traps would present the same deformation (notice that they are arranged symmetrically to the center of the device).



**Fig. 6.2** Micrograph showing the three liner dimensions (exit, entrance, and gap between traps) that were examined on 80 traps for experiment 1.



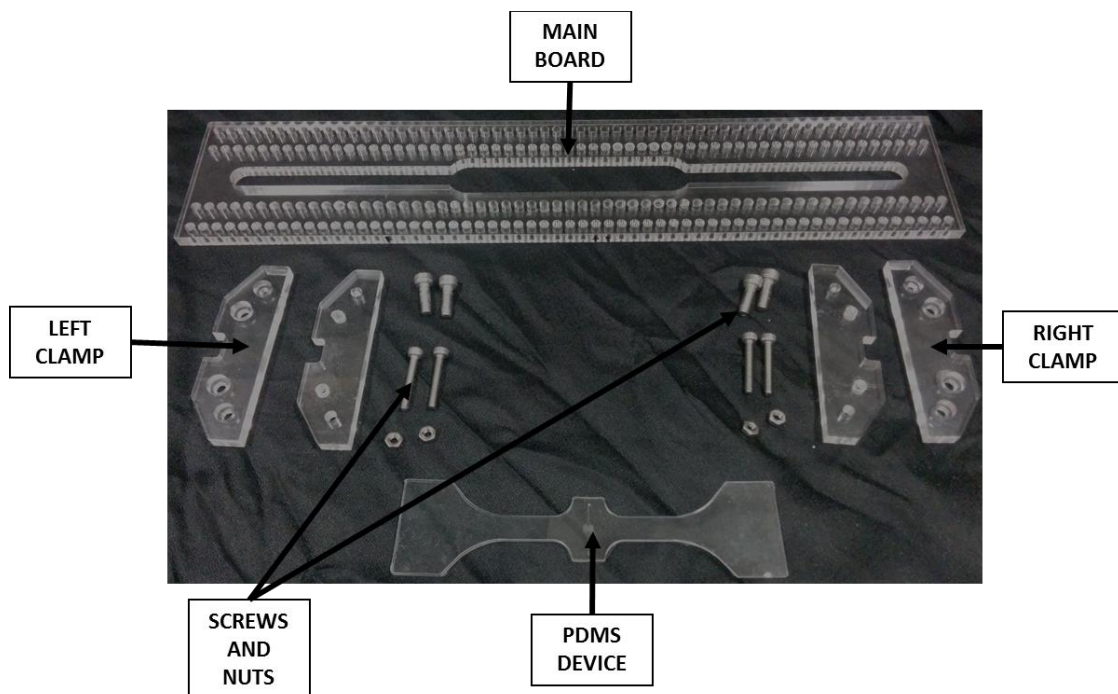
**Fig. 6.3** Schematic diagram showing the selection of traps. The device was divided on two arrays A1 and A2, later each array was divided in 5 regions denoted by the letters A to E. From each zone 8 different traps were selected to be examined on three linear dimensions, exit, entrance, and gap between traps.

After defining the traps to be measured, the experiment procedure was as follows:

1. The PDMS device was mounted on the clamps of the stretching apparatus.
2. The “left” clamp was secured to the motherboard, while the “right” clamp was left loose in order to choose its desired position. The components used as well as the procedure for the mounting of the device is depicted in figures 6.4 and 6.5, respectively.
3. First, the “right” clamp was secured at position zero (hole 0), which is equal to a zero strain applied. Then micrographs of each zone (A to E) focusing on the 8 selected traps were taken on both arrays using a 10X objective.
4. The “right” clamp was unscrewed and moved to the immediate next hole to the right (hole 1), resulting in a stretch of 5mm on the PDMS device.

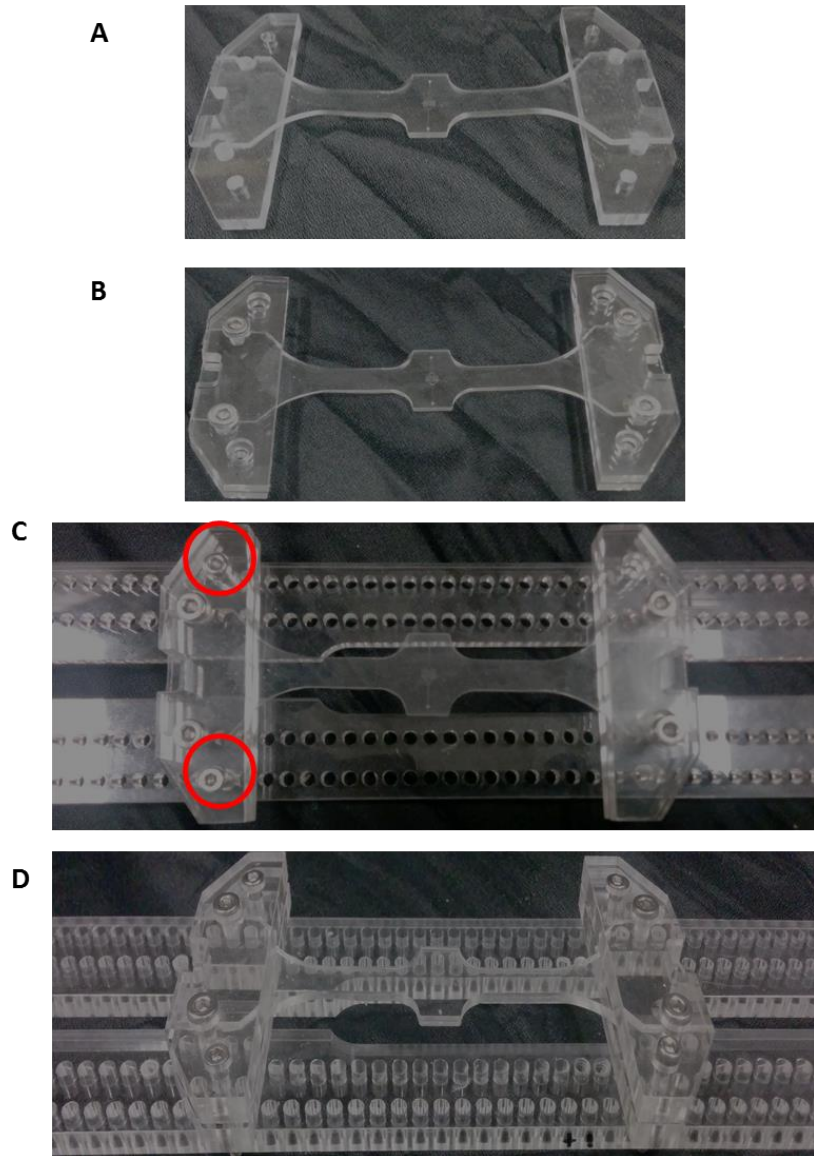
5. After securing the clamp on the new position (hole 1), micrographs of the same 8 traps were taken again at each zone of the arrays. This process was consecutively repeated for each new position (hole) until reaching the hole number 5.
6. All the 60 micrographs obtained from the above process were later transferred to an image processing software called Image J, where the measurements were done manually.
7. Exit, entrance, and gap of all the 8 traps on each micrograph were measured and recorded in a spread sheet following the same order.

In order to display the results, the three linear dimensions of each trap were averaged separately. As a result, for zone A at hole zero, only one value for the exit, the entrance, and the gap is shown. The above was done for each zone and array. In addition, since all the traps are identical in theory, the dimensions of all the traps should be very similar. In order to corroborate this argument, the coefficients of variation (CV) are also calculated. The results obtained are presented in the next section.





**Fig.6.4** Components required for the assembling of the new microfluidic single cell trapping device onto the stretching apparatus.



**Fig. 6.5** Procedure to mount the new cell trapping device onto the stretching apparatus. (A) Put the PDMS chip on top of the bottom sections of the clamps. (B) In a sandwich manner locate and align the top sections of the clamps on top of the PDMS chip, and secure the device on the clamps using the short screws. (C) Fix the left clamp to the main board by using two large screws, the position could be arbitrary. (D) Determine the strain or size increment you want to apply to the traps and fix the right clamp in the corresponding hole. Remember that the

stretching direction is to the right side and you can choose from 6 holes (6 positions); hole 0 means no deformation and hole 5 means maximum deformation.

## 6.4 Experimental Results (Experiment 1)

This section will present some of the experimental results obtained from measuring the traps under different strains. Many results were taken for repeatability using not only a single device, but 4 devices. Since the devices were fabricated under the same condition and no considerable variations were observed on the features among devices, we only focus on one device to conduct experiments. Although only representative results are presented here, more results such as micrographs and measurements are provided as supplemental material. Also, on the measurements obtained there is no evidence of a considerable variation on the size of the traps that could indicate the need of measuring more or other traps than the previously selected.

### 6.4.1 Measuring in ImageJ

Image J, an image processing software very popular among the scientific community, was selected in order to conduct the measurements of the traps in the micrographs obtained from the microscope. Image J can measure distances and angles on pixels or if provided on a real scale such as millimeters. Thus, when opening the micrographs in Image J a complication arises because the original dimension units of the images are given in pixels, so a conversion back to micrometers is necessary. Such conversion is done using specific information from the characteristics of the microscope (Olympus IX70) and the recording camera (JVC TK-1270 U). Thus, the pixel size is given by

$$Pixel\ Size = \frac{CCD\ element\ size}{Magnification\ of\ objective} \quad (6.1)$$

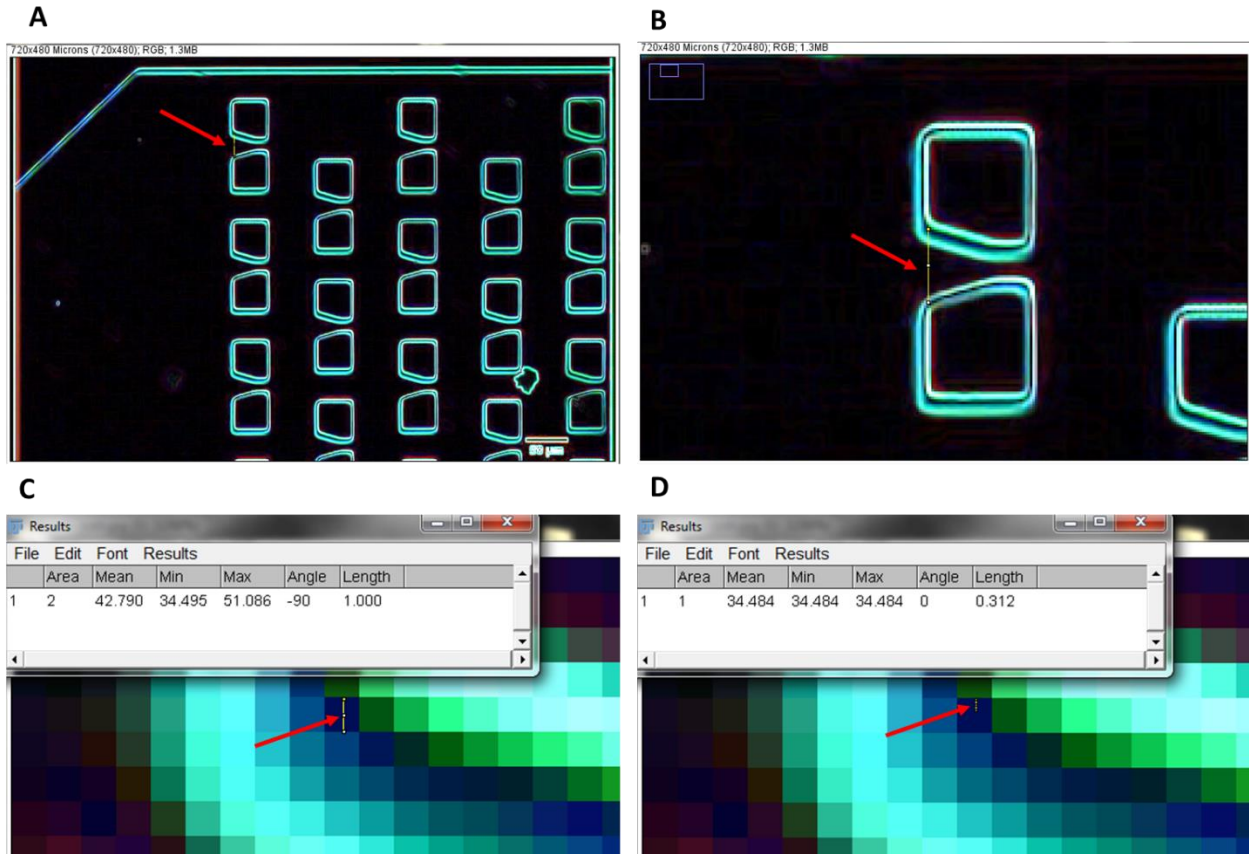
Where the CCD element size is determined by dividing the length of the camera's CCD by the size of the image in pixels. The camera used has a 1/2" CCD which size is of 6.4mm by

4.8mm, and the output image is of 720 pixels by 480 pixels. Thus, dividing 4.8mm over 480 pixels yields an element size of  $10\mu\text{m}$ . Now considering the magnification of 10X used on the microscope and substituting values into equation (6.1), one has that the real pixel size is:

$$\text{Pixel Size} = \frac{10\mu\text{m}}{10} = 1\mu\text{m in the vertical direction.} \quad (6.2)$$

Before making any measurement the pixel size value obtained was confirmed measuring known distances.

When using an image processing program some confusions might arise; therefore, one must have very clear what the software is doing. In particular the resolution of the images and measurements are of high interest for this research work. Although the software allows the user to measure distances in images, the measurements are done manually; i.e., the user has to select a point A (start point) and a point B (end point) using the cursor. As a consequence of this manual selection, human error is a considerable factor on the variance of the measurements recorded. In order to reduce the unavoidable error of eyeballing the selection of points A and B, we use the zoom tool to increase the size of the original image. Zooming in an image does not increase its resolution, but it allows us to have a closer look in it, to be able to select the edges of the traps more accurately. Moreover, the step increment of the measuring tool in Image J is independent to the pixel size of the image; therefore, it can measure lengths smaller than the pixel size (Fig. 6.6). So, although the resolution of the images is given by the microscope resolution, which is of 1 micron, the length values obtained from Image J, present decimal values corresponding to nanometers.



**Fig. 6.6** Example of measuring the traps using Image J. (A) Shows an original size micrograph with a size of 720x480 pixels. (B) Shows the same image in (A), but enlarged 300%. The red arrow in (A) and (B) is pointing at a measuring line to exemplify that it is easier to select the edges of a trap by zooming in the image. (C) Depicts the real vertical length of a pixel in image (A), which is of 1 micron; the image has a zoom of 3200%. (D) Shows that Image J is capable of measuring lengths smaller than the pixel size of the image being analysed. The resolution of the measuring tool was empirically determined to be approximately of 1/30 pixels for the image size used.

#### 6.4.2 Maximum Deformation and Strain

As discussed earlier, instead of displaying all the dimensions recorded for all the 80 traps examined (which are 240 measurements per hole), an average of the measurements taken of

the 8 traps in each zone is presented, as well as the coefficients of variation. All the data and results can be seen in the supplementary material. Hence, the following tables (Table 6.1 and Table 6.2) show the average dimension of the exit, the entrance, and the gap per zone at different strains; i.e., hole 0, 1, 2, 3, 4, and 5. While tables 6.3 and 6.4 present the corresponding coefficients of variation.

**Table 6.1** Average dimensions of the traps in the array one (A1).

ARRAY OF TRAPS 1							
ZONE		HOLE 0	HOLE 1	HOLE 2	HOLE 3	HOLE 4	HOLE 5
A	EXIT [ $\mu\text{m}$ ]	12.17	14.39	16.20	18.37	20.47	22.12
	ENTRANCE [ $\mu\text{m}$ ]	28.43	30.17	32.36	34.32	36.32	38.37
	INTER-TRAPS GAP [ $\mu\text{m}$ ]	33.75	36.80	39.42	42.44	45.70	47.44
B	EXIT [ $\mu\text{m}$ ]	12.07	14.32	16.39	18.68	20.26	22.02
	ENTRANCE [ $\mu\text{m}$ ]	27.73	30.52	32.38	34.36	36.32	38.37
	INTER-TRAPS GAP [ $\mu\text{m}$ ]	33.84	36.89	39.33	42.56	44.65	47.21
C	EXIT [ $\mu\text{m}$ ]	11.51	13.34	15.39	17.24	19.21	21.33
	ENTRANCE [ $\mu\text{m}$ ]	27.73	29.74	31.88	33.64	35.84	37.67
	INTER-TRAPS GAP [ $\mu\text{m}$ ]	33.31	36.05	38.98	41.56	43.65	46.64
D	EXIT [ $\mu\text{m}$ ]	12.09	14.07	16.02	18.07	20.29	22.29
	ENTRANCE [ $\mu\text{m}$ ]	28.01	30.26	32.53	34.36	36.54	38.46
	INTER-TRAPS GAP [ $\mu\text{m}$ ]	33.58	36.98	39.33	43.02	45.82	47.79
E	EXIT [ $\mu\text{m}$ ]	12.24	14.15	16.12	18.05	20.12	22.16
	ENTRANCE [ $\mu\text{m}$ ]	28.52	30.35	32.27	34.54	36.45	38.28
	INTER-TRAPS GAP [ $\mu\text{m}$ ]	34.27	36.54	39.07	42.56	45.23	48.37

**Table 6.2** Average dimensions of the traps in the array two (A2).

ARRAY OF TRAPS 2							
ZONE		HOLE 0	HOLE 1	HOLE 2	HOLE 3	HOLE 4	HOLE 5
A	EXIT [ $\mu\text{m}$ ]	11.90	13.97	16.05	18.07	20.38	22.08
	ENTRANCE [ $\mu\text{m}$ ]	27.82	30.35	32.15	34.23	36.32	38.46
	INTER-TRAPS GAP [ $\mu\text{m}$ ]	33.58	36.80	39.42	42.33	45.35	47.67
B	EXIT [ $\mu\text{m}$ ]	12.03	14.15	16.12	18.47	20.32	22.20
	ENTRANCE [ $\mu\text{m}$ ]	28.08	29.83	32.09	34.27	36.28	38.37
	INTER-TRAPS GAP [ $\mu\text{m}$ ]	33.75	36.89	39.59	42.56	45.47	47.91
C	EXIT [ $\mu\text{m}$ ]	11.91	13.98	15.92	18.17	20.10	22.07
	ENTRANCE [ $\mu\text{m}$ ]	28.00	30.17	32.05	34.19	36.28	38.37
	INTER-TRAPS GAP [ $\mu\text{m}$ ]	33.79	36.89	39.42	42.79	45.35	47.09

<b>D</b>	EXIT [ $\mu\text{m}$ ]	12.19	14.41	16.20	18.38	20.44	22.02
	ENTRANCE [ $\mu\text{m}$ ]	28.34	30.35	32.62	34.19	36.28	38.35
	INTER-TRAPS GAP [ $\mu\text{m}$ ]	33.66	36.72	38.98	42.56	45.23	47.44
<b>E</b>	EXIT [ $\mu\text{m}$ ]	12.17	13.96	16.02	18.37	20.47	22.20
	ENTRANCE [ $\mu\text{m}$ ]	28.17	30.09	32.09	34.32	36.45	38.37
	INTER-TRAPS GAP [ $\mu\text{m}$ ]	33.93	36.63	39.33	42.91	45.58	48.02

Note in tables 6.1 and 6.2 that among zones the size of traps, meaning the exit space, the entrance space, and gap are very similar and consistent. For instance, in table 6.1 at hole 0 the exit of the traps in all zones is about  $12\mu\text{m}$ , being the zone C the smallest with  $11.5\mu\text{m}$  and zone E the largest with  $12.24\mu\text{m}$ ; however, this difference is attributed to experimental measurement, and thereby they are negligible. Same exemplification can be made for the rest of the dimensions in the table and a similar variance will be found.

**Table 6.3** Coefficients of variance of the measured traps in array one (A1).

<b>ARRAY OF TRAPS 1</b>							
<b>ZONE</b>		<b>HOLE 0</b>	<b>HOLE 1</b>	<b>HOLE 2</b>	<b>HOLE 3</b>	<b>HOLE 4</b>	<b>HOLE 5</b>
<b>A</b>	EXIT	0.02	0.02	0.02	0.02	0.02	0.01
	ENTRANCE	0.02	0.01	0.01	0.01	0.00	0.00
	INTER-TRAPS GAP	0.01	0.02	0.02	0.01	0.01	0.01
<b>B</b>	EXIT	0.04	0.03	0.03	0.02	0.01	0.01
	ENTRANCE	0.02	0.01	0.01	0.01	0.00	0.00
	INTER-TRAPS GAP	0.02	0.01	0.01	0.02	0.00	0.01
<b>C</b>	EXIT	0.04	0.04	0.03	0.03	0.02	0.02
	ENTRANCE	0.02	0.02	0.02	0.02	0.02	0.02
	INTER-TRAPS GAP	0.02	0.01	0.01	0.01	0.01	0.01
<b>D</b>	EXIT	0.02	0.02	0.00	0.00	0.02	0.01
	ENTRANCE	0.02	0.02	0.01	0.01	0.01	0.01
	INTER-TRAPS GAP	0.02	0.01	0.01	0.02	0.01	0.01
<b>E</b>	EXIT	0.03	0.02	0.01	0.00	0.01	0.01
	ENTRANCE	0.02	0.02	0.01	0.01	0.01	0.01
	INTER-TRAPS GAP	0.01	0.01	0.02	0.01	0.01	0.01

**Table 6.4** Coefficients of variance of the measured traps in array two (A2).

<b>ARRAY OF TRAPS 2</b>							
<b>ZONE</b>		<b>HOLE 0</b>	<b>HOLE 1</b>	<b>HOLE 2</b>	<b>HOLE 3</b>	<b>HOLE 4</b>	<b>HOLE 5</b>

<b>A</b>	EXIT	0.01	0.00	0.00	0.00	0.02	0.01
	ENTRANCE	0.02	0.01	0.00	0.01	0.00	0.01
	INTER-TRAPS GAP	0.02	0.01	0.02	0.02	0.00	0.01
<b>B</b>	EXIT	0.02	0.02	0.01	0.02	0.02	0.01
	ENTRANCE	0.02	0.02	0.01	0.01	0.00	0.00
	INTER-TRAPS GAP	0.01	0.01	0.01	0.00	0.01	0.01
<b>C</b>	EXIT	0.03	0.03	0.01	0.01	0.02	0.01
	ENTRANCE	0.01	0.02	0.01	0.00	0.00	0.00
	INTER-TRAPS GAP	0.01	0.02	0.02	0.01	0.01	0.01
<b>D</b>	EXIT	0.02	0.02	0.02	0.02	0.02	0.01
	ENTRANCE	0.01	0.02	0.01	0.00	0.00	0.01
	INTER-TRAPS GAP	0.02	0.02	0.02	0.01	0.01	0.00
<b>E</b>	EXIT	0.02	0.03	0.00	0.02	0.02	0.02
	ENTRANCE	0.02	0.01	0.00	0.01	0.01	0.00
	INTER-TRAPS GAP	0.01	0.01	0.01	0.01	0.01	0.01

Note that tables 6.3 and 6.4 present very small values, lower than 0.04, which means that the traps are indeed almost identical, and the values obtained when measuring the exit, the entrance, and the gap between traps are all very close to its corresponding mean value. Such variations in sizes can be explained by considering the accuracy limitation of the fabrication process and the measuring error. In particular, the process used to fabricate the device has a tolerance of fabrication of  $\pm 8\%$ , and the measuring error comes from the manual selection of the characteristics of the traps in Image J.

To determine the maximum deformation achieved in the traps after applying the maximum strain, the dimensions recorded at hole 0 (no strain) and the ones recorded at hole 5 (maximum strain) were subtracted yielding a maximum growth of the traps of about  $10\mu\text{m}$ . An example of the calculations done is provided considering only zone A.

$$\text{Max. size increment of exit} = 22.122 - 12.174 = \mathbf{9.948\mu\text{m}}$$

$$\text{Max. size increment of entrance} = 38.372 - 28.430 = \mathbf{9.942\mu\text{m}}$$

$$\text{Max. size increment of gap} = 47.442 - 33.750 = \mathbf{13.692\mu\text{m}}$$

### 6.4.3 Uniform Deformation

Using tables 6.1 and 6.2 in the previous section, a size increment tables were obtained (tables 6.5 and 6.6). In these tables, each column states the magnitude increment of the exit, entrance, and gap of the traps when the device is stretched. This is done aiming to showing that the increment is the same every time that the device is stretched 5mm.

**Table 6.5** Size increments of the traps on each zone of array A1.

ARRAY OF TRAPS 1						
ZONE		$\Delta$ (0-1) [ $\mu\text{m}$ ]	$\Delta$ (1-2) [ $\mu\text{m}$ ]	$\Delta$ (2-3) [ $\mu\text{m}$ ]	$\Delta$ (3-4) [ $\mu\text{m}$ ]	$\Delta$ (4-5) [ $\mu\text{m}$ ]
A	EXIT	2.211	1.819	2.163	2.099	1.657
	ENTRANCE	1.744	2.181	1.961	2.006	2.049
	INTER-TRAPS GAP	3.053	2.616	3.023	3.256	1.744
B	EXIT	2.249	2.073	2.291	1.579	1.762
	ENTRANCE	2.789	1.853	1.984	1.962	2.049
	INTER-TRAPS GAP	3.052	2.443	3.226	2.093	2.558
C	EXIT	1.833	2.048	1.858	1.962	2.128
	ENTRANCE	2.006	2.137	1.766	2.202	1.831
	INTER-TRAPS GAP	2.732	2.936	2.579	2.093	2.990
D	EXIT	1.983	1.954	2.047	2.221	2.000
	ENTRANCE	2.256	2.267	1.830	2.181	1.918
	INTER-TRAPS GAP	3.401	2.355	3.692	2.792	1.976
E	EXIT	1.907	1.966	1.936	2.064	2.044
	ENTRANCE	1.832	1.919	2.268	1.919	1.831
	INTER-TRAPS GAP	2.268	2.528	3.488	2.675	3.139

**Note:** The notation  $\Delta$  (0-1) means the size increment resulted when the device was stretched from position 0 (hole 0) to position 1 (hole 1); thus,  $\Delta$  (1-2) means size increment resulted when the device was stretched from position 1 to position 2, and so on.

**Table 6.6** Size increments of the traps on each zone of array A2.

ARRAY OF TRAPS 2						
ZONE		$\Delta$ (0-1) [ $\mu\text{m}$ ]	$\Delta$ (1-2) [ $\mu\text{m}$ ]	$\Delta$ (2-3) [ $\mu\text{m}$ ]	$\Delta$ (3-4) [ $\mu\text{m}$ ]	$\Delta$ (4-5) [ $\mu\text{m}$ ]
A	EXIT	2.075	2.076	2.023	2.308	1.698
	ENTRANCE	2.529	1.799	2.082	2.093	2.137
	INTER-TRAPS GAP	3.227	2.616	2.907	3.023	2.326
B	EXIT	2.110	1.977	2.349	1.849	1.884
	ENTRANCE	1.745	2.267	2.180	2.006	2.093
	INTER-TRAPS GAP	3.140	2.703	2.966	2.906	2.442

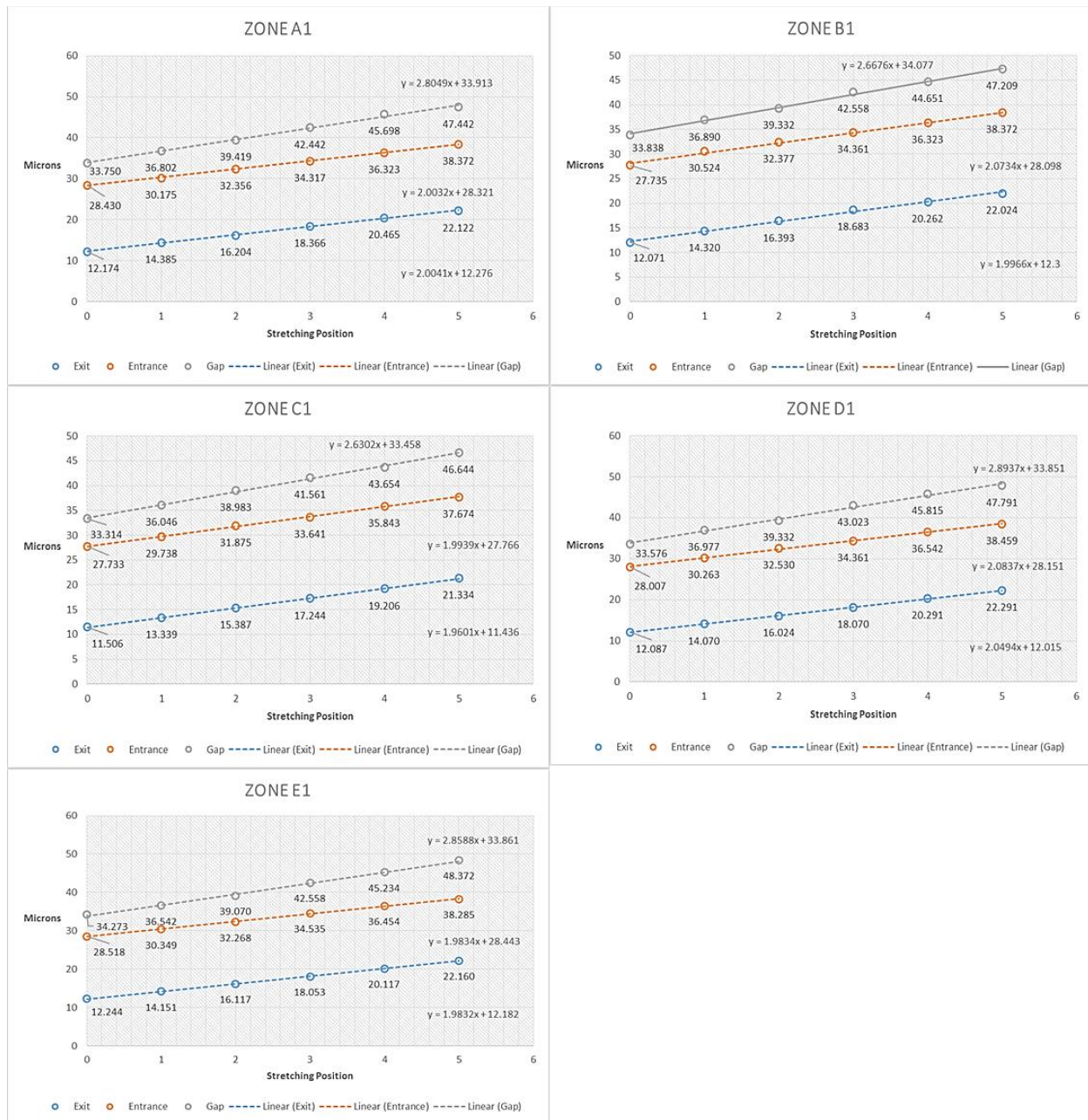


C	EXIT	2.064	1.948	2.250	1.921	1.974
	ENTRANCE	2.179	1.875	2.137	2.093	2.093
	INTER-TRAPS GAP	3.096	2.529	3.372	2.558	1.744
D	EXIT	2.215	1.791	2.186	2.052	1.587
	ENTRANCE	2.007	2.267	1.570	2.093	2.072
	INTER-TRAPS GAP	3.054	2.266	3.576	2.675	2.209
E	EXIT	1.791	2.053	2.349	2.099	1.738
	ENTRANCE	1.919	2.006	2.224	2.137	1.919
	INTER-TRAPS GAP	2.703	2.702	3.576	2.675	2.442

**Note:** The notation  $\Delta$  (0-1) means the size increment resulted when the device was stretched from position 0 (hole 0) to position 1 (hole 1); thus,  $\Delta$  (1-2) means size increment resulted when the device was stretched from position 1 to position 2, and so on.

In the above tables it is seen that all the size increments of the trap features examined, exit, entrance, and gap are approximately equal to 2  $\mu\text{m}$ . In particular, this is the case for the exit and entrance, while the gap has a larger increment of more 2.8  $\mu\text{m}$ .

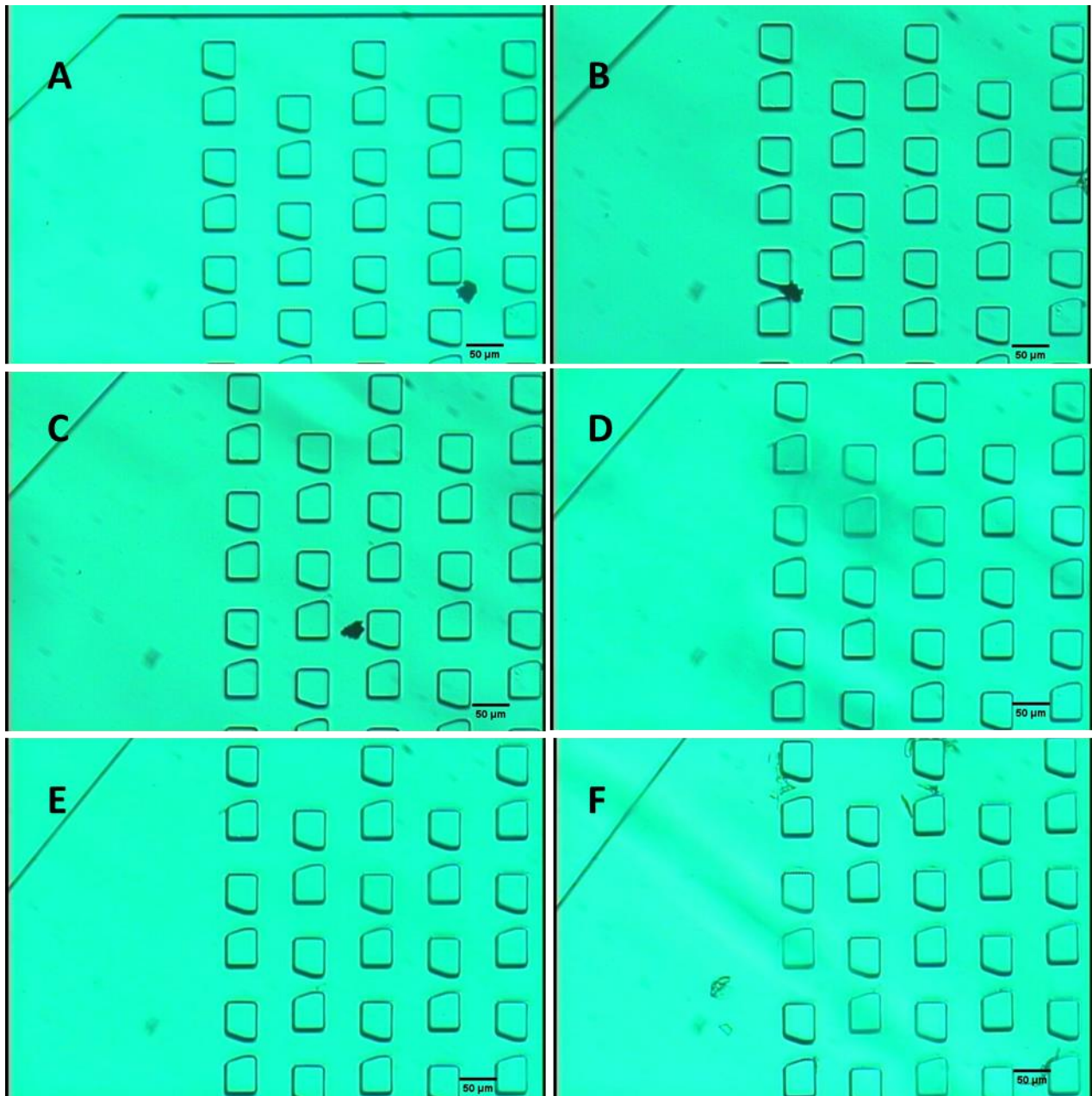
The data in tables 6.5 and 6.6 were plotted in ten separated scatter charts, five charts per array. Each of the following charts in figure 6.7 represents graphically the size increments obtained on each zone of the array, so that if a uniform deformation was achieved in all the traps, all the charts must be if not identical very similar. Here only the charts corresponding to the array A1 are shown; the plots for array A2 and larger images of the charts can be found in Appendix B.



**Fig. 6.7** Charts in this figure displays the average magnitudes recorded for the exit (blue dots), the entrance (orange dots), and the gap between traps (grey dots) at all the stretching position tested (hole 0 to 5) for the traps in all the regions, such that the x-axis is the stretching position and the y-axis is the trap dimension expressed in microns. In addition to the scattered dots, a trend line has been included with its corresponding equation for each series in order to

show that the deformation of the traps follows a linear and constant tendency, which can be represented by a linear equation of first order.

In addition, figure 6.8 shows how the traps keep their triangular shape and the microstructures did not experiment a visible deformation when the PDMS device was subject to various strains. The figure shows six micrographs of the zone B in array A1.



**Fig. 6.8** Micrographs taken at array one section B. (A) Image taken when the device was not stretched. (B) Micrograph obtained when the device was expanded to position hole 1. (C)-(F) Pictures taken when the device was stretched from hole 1 to hole 5 progressively. By looking at all the micrographs one can observe the increase on size of the traps as they go from A to F, but a small deformation of the microstructures.

#### **6.4.4 Minimum Deformation**

From figure 6.7 is also evident that the minimum deformation possible on the actual device is of  $2\mu\text{m}$  which correspond to a stretching of 5mm or a strain of 0.06. Moreover, the minimum deformation of the single-cell trapping device is of particular interest because it also defines the capturing resolution of the device.

#### **6.5 Discussion (Experiment 1)**

From the data in tables 6.5 and 6.6 it was determined that the trap's exit and entrance grow  $10\mu\text{m}$  when the trapping device is stretched up to the hole 5, which represent the maximum strain of 0.48. This growth is exactly the increment proposed in the design stage to be able to capture particles of  $30\mu\text{m}$  in diameter and avoid plastic deformation when the device is stretched. Thus, the device should be capable of capturing particles from  $20\mu\text{m}$  to  $30\mu\text{m}$  as it was originally designed.

Besides the maximum trap size achieved by the device, more important for its correct functioning is to be able of producing a uniform deformation through all of its features. Thus, if a uniform deformation is achieved, then all the traps in the device must present the same or similar size increment and deformation. In addition, the microstructures that form the traps must present a very little deformation in order to keep the shape of the traps. Reviewing the charts of figure 6.4, one can clearly recognize that the discrete points representing the size increment of the traps follow with a negligible difference the trend line; consequently, it can be said that

indeed the traps on each zone have a linear and uniform deformation when a strain below the maximum limit is applied. Further, if the charts are analyzed altogether it is noticeable at sight that all of them are very similar. Even more, looking at the slopes compiled in the next table below (Table 6.7), one can tell that their values are very close to each other and they are around  $m = 2$  for the exit and entrance and  $m = 2.8$  for the gap, regardless of the zone in the array considered. The largest elongation produced on the gaps between traps is attributed to the larger space between the neighboring microstructures. If one thinks on the microstructures as pillars that hold together the top and bottom layer of the device, when the device is stretched the microstructures oppose the deformation trying to hold the layers in the same position. However, as the length of the gap between traps is larger than that of the entrance and exit; the microstructures (pillars) cannot oppose with the same force to the deformation. Thereby, the larger the length of the gap, the lower the resistance to deform, which also explains the fastest deformation rate, shown on the plots. Nevertheless, the requirement of having the same deformation in all the traps has been met as shown by the experimental evidence.

**Table 6.7** Size increments of the traps on each zone of array A2.

ZONE		TREND LINE SLOPE	
		Array A1	Array A2
A	EXIT	2.004	2.061
	ENTRANCE	2.003	2.091
	INTER-TRAPS	2.804	2.829
	GAP		
B	EXIT	1.996	2.049
	ENTRANCE	2.073	2.085
	INTER-TRAPS	2.667	2.842
	GAP		
C	EXIT	1.96	2.039
	ENTRANCE	1.993	2.066
	INTER-TRAPS	2.63	2.721
	GAP		
D	EXIT	2.049	1.983
	ENTRANCE	2.083	1.982

E	INTER-TRAPS GAP	2.893	2.8
	EXIT	1.983	2.057
	ENTRANCE	1.983	2.066
	INTER-TRAPS GAP	2.858	2.883

The resolution of  $2\mu\text{m}$  shown in the results is directly related to the displacement increment permitted by the stretching apparatus. Therefore, if a smaller step increment was possible by the stretching apparatus, the size increment of the traps would be smaller, and consequently the resolution of the trapping device would be higher. Thus, the smaller the displacement of the stretching device, the larger the resolution of the PDMS device. Here, the resolution is understood as the minimum variation in the diameter of particles that can be differentiated by the traps. In other words, how small the increment of the particle size is that the traps are capable of reflecting in their deformation to capture specific sizes. In this line, a higher resolution would imply that cells with smaller differences to  $2\mu\text{m}$ , could be identified by the device. For instance, with the actual resolution of the device, particles (either cells or microspheres) from  $20\mu\text{m}$  to  $30\mu\text{m}$  can be captured with the device; however, the traps cannot differentiate between cells of  $20\mu\text{m}$  and  $22\mu\text{m}$ . As a consequence, the particles which the device would work properly with, must have average diameters of  $20\mu\text{m}$ ,  $22\mu\text{m}$ ,  $24\mu\text{m}$ ,  $26\mu\text{m}$ ,  $28\mu\text{m}$ , and  $30\mu\text{m}$ .

## 6.6 Experiment 2: Trapping of Particles

Experiment two was conducted to demonstrate the compliance of the traps (attribute B) of the new single-cell trapping device. Such attribute involves two main aspects that the traps must cover. The first is that the device must be capable of capturing single particles of a predetermined size at different strains and the second is to produce no damage onto the captured cells. These two aspects were assessed separately in two parts. In part one, 6 different

particle-size batches of water-in-oil microsphere were used to test the trapping performance of the traps, whilst in part two, melanoma cells were captured to demonstrate their viability within the device.

### **6.7 Experiment 2: Part I**

In experiment one it was shown that the device works well and behaves as designed in the mechanical domain. Now in this part of experiment two, the device is tested in the microfluidics domain to assess its function (capture single particles). It is important to mention that although the device was introduced as a cell trapper, to facilitate the experiments, microspheres instead of cells were used in this experiment. The main reason is because water-in-oil microspheres of specific sizes can be relatively easy to produce in large quantities, very fast, and at low costs in our lab. In the literature review it was shown that the exchange of cells by microspheres is a common practice when testing microfluidic trapping devices. Therefore, for this research it has been assumed that the nature of the particles used should not affect the objective of proving the concept of adaptability of the device to trap a wide range of particle sizes. Nevertheless, in the second part of this experiment it is shown that the device is suitable to working with cells too.

The experiment on part one consisted of a series of tests to exhibit: (i) the device ability of trapping single particles; (ii) that the deformation of the traps does not have negative effects on the trapping function; (iii) that the device is able to capture particles of different sizes when modulated; and (iv) the behaviour of the device when larger and smaller particles than the ideal size are used. In order to achieve the above goals, the following procedure was followed.

### **6.8 Experimental Procedure (Experiment 2: Part I)**

Batches of water-in-oil microsphere of different sizes were produced in a modified T-junction device (Lei, 2016) to later be fed into the PDMS single-cell trapping device. The average size of the microspheres of each batch was controlled at 20 $\mu$ m, 22 $\mu$ m, 24 $\mu$ m, 26 $\mu$ m,

28 $\mu\text{m}$ , and 30 $\mu\text{m}$ , respectively. The trapping device was tested with a single batch at a time. The whole trapping process was observed at all times under an optical microscope (Olympus IX70), and micrographs were taken as evidence of the process, in particular when the traps were filled. Later, the micrographs were transferred to Image J in order to measure the size of the particles captured. The detail procedure carried out for the experiments is outlined below.

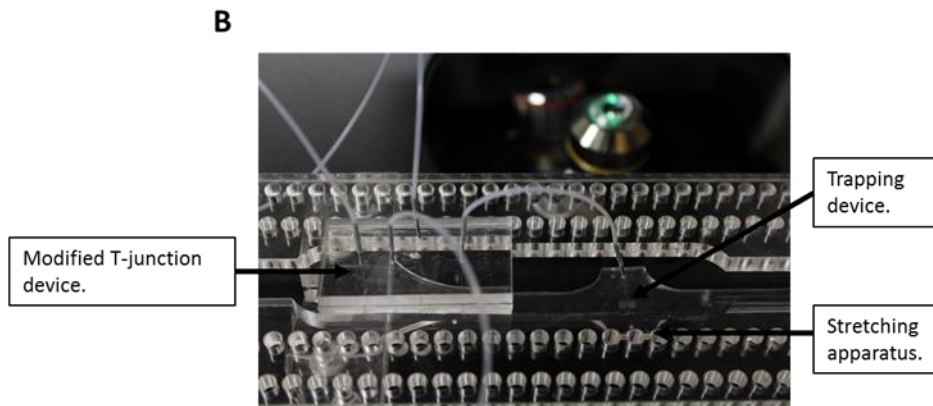
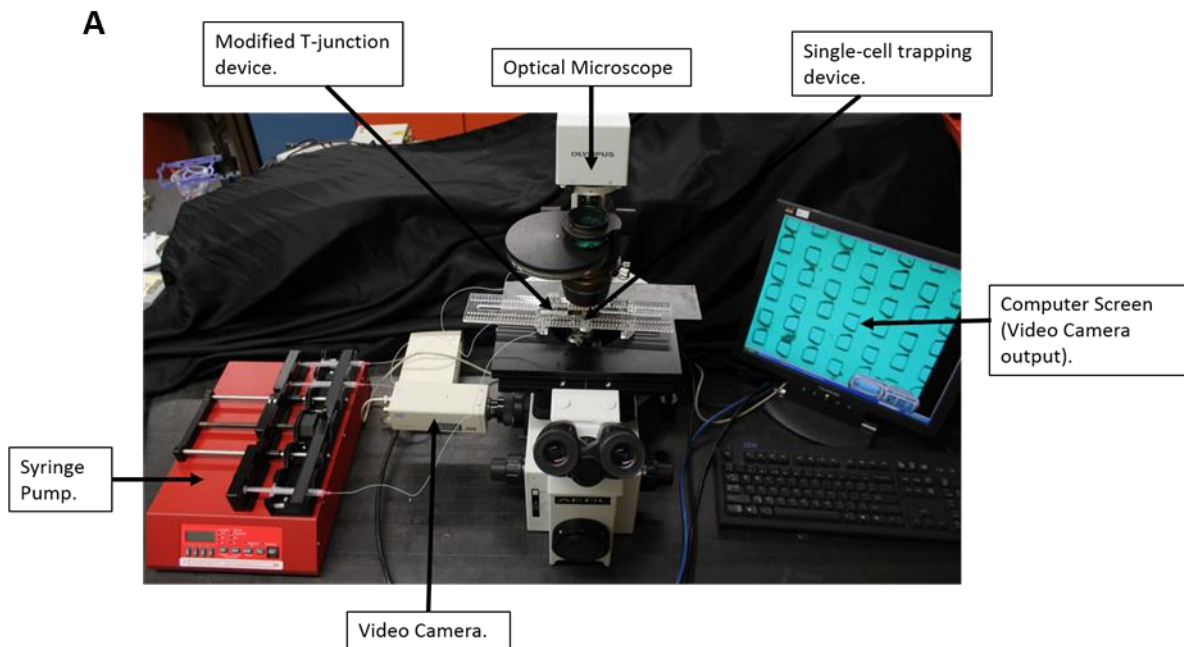
1. Prior to experimentation, the microfluidic channel walls of both PDMS devices (the trapping device and the microsphere producer) were rendered hydrophobic by inducing a constant flow of RainX® in the channels for 30min at 50 $\mu\text{l/hr}$ . Two syringe pumps (Multi-Phaser™ NE-1600 and Genie™ Plus) were used in order to feed fluids into the devices plus 3cc syringes and Teflon tubing.
2. Water-in-oil microsphere of more 20 $\mu\text{m}$  of diameter were produced using a modified T-junction device. In order to produce the microspheres, two phases are required. The continuous phase was paraffin oil (Sigma-Aldrich 18512) containing 2% (w/w) Span 80 (Sigma-Aldrich S6760), while the disperse phase was distilled water. The continuous phase was used as the focusing flow and the crossflow, and the disperse phase was used as the middle flow in the modified T-junction device. The interaction of these three flows at specific flowrates in the device, results in water-in-oil microsphere formation of different sizes which depend upon the flowrate selection of the flows. For instance, to produce microspheres between 20 $\mu\text{m}$  and 30 $\mu\text{m}$ , in this experiment the focusing flow was keep constant at 60 $\mu\text{l/hr}$ , while the middle flow was changed between 5 $\mu\text{l/hr}$  and 12 $\mu\text{l/hr}$  where a flowrate of 5 $\mu\text{l/hr}$  would result in microspheres of about 20 $\mu\text{m}$  and a flowrate of 12 $\mu\text{l/hr}$  on microspheres of about 30 $\mu\text{m}$ . The cross flow was modified along with the middle flow.



3. At the same time of microsphere generation, a constant flow at  $30\mu\text{l/hr}$  of paraffin oil was induced into the single-cell trapping device in order to remove the air and permeate the walls of the microchannels before the loading of microspheres.
4. The outlet of the microsphere generator device was connected by a Teflon tube to the inlet of the single-particle trapping chip, so that the recent formed microspheres would flow directly to the trapping device. The modulation of the traps was pre-set in relation to the size of microsphere to capture. For instance, in the mechanical tests it was found that the device has to be set on position zero (hole 0) to capture particles of  $20\mu\text{m}$ , at position 1 (hole 1) to capture particles of  $22\mu\text{m}$ , at position 2 (hole 2) to capture particles of  $24\mu\text{m}$ , and so on until reaching position 5.
5. After the introduction of microspheres into the trapping device, the trapping performance was observed through the microscope focusing in different areas of the trap arrays. It was observed that less than a minute is enough time for the device to fill all its traps; therefore, after couple minutes of loading cells the feeding of microspheres is stopped and replace it by a constant flow of paraffin oil at  $30\mu\text{l/hr}$ , so that the captured microspheres keep their trapping positions.
6. Several micrographs of various zones of the trap arrays were taken to show and prove the trapping properties of the device, followed by an analysis of the obtained images in Image J.
7. Once several images were taken, the flow of oil was reversed in the trapping device in order to extract all the trapped microspheres. The inversed flow was increased up to  $100\mu\text{l/hr}$  in order to speed up the extraction of the trapped microspheres.
8. Having all the particles extracted from the device, the microfluidic channels have to be cleaned. To clean the channels, the device is flushed with 70% ethanol at a rate

of 100  $\mu\text{l/hr}$  for about 5 min. Later the channels are optically examined under the microscope to determine whether the channels are cleared. If the channels are cleaned, then we proceed to the next test.

The above process was carried out six times in total (more trials were conducted, but only the most relevant results are here presented), one time per trap size increment. In total six batches with a different average size of microspheres were tested: 20 $\mu\text{m}$ , 22 $\mu\text{m}$ , 24 $\mu\text{m}$ , 26 $\mu\text{m}$ , 28 $\mu\text{m}$ , and 30 $\mu\text{m}$ . The equipment and setup used for this experiment is depicted and described below in figure 6.9.



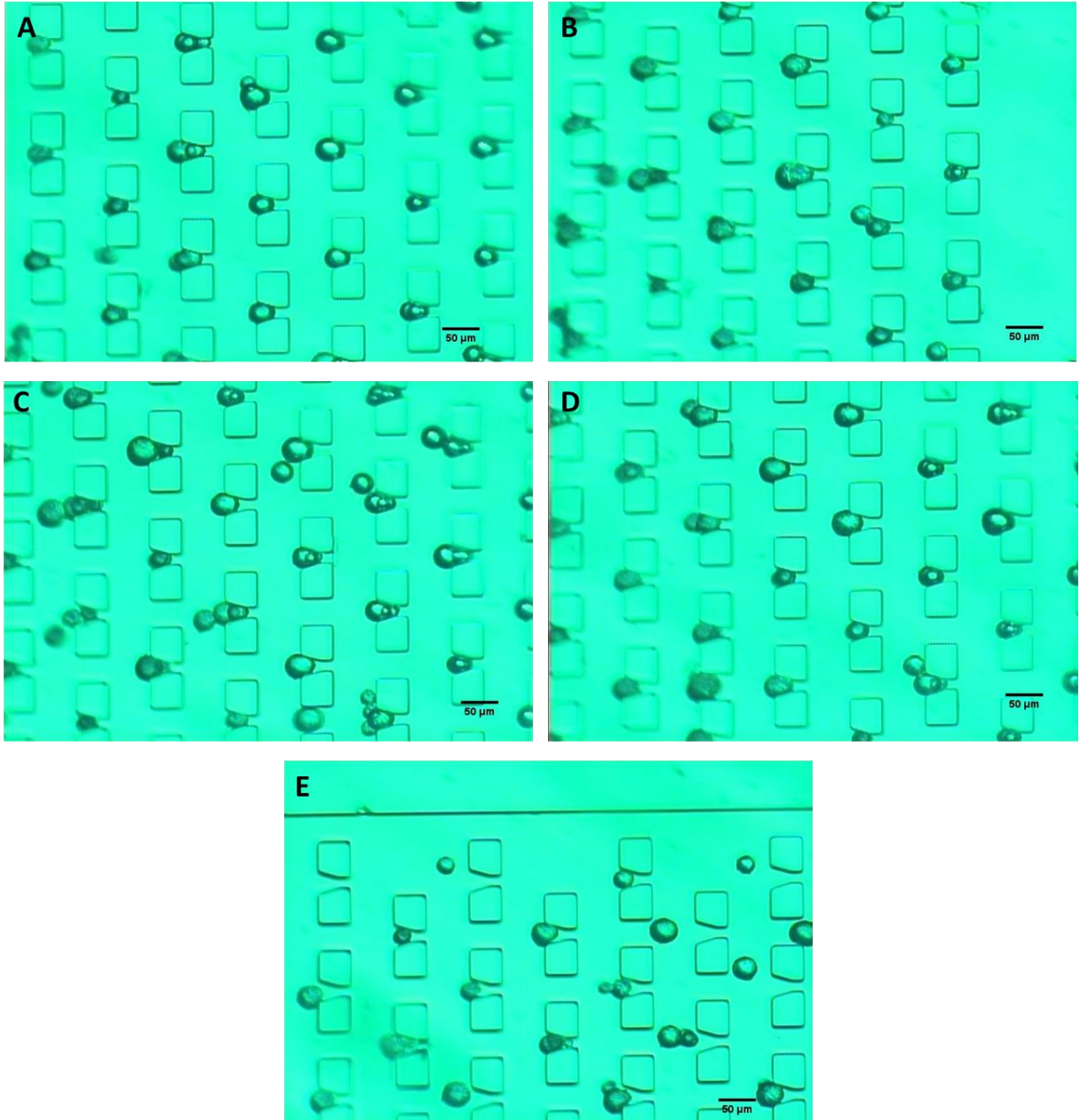
**Fig. 6.9** Picture of the equipment used to conduct Part I of experiment 2. In the picture (A), one of the two syringe pumps used is showed loaded with three plastic syringes (BD) of 3ml which are connected to the modified T-junction device for the microsphere production by Teflon tubing (two syringes were actually used during the experiments, this setup is just proposed as an example). The microsphere generator device and the trapping devices are located at all times under the optical microscope for visualization. A computer which is connected to the output of the video camera displays the image obtained by the microscope. Picture (B) shows in a close up, the modified T-junction device and the trapping chip, as well as, how these two are connected by a Teflon tubing to allow the direct flow of microspheres.

## **6.9 Experimental Results (Experiment 2: Part I)**

The following results are mainly the micrographs taken when microspheres were introduced into the microfluidic single-cell trapping device.

### **6.9.1 Trapping of single microspheres**

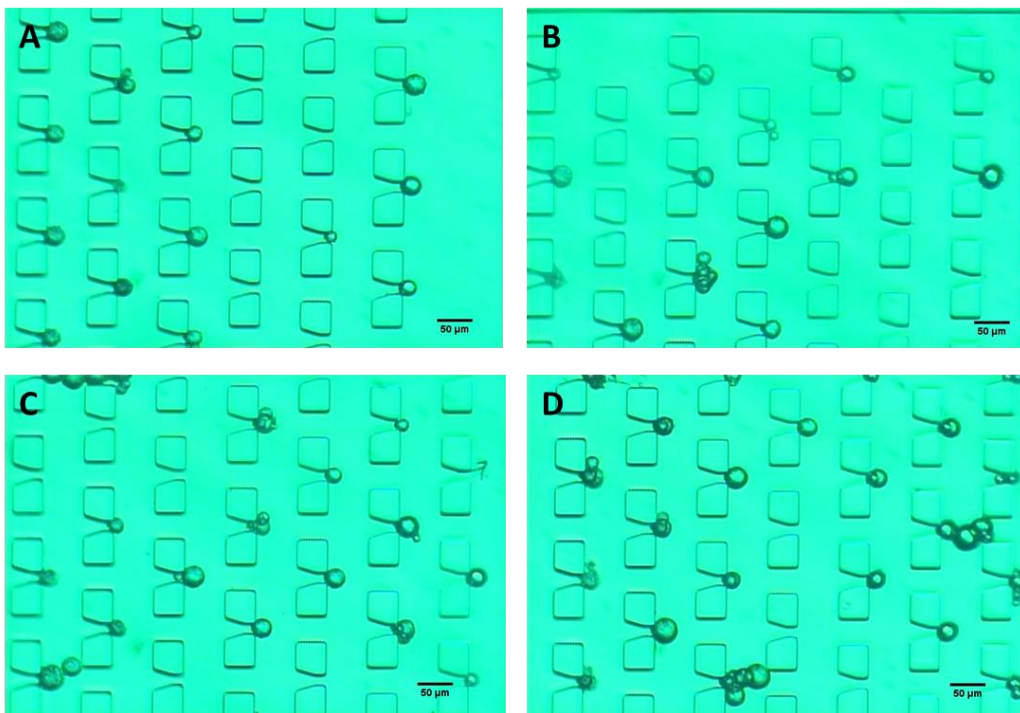
In this section some micrographs obtained when microspheres of about 20 $\mu$ m were introduced into the trapping device, are presented to simply demonstrate that the device is indeed capable of capturing large batches of single particles. As it was already said in the procedure, the input of the microspheres was conducted at 60 $\mu$ l/hr for couple minutes. In addition to the trapping images, some pictures taken during the extraction of the captured microspheres are also provided. The loading images can be seen in figure 6.10, and the releasing images on figure 6.11.



**Fig. 6.10** Micrographs showing the trapping of single 20 $\mu\text{m}$  particles at various zones of the trap arrays. In (A) most of the traps are filled with a single microsphere, while in (C) several traps captured multiple particles. (E) and (C) shows that undesired particles larger than 20 $\mu\text{m}$  were captured. However, among all the images single trapped microspheres predominate.

From figure 6.10 some important discoveries emerge. First, it is confirmed that the device, at least without deformation, is capable of capturing single particles within the traps. Second, during the loading process it was observed that the device complies with the hydrodynamic trapping principle of “least path resistance”; however, the interaction among particles also plays a big role in the trapping performance. Third, unfortunately several sizes of microspheres were introduced into the device which might result in undesired effects on the trapping function, such as trapping of multiple particles and clogging of the channels. Next, very few traps remained empty at the end of the loading process; it was observed that the empty traps were mainly those on the lateral ends of both arrays. Also it was noticed that at the entrance of the trap arrays the flow of microspheres is quite chaotic, but the flow recovers its laminar behaviour as the microspheres move on through the device.

When inverting the flow to release the captured microspheres, the following results were obtained (Fig. 6.11).



**Fig. 6.11** Micrographs showing the release of previously trapped microspheres at various zones of the trap arrays. In all the micrograph here presented it can be seen than all the traps

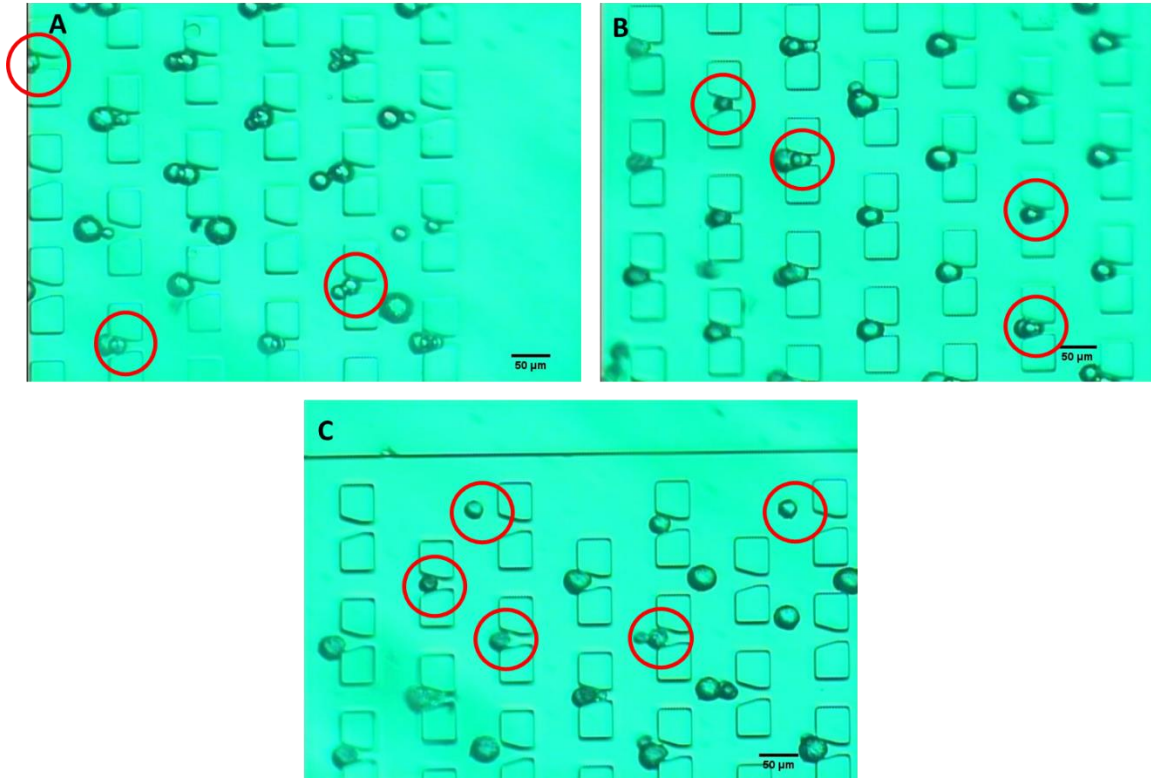
are empty due to the reversed flow; however, many microspheres are retained at the rear of the traps.

In figure 6.11 it can be seen that the device has a low release efficiency since many of the particles remain within the arrays. Although all the microspheres are removed from the traps, many of them are recaptured by the rear opening (exit) of adjacent traps. Therefore, in order to extract all the particles several iterations of the releasing process have to be done.

### **6.9.2 Trapping of single microspheres of different sizes.**

Having corroborated that the device is capable of capturing single particles, it was necessary to test whether the device is capable of working with different batches that vary on their particle average size when the size of the traps is tuned. To test the trapping behaviour at different strains, the device was stretched gradually from hole 0 to hole 5, and on each position, microspheres corresponding to the trap size were introduced. The following results depicted in figure 6.12 to figure 6.17 are organized according to the size of particle fed, and by the extension applied on the device, starting from none deformation of the traps up to the maximum deformation achieved when the clamp holding the trapping device is placed at hole 5 of the stretching apparatus.

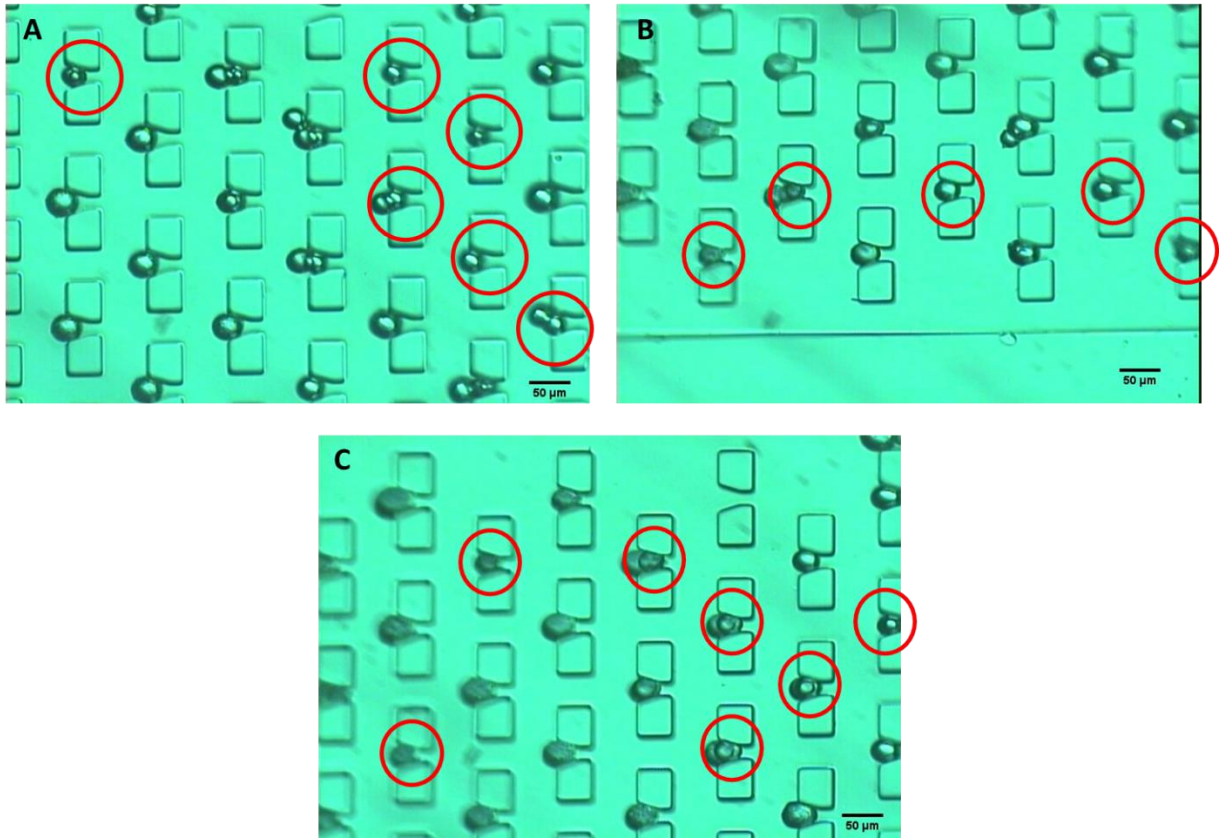
1. Trapping device position: 0 / average microsphere-size input: 20 $\mu$ m.



**Fig. 6.12** Micrographs showing the capturing of single particles at different zones of the trap arrays. The red circles highlight particles with a diameter of  $20\mu\text{m}$  or close.

2. Trapping device position: 1 / average microsphere-size input:  $22\mu\text{m}$ .

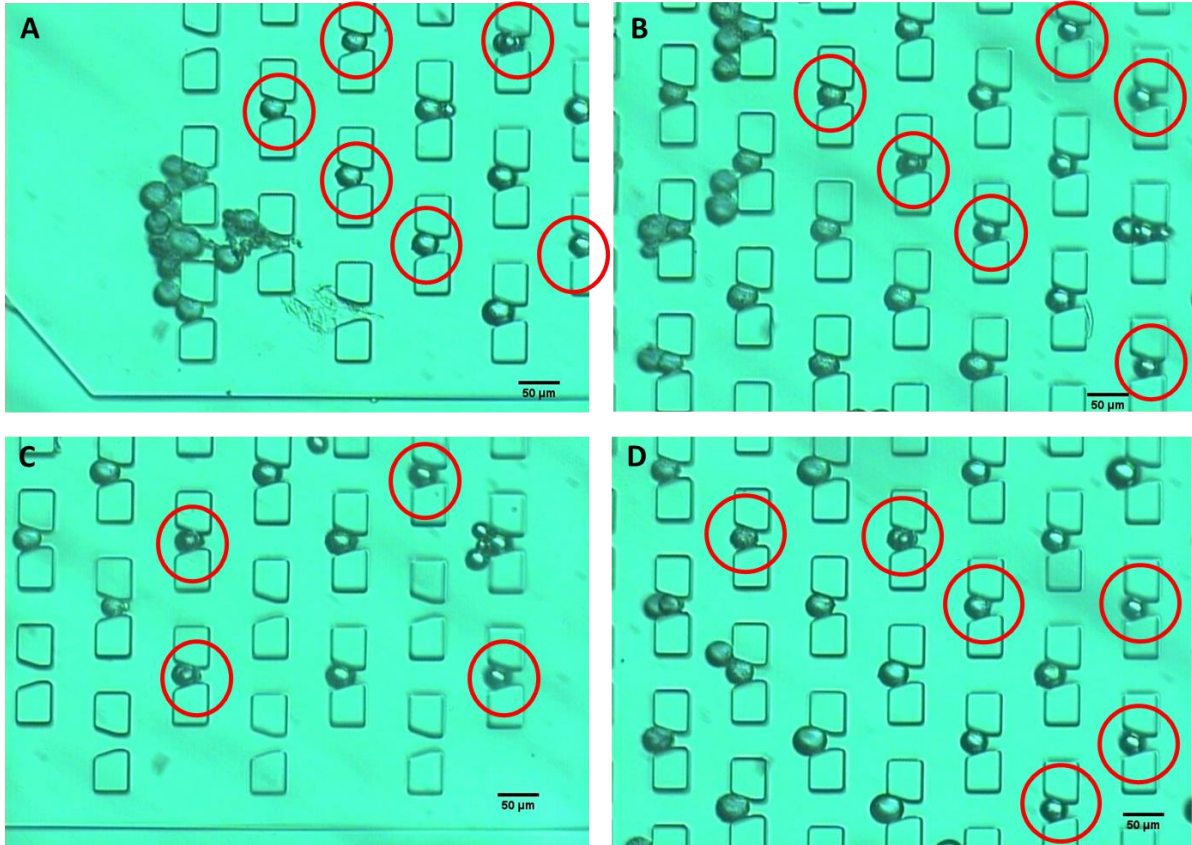




**Fig. 6.13** Micrographs showing the capturing of single particles at different zones of the trap arrays. The red circles highlight particles with a diameter of  $22\mu\text{m}$  or close. Among the three images showed it can be seen that some traps have two microspheres; however, they are highlighted because one of the microspheres has the ideal size.

3. Trapping device position: 2 / average microsphere-size input:  $24\mu\text{m}$ .

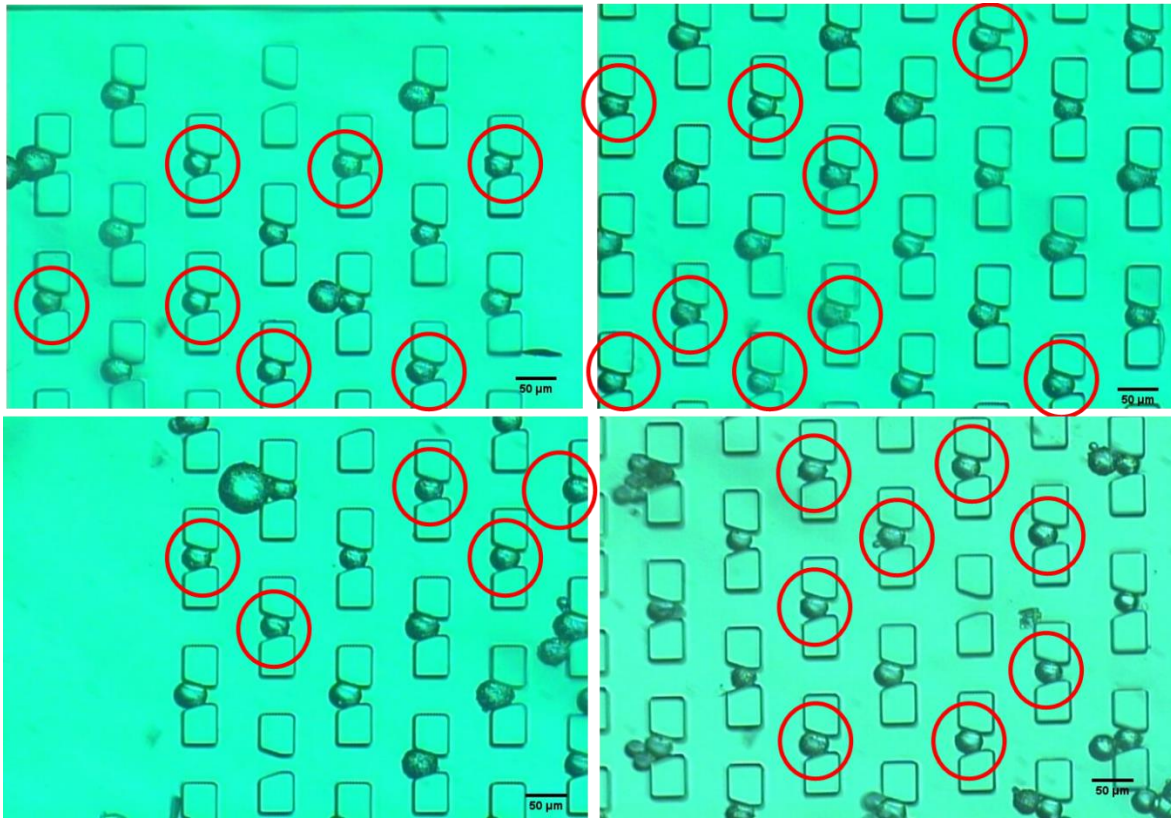




**Fig. 6.14** Micrographs showing the capturing of single particles at different zones of the trap arrays. The red circles highlight particles with a diameter of  $24\mu\text{m}$  or close.

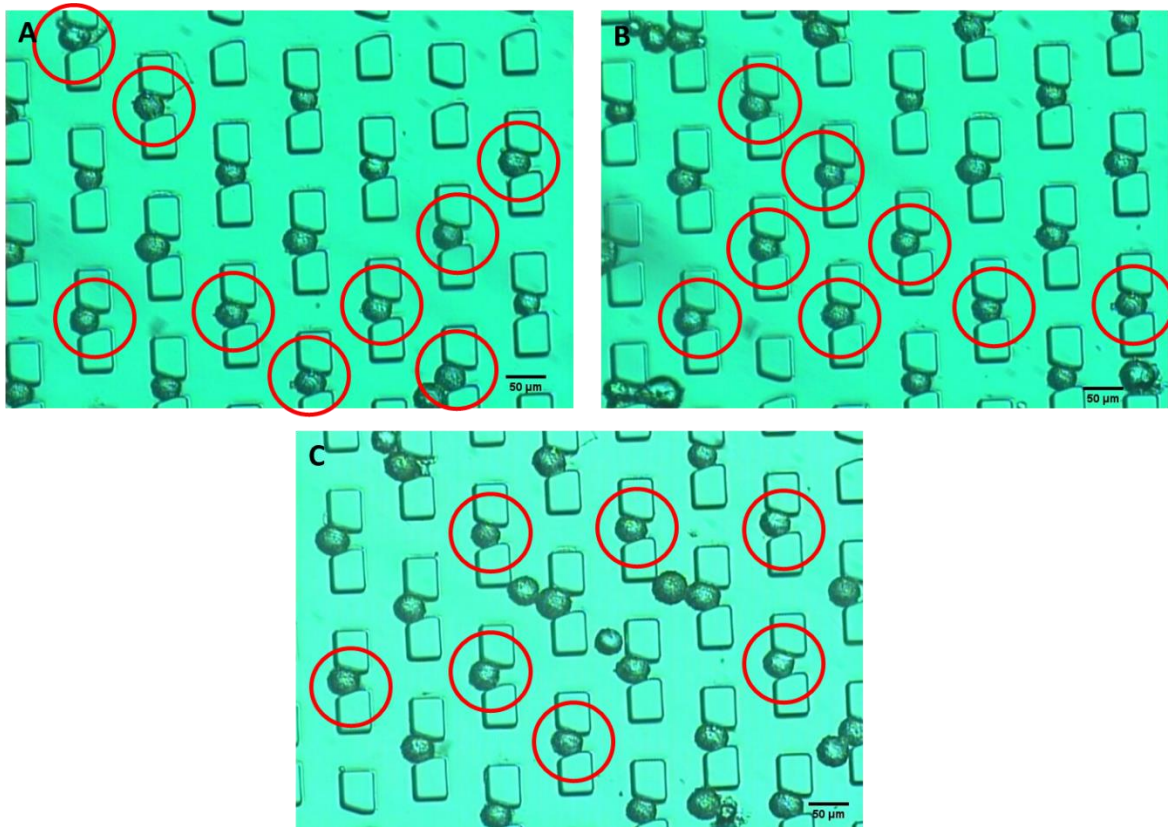
In image (A) of figure 6.14 a big clog of microspheres is observed. This picture exemplifies the issue observed due to the small distance between the inlet channel and the trap zones. Also notice that the size of the particles is more regular in comparison to previous images, which shows that when producing the microspheres, it was very difficult to obtain and control the size of small microspheres such as the ones with a diameter of  $20\mu\text{m}$ .

4. Trapping device position: 3 / average microsphere-size input:  $26\mu\text{m}$ .



**Fig. 6.15** Micrographs showing the capturing of single particles at different zones of the trap arrays. The red circles highlight particles with a diameter of 26 $\mu\text{m}$  or close.

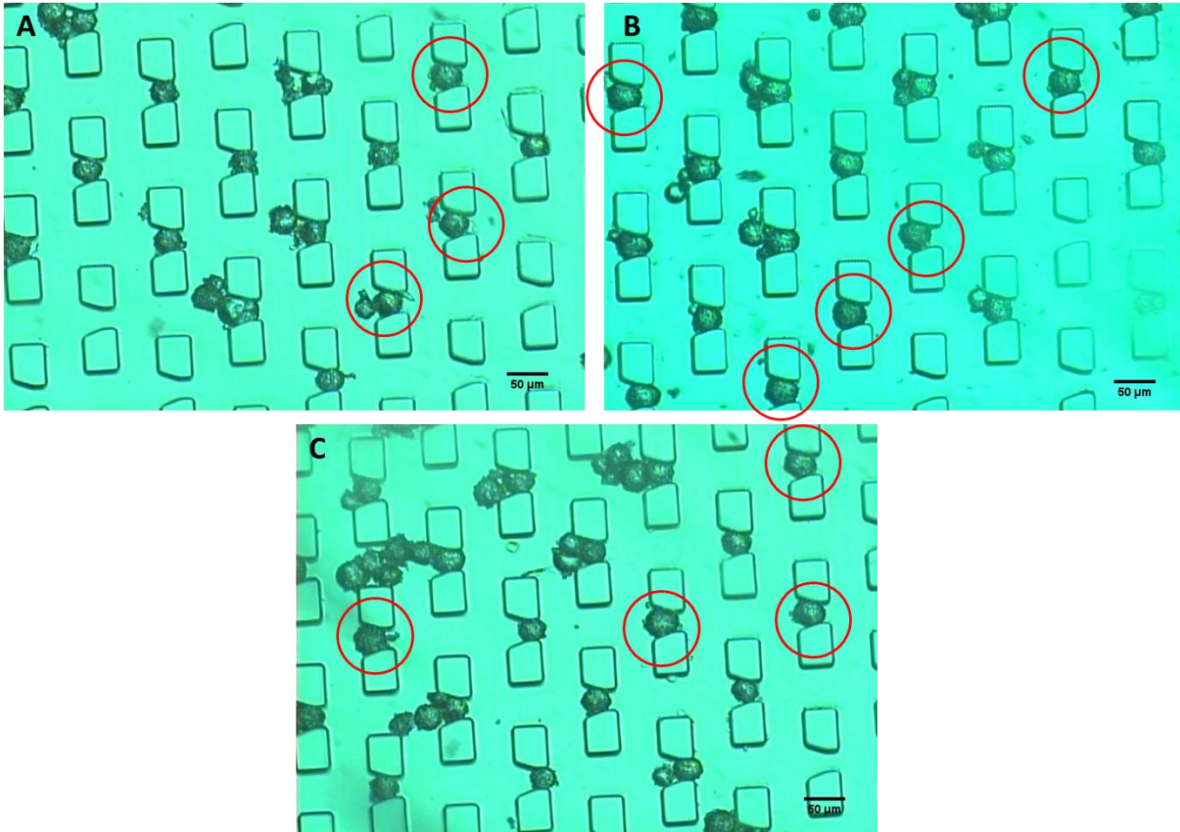
5. Trapping device position: 4 / average microsphere-size input: 28 $\mu\text{m}$ .



**Fig. 6.16** Micrographs showing the capturing of single particles at different zones of the trap arrays. The red circles highlight particles with a diameter of  $28\mu\text{m}$  or close.

6. Trapping device position: 5 / average microsphere-size input:  $30\mu\text{m}$ .



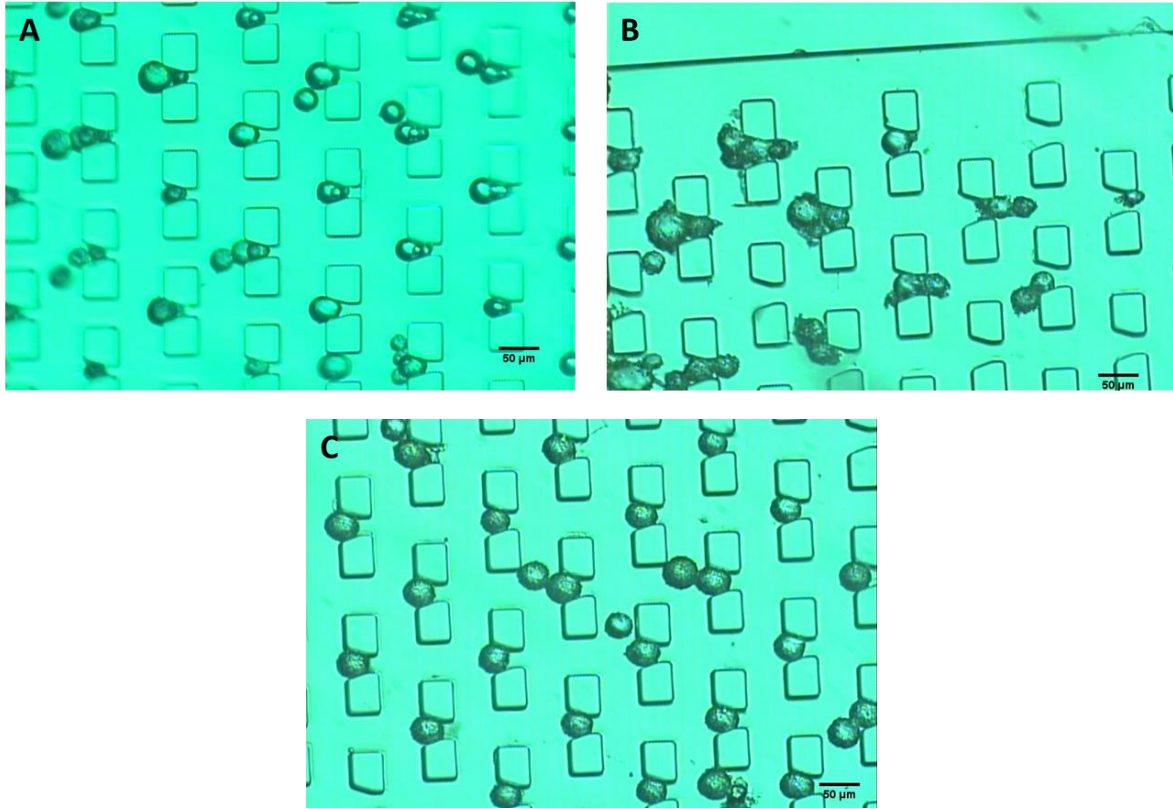


**Fig. 6.17** Micrographs showing the capturing of single particles at different zones of the trap arrays. The red circles highlight the particles with a diameter of  $30\mu\text{m}$  or close.

It was already mentioned that unfortunately the size of microspheres produced was difficult to control, in particular the smaller sizes like  $20\mu\text{m}$ . For this reason, a variation of sizes is observed in all the micrographs presented above. However, this issue should not diminish or refuse the fact that the device can capture particles of various sizes when the traps are modulated. In addition, every time that the device was stretched to produce a large size of trap the trapping behaviour of the device remains the same; i.e., along the experiment no notable differences were observed on the trapping performance, except for some issue related to the size of particles used. For example, when particles of  $20\mu\text{m}$  or less were introduced into the device it was detected that a considerable number of traps corralled multiple particles, and when larger particles of  $30\mu\text{m}$  were used several channels were clogged. Nonetheless, this behaviour

was expected since these situations occur at the limit size operation of the device, where the particle to trap size ratio is critical. In the lower limit the device has big traps with a height that can fit two particles of  $20\mu\text{m}$ , and at the upper limit the bypass channels or gaps between traps and rows of traps are reduced in size, so bigger particles than  $30\mu\text{m}$  will more likely get stuck, as depicted in figure 6.17 (C).

Among all the micrographs displayed above, it can be seen that the traps captured microspheres of various sizes without the need of any adaptation or modification. Therefore, the following question is forwarded. Is it really necessary to adapt the size of traps in order to trap various sizes of particles? The answer is yes for two main reasons. First, with smaller particles the traps will more likely capture multiple particles per trap or the particles could escape the trap. Second, if particles larger than the optimal size are used, they would get stuck in the channels clogging them. These undesired situations, depicted in figure 6.18, are overcome by using an adaptable trapping device such as the one presented in this thesis.



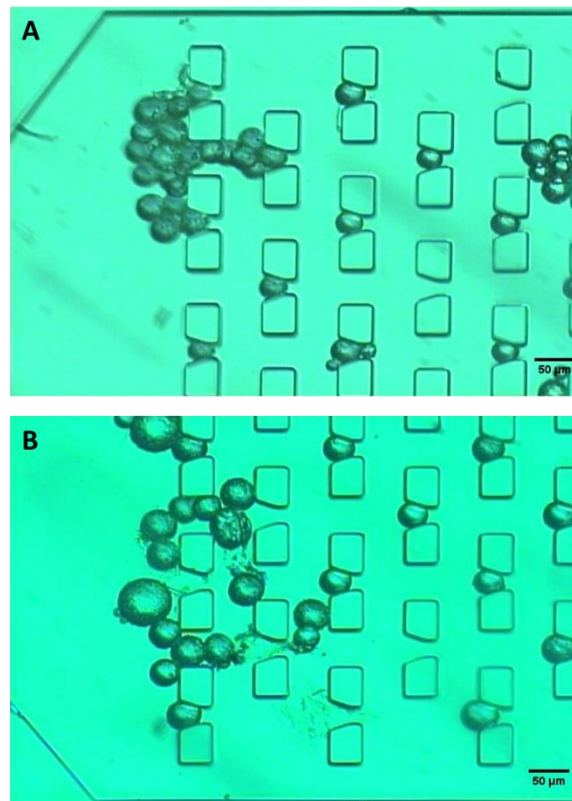
**Fig. 6.18** Traps filled with multiple particles, particles escaping traps, and clogged channels are common issues that occur when an improper size of particle is used. Image (A) shows several traps filled with two or more microspheres. In (B) it can be seen how some small microspheres are flowing out the traps through the trap's exit. (C) depicts some channels blocked by large microspheres trying to go through the same channel. Although the big particles are captured within the trap, half of its body protrudes out of the trap narrowing the microfluidic channel.

### 6.10 Discussion (Experiment 2: Part I)

Although the trapping device performs its main function of capturing large batches of single particles of different sizes when its trap dimensions are modulated, reasonably well as evidenced by the results, some issues during the process were encountered. The trapping function was supposed to be mainly governed in theory by the hydrodynamic working principle of "the least path resistance"; however, during the experiments the random interaction among

the particles flowing at the same time through the arrays did play an important role on the trapping performance. Therefore, it was empirically speculated that the device, as it is right now, works better and fills more traps when large concentrations of particles are used. On the other hand, large amounts of particles flowing through the micro-channels at the same time could clog the smaller channels. To avoid this, the loading process has to be supervised all the time, so the feeding could be stopped when most of the traps are filled.

An important drawback of the device that has to be improved in the future is the small distance between the inlet-channel exit and the first row of traps in the arrays. Such a small distance does not allow the flow to recover its laminar behaviour after the channel expansion, so the microspheres arrive to the array at high speeds and disorderly, which results in huge agglomerations of microspheres at the first row of the array that clog the channels and the traps. This is depicted in figure 6.19.



**Fig. 6.19** Micrographs showing massive clogs of microspheres at the first row of the arrays. Image (A) was taken at array A2 when microspheres of 24 $\mu\text{m}$  were introduced into the device. The clog depicted on (B) was developed when microspheres of 26 $\mu\text{m}$  were used; here it can be seen that larger microspheres help on building up such huge obstructions.

Regardless of the issues just discussed and the difficulties faced to produce microspheres with low size variations, it has to be recognized that the main objectives of the experiments of demonstrating that the new trapping device can capture single particles and that the deformation of the traps actually works in order to capture larger particles with the same trapping performance, were met.

### **6.11 Experiment 2: Part II**

In part I of this experiment, the trapping performance of the new cell-trapping device was evaluated using water-in-oil microspheres. Now in part II, as previously mentioned, the second aspect related to the compliance of the traps is assessed. It was mentioned earlier that the traps must not only capture single cells, but also capture them on a safely manner. In other words, the trapped cells within the traps must remain alive. Thus, the single objective of this second part of experiment two is to demonstrate that the new device in particular its traps do not produce any damage onto living human cells when introduced into the microfluidic device.

### **6.12 Experimental Procedure (Experiment 2: Part II)**

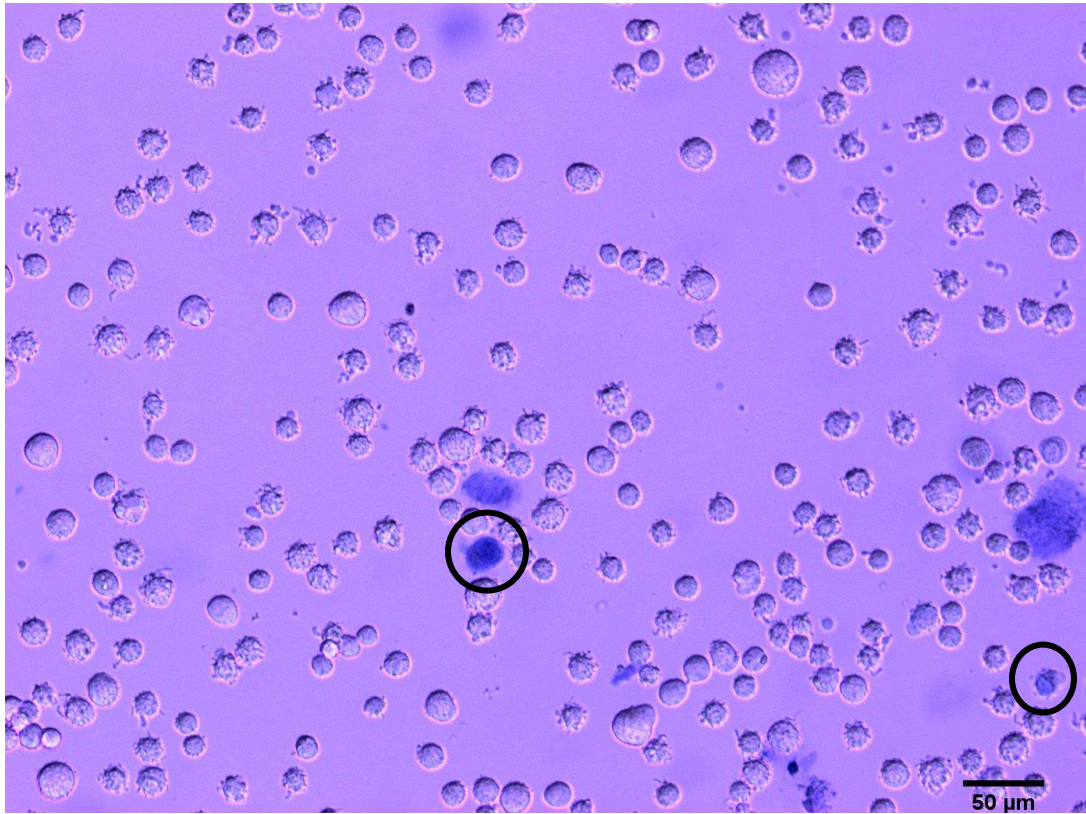
In order to achieve the above objective, melanoma human cells obtained from the College of Pharmacy and Nutrition of the University of Saskatchewan, were fed into the device as a cell solution, and their viability within the traps was determined using a dye exclusion method. The dye used was Trypan-blue, which is a vital stain used to selectively colour death cells blue. In addition, all the steps and procedures of this experiment were conducted in a Level 2 safety lab



in the department of Pharmacology. Briefly, melanoma cells were cultured in culture flasks with fetal bovine serum (FBS) for 7 days to obtain a large population of healthy cells. Prior to the trapping experiments, the cells were detached from the flask by removing the FBS, and adding trypsin to deactivate the FBS. Then the trypsin was replaced with fresh trypsin and let it repose for 2 to 3 minutes. To neutralize the trypsin, same amount of FBS (10ml) was input in the flask followed by the collection of the detached cells. The cell solution obtained from the flask was centrifuged for 5 minutes at 5°C. Finally, the cells were collected and re-suspended in fresh culture media (FBS) at a cell concentration of approximately 2 000 000 cells/ml. In order to conduct the trapping experiments, the procedure outlined below was followed.

1. In the biosafety cabinet (BSC) the microfluidic cell-trapping device was incubated with fresh culture media (FBS) for about 20 min. The culture media was input into the device at room temperature, of approximately 25°C at a flowrate of 60µl/hr.
2. A sterile syringe of 3cc was fully loaded with the cell solution and mounted on the syringe pump. Since the cells in the syringe tend to sediment on the bottom, the pump was tilted to 60°, so that the cells would concentrate on the outlet of the syringe.
3. In order to determine the cells viability after the capturing process a control sample was taken from the cells in the syringe and observed under the microscope to determine whether the cells in the syringe and about to be introduced in the device were alive (Fig. 6.20) After optical evaluation, the sample was taken to a cell counter machine which determined that 98% of the cells in the solution were alive.
4. During the incubation of the microfluidic channels with FBS it was observed the formation of air bubbles. Therefore, the process had to be supervised at all times to avoid this phenomenon.

5. After the channel's incubation period with FBS, the input of the device was replaced it with the cell solution. The cells were introduced at  $30\mu\text{l/hr}$ . for couple min. It has to be mentioned that the loading time sometimes increased due to the formation of air bubbles within the device, which retarder the process. However, when air bubbles were avoided the loading process was very fast.
6. Once the cells were loaded into the trapping device, the device was taken out of the BSC to be examined under an optical microscope and observe whether or not cell were corralled in the traps.
7. If a considerable number of cells were docked in the traps, the next step was carried out; otherwise, the loading process was continued until reaching a considerable number of trapped cells.
8. The input of the device was replaced by the syringe containing the vital dye. Previously a 3ml syringe was loaded with trypan-blue dye. The trypan-blue was introduced at a flowrate of  $20\mu\text{l/hr}$  for 1 min.
9. Once it was observed that the trypan blue had filled all the channels, the trapping device was taken now to another optical microscope equipped with a camera to take micrographs of the trapped cells. The trypan blue syringe was taken along with the device without plugging it out to avoid the reverse of the flow.
10. Finally, the viability of the trapped cells was determined thanks to the dye. If the cells were alive the dye should not have penetrated their membrane, remaining transparent.



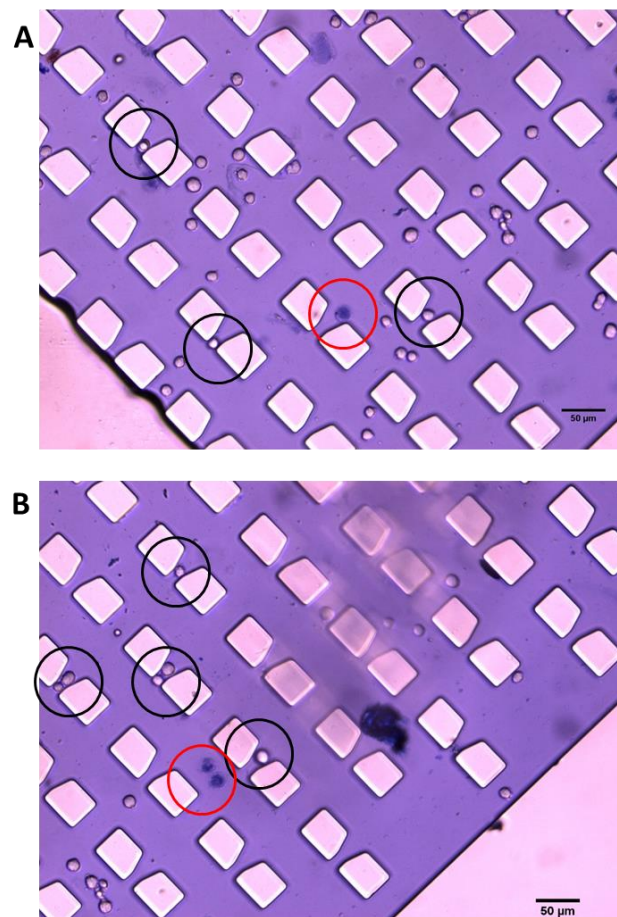
**Fig. 6.20** Micrograph of a sample of melanoma cells. The cells were placed on a microscope slide flowed by the addition of a drop of trypan blue. The black circles highlight two cells stained on blue which are actually death.

### 6.13 Experimental Results (Experiment 2: Part II).

Before proceeding to the results, it is important to notice that the size of the melanoma cells is smaller than the ideal particle size for which the device was designed; therefore, it is expected to have a very low number of cells captured or have traps with multiple cells. The average size measured for the used cells was about  $13\mu\text{m}$  being the smallest, of approximately  $10\mu\text{m}$  and the larger of  $18\mu\text{m}$ . Regardless of this known disadvantage, the experiment was still carried out to demonstrate that the device is capable of working with living cells, and it is assumed that the device should work the same if it is just rescaled down to work with smaller particles of dimeters between  $7\mu\text{m}$  to  $17\mu\text{m}$ .

Although the result of this part of the experiments only consist of a couple of micrographs of the trapped cells after being stained with trypan blue, the real output obtained from them is of great value for this investigation.

The micrographs depicted in figure 6.21 show some cells within the device, few of them were trapped and many other were not, as expected. Moreover, after introducing trypan blue to assess their viability, as it can be seen, it was found that the cells were alive and therefore viable for further analyses within or out of the device.



**Fig. 6.21** In pictures A and B very few single cells were captured by the traps. (B) shows couple traps with multiple cells and only one trap with a large cell properly captured (black circles). Only couple cells were found death and they are highlighted by the red circles.

From figure 6.21 above two very important inferences can be made. First, the new cell-trapping device is capable of capturing cells as it did with the microspheres, even when the device was not designed to work with such a small cell sizes. Second, the device features and operation does not damage living cells, making it an option for actual experimentation with living cells.

#### **6.14 Discussion (Experiment 2: Part II)**

The experiments to determine the viability of the cells, were restricted and limited by the equipment and setup used. In particular, it was difficult to control the trapping device without supervising the loading processes through a microscope as before. Unfortunately, it was not possible to have a microscope inside the biosafety cabinet due to its architecture and design. This limitation resulted in not obtaining the best micrographs because the capturing process was done “blind”. Also, the device had to be constantly moved from the BSC to a microscope outside, which might have resulted arguably in disturbances on the cells already captured.

In addition, it was observed during the incubation of the microfluidic channels with culture media (FBS) that air bubbles tend to form within the device, which never happened when using paraffin oil in the previous experiments. This was surprising also because such phenomenon was not reported on any of the previous research works reviewed on the literature review. In order to overcome this air bubble issue, the culture media was warmed up to the room temperature. Although the problem was slightly reduced, it was not eliminated. Thus, this issue becomes another point to solve for a new optimized and improved cell trapping device.

#### **6.15 Conclusion**

The results were divided in three sections which correspond to the three main attributes that a new adaptable single cell-trapping device must meet in order to comply with its desired function. Therefore, several experiments were conducted in order to prove that the new cell-

trapping device is characterized by: (A) deformation of the elastomeric polymer (PDMS) feasible to stretch, (B) compliance of the traps, and (C) uniformity of the deformation of the traps.

On regards of attribute A, it was found that the trapping device is capable of being stretched 25mm without presenting plastic deformation. Such stretch represents a strain of 0.48 which results in a deformation of the traps, of approximately 80%, which is equal into an increment of 10 $\mu$ m in their size.

Considering attribute C, it was found that the minimum trap-size increment possible with the stretching apparatus, is of 2 $\mu$ m, and the deformation of the traps is uniform through all the traps.

On the other hand, for attribute B, the trapping results demonstrated that every time that the size of the traps is modulated by stretching mechanically the device, it is capable of capturing single particles (water-in-oil microspheres) of various sizes which goes from 20 to 30 $\mu$ m. The compliance of the traps was also evaluated using melanoma cells, and the experiments showed that the device does not produce visible damage to living cells.

During the experiments some unexpected behaviours of the device operation were found. For instance, it was determined that the device performs better when high-concentration of particles are used as inputs because the trapping function is characterized by the hydrodynamic trapping principle and the random interaction among particles. It was also found that air bubbles tend to form when culture media (FBS) and cells are introduced into the microchannels, which have negative impacts on the device performance. Nevertheless, the results demonstrate that the device meets all the proposed attributes and it is an option to be used on biological analysis.

## CHAPTER 7: CONCLUSION AND RECOMMENDATIONS

### 6.9 Overview

Microfluidic technology has gained ground last two decades in biological and medical research, where several analysis and assays require separation, isolation, positioning, trapping, and sorting of various types of cells. In particular, microfluidic cell-trapping devices based on hydrodynamic principles, which are capable of capturing, isolation, and positioning have been widely reported in the literature. However, it has been found and reiterated their lack of flexibility to adapting to different types of cell sizes, which limits their operation to a fixed size of particle. This results in a waste of time and resources, because new devices have to be designed and fabricated for each different size of cell that wants to be studied or analyzed. Thus, the idea of investigating the possibility of developing a microfluidic device capable of adapting its geometrical features to deal with more than a fixed particle size, arose.

This thesis has then proposed the design and development of a new adaptable microfluidic single-cell trapping device capable of capturing large batches of single particles within a wide range of sizes. Since in the beginning some limitations were foreseen; for example, it was mentioned that the range of sizes would be limited, and that the experimental tests would be conducted using microspheres. However, it was also clearly established that these decisions should not interfere with the verification of the device functionality. These considerations, also, obey to the intrinsic limits of this research such as resources and time.

The new and unique device proposed in this thesis, as a general objective, was designed, fabricated, and tested in accordance to the methods found in the literature.

This chapter will consider the objectives of the research and will compare them to the results obtained to demonstrate how they were met and present conclusions that arise from each. In addition, contributions of the work will be summarized and a discussion on future work will be also provided.

## 7.2 Outcome

The general objective of this research was as follows (Section 1.5): to design a new microfluidic cell-trapping device capable of modifying its features in order to capture multiple single-cells of different sizes without compromising its capture efficiency. The general methodology is to apply a uniform distributed strain on the device via a mechanical stretching. Therefore, the key attributes of such a device include: (A) the deformation of the elastomeric polymer (PDMS) feasible to stretch, (B) compliance of the traps, and (C) uniformity of the deformation of the traps. This general objective was attempted considering the following specific objectives and conclusions.

**Objective 1:** Analysis of the existing principles of single cell trappers to lead to the classification of the principles with their pros and cons;

This was achieved in Chapter 2 through a literature review, in which the most relevant devices reported were analysed and classified under the FCBPSS framework. It was concluded that, the best and more suitable structure and trapping principle for a new device is the array of traps and the hydrodynamic trapping principle of “less path resistance” respectively due to their simplicity and efficiency on capturing single cells. In addition, the literature review has shown that very little has been published on adaptable trapping devices, such as the one presented in this thesis.

**Objective 2:** Development of a simulation system for the device, as well as its deformation process, to guide the design optimization;

The mechanical simulation of the new design was conducted using ANSYS to predict the deformation of the traps and the microstructures, and to determine numerically the maximum strain possible to applying before exceeding the elastic region. This point was very important and represented a keystone for the design because if the material (PDMS) results not to be adequate for the large deformability desired, the whole design or tuning method would have to be rethought. On the other hand, Fluent was employed to create a simulation model of the flow



profile in order to characterize the flow of the cells within the microchannels, and to determine the wall shear stress exerted on the cells, which has to be lower than 4.5 Pa as determined by Dimmeler et al. (1996) to guarantee their viability. By the results obtained from the models it was concluded that both mechanically and hydrodynamically the design proposed in Chapter 3 complies with all requirements originally established.

**Objective 3:** Design of the device to achieve a large deformation as possible (which is at least a size increment of 60% on the traps) and a uniform deformation of each trap;

This part of the study is directly related to the experimental section (Chapter 6) where not only Objective 3, but also the three attributes A, B, and C proposed in the general objective were addressed. In order to demonstrate and confirm the deformation of the traps (attributes A and C), the cell trapping device was induced to various strains and the resulting increment size in the traps was measured at different locations of the arrays. The results obtained confirmed that the traps experienced a maximum relative size-increment of 80%, and the deformation of the traps is the same and uniform throughout the entire device. Finally, the compliance of the traps, which is related to attribute B, was addressed on two parts. First, the trapping behaviour of the device was tested using water-in-oil microspheres between 20 $\mu$ m and 30 $\mu$ m of diameter. Second, melanoma cells were used to determine their viability after being fed and captured by the cell trapping device. It was concluded that the device in particular its novel property of trap modulation could be used in biological applications and medical researches where within the cell type to study, various cell sizes are encountered.

**Objective 4:** Development of the fabrication approach to the device in accordance with the design specifications resulting from the research in objective 2;

After designing and defining the characteristics of the device, it was determined that soft lithography in particular a replica molding process would be a suitable microfabrication process to fabricate the PDMS device. On the other hand, the stretching apparatus and all its components were fabricated by a traditional CNC machining process. The conclusion was that a

novel microfabrication process was not necessary to fabricate the device, which is an advantage because it reduces the time and cost of fabrication making the device suitable and affordable for research applications.

### **7.3 Discussion on the Limitations of Using Microspheres instead of Cells**

As mentioned several times throughout this document, due to several considerations, the device was designed to test its trapping function using water-in-oil microspheres. Whether this affected or interfered with the validation of the device trapping function, might remain unclear. However, supported by other studies presented in the literature review (Chapter 2), biological cells can be replaced for microspheres. Indeed, some devices were before tested with microspheres, such as the ones presented by Tan and Takeuchi (2006) and Lawrenz et al. (2013). Moreover, to reduce this skepticism regarding the trapping of cells, experiments with real cells were conducted. And it was concluded that the device is in fact suitable to work with cells, and there is not clear evidence found to not saying that it should behave similarly as it did when using microspheres. Still, the device has to be rescaled to work with smaller cells, and be tested in a biological assay, which is a point proposed as a recommendation for future work.

### **7.4 Conclusions**

Based on the outcomes of this research, it was concluded that microfluidic devices that relay solely on hydrodynamic principles are simple but efficient on capturing single particles. Also, it was determined that within the different types of cell trappers the ones using arrays of traps are the best when large batches of single particles are considered. As a result, the new adaptable trapping device presented in this thesis bears two arrays of traps.

The experimental results obtained showed that the silicone PDMS is capable of large elastic deformation, even molded in different shapes and therefore it was ideal for the application proposed in this thesis. In addition, it was concluded that the traps were able to

increase their size uniformly in all the regions of the arrays when mechanically stretching the device.

After conducting experiments with microspheres, it was surprising to find out and conclude that the trapping behaviour of the device depends in great measure on the multiple physical interactions of the particles flowing at the same time through the channels; rather than on the hydrodynamic principle of least path resistance. This opens the opportunity for optimization of the trapping function in the future. It was also concluded that the trapping performance of the device was not affected when the size modulation of the traps was conducted, and the traps actually were capable of capturing batches of single particles each time the batch particle-size was increased. This is the most important conclusion because the main objective of this research was to demonstrate that it is possible to have a trapping device capable of modulation to work with various sizes of cells, and not with a fixed size as all the previous cell-trapping devices published. Currently, in order to capture large batches of single cells or particles that vary on size one has to change the trapping device; however, with the device resulting from this research it is possible to work with different particle-sizes by simply tuning the size of the traps using the stretching apparatus. For the device here presented the average particle-size of the batches has to be within a range between 20 and 30 microns, and the particles have to be sorted considering their size previous to be feed into the device.

A possible sorting application of the device was observed. Although the function of the microfluidic device designed is to trap large batches of single cells, due to its adaptive quality and its traps, it was found that the device might be able to work also as particle-size sorter. The device could work as a particle-size sorter thanks to the geometry of the traps. Since the traps have an exit channel, particles with a smaller diameter than the channel cross section can flow through the traps without being captured. Moreover, the device is capable of increase the size of the traps by stretching it, so it could sort larger particles. For instance, suppose that one is interested in obtaining or separating only the particles with an average diameter larger than 15

$\mu\text{m}$ . Then if a batch with mixed particle diameters is fed, only the particles larger than  $15 \mu\text{m}$  will be captured by the traps, while the rest will flow through the traps. Once all the traps are filled, one can remove the trapped particles in the device by simply reversing the input flow, and maybe repeat the process. Due to the adaptability feature of the new device, also larger particles could be sorted. For example, consider now the case where only particles larger than  $20 \mu\text{m}$  are desired. Then, simply one has to tune the size of the traps in order to capture particles of  $26 \mu\text{m}$ , which will result on an exit channel of  $18 \mu\text{m}$ . Therefore, when particles of various sizes are fed at the same time, only particles larger than 20 microns will remain in the traps. Again one can repeat the process to sort more particles. Thus, the device could work as a particle-size sorter by discriminating of particles smaller than the size of the exit channel of the traps.

Finally, experiments with melanoma cells were conducted in order to assess whether living cells would experience any negative effect or damage due to the trapping process within the device. It was concluded that the device does not represent any observable threat to the cells when they are captured within the traps, which makes the device to be a suitable platform for biological or medical applications.

## **7.5 Future Research Recommendations**

The following recommendations for future work on this new trapping platform or on the seek of better cell trapping devices, were drawn from the experiences obtained and the behaviors observed during the tests the device.

### **7.5.1 Design Modifications**

Increasing the space between the exit of the inlet channel and the first row of traps in the arrays will help the incoming flow recover its laminar behaviour and thus solve the problem of massive concentrations of particles at the first row of traps (Section 6.7.3). Also, changing the

rear side of the traps should improve the extraction of the cells from the device. It is recommended to change only the vertical rear wall to an angle of  $110^\circ$  as proposed by Huebner et al. (2008).

Since it is desired to have different kinds of inputs into the device, it could be helpful to have various parallel inlet holes and channels. This might also help in reducing the air bubbles formation in the channels, which might be a result of the constant plug and unplug of inputs.

### **7.5.2 Rescale and Optimization**

The device presented in this work was designed in order to capture particles between  $20\mu\text{m}$  and  $30\mu\text{m}$  and tested with water-in-oil microspheres. Therefore, to test a new platform with different sizes of cells, its dimensions have to be rescaled down. For example, it should be rescaled and tested with cells between  $10\mu\text{m}$  and  $20\mu\text{m}$ . In addition, the device should be optimized in order to maximize the packing density and the trapping efficiency. The optimization process could be done by following the approach proposed by Xu et al. (2013).

### **7.5.3 Air bubbles and Filters**

It is important to understand the reasons of the air bubbles formation when culture media (FBS) is introduced into the microfluidic channel and find a method to avoid them. This will considerably improve the device function and facilitate its use. Although it was not mentioned before, during the trapping experiments it was observed the apparition of undesired particles (pollutants) in the microchannels, which might come from the fluids used or the debris of the device itself. Therefore, it is recommended to filter the fluids that will be used before experiments.

#### **7.5.4 Assess the device on a biological assay**

Although in this work some experiments with living cells were conducted in order to determine the cell's viability, the device must be used on a biological assay. At the end, the main goal of the trapping device presented on this research is to be a tool that could help on investigations conducted on cancer research, drugs development, medical analyses, etc. Thus, it is proposed as a recommendation to use the device as a tool in experiments and works on which the focus is not the device by itself. Nevertheless, as it was previously mentioned, the device might not be ready for such experiments because it has to go through some improvements and optimization.

#### **7.5.5 Single-cell retrieving system**

As discussed on Chapter 2 (section 2.3.5), Tan and Takeuchi did not develop a simple microfluidic single-cell trapping device, but incorporated a unique retrieving system for individual cells. By using an optical method with IR laser and aluminum plates, they achieved to producing air bubbles within the microfluidic device at will. As a result, they were able to retrieve determined single cells rather than the approach of taking all the trapped cells by reverting the flow. Therefore, it would be very interesting to assess whether it is possible to add such a retrieving system on the novel device presented on this thesis.

## LIST OF REFERENCES

- Andersson, H., & van den Berg, A. (2003). Microfluidic devices for cellomics: a review. *Sensors and Actuators B*, 92(3), 315-325. doi: 10.1016/S0925-4005(03)00266-1
- Beech, J. P., & Tegenfeldt, J. O. (2008). Tunable separation in elastomeric microfluidics devices. *Lab on a Chip*, 8(5), 657-659. doi:10.1039/B719449H
- Benavente-Babace, A., Gallego-Pérez, D., Hansford, D.J., Arana, S., Pérez-Lorenzo, E., & Mujika, M. (2014). Single-cell trapping and selective treatment via co-flow within a microfluidic platform. *Biosensors and Bioelectronics*, 61(2014), 298-305. doi: 10.1016/j.bios.2014.05.036
- Charnley, M., Textor, M., Khademhosseini, A., & Lutolf, M. P. (2009). Integration column: microwell arrays for mammalian cell culture. *Integrative Biology*, (12) 625-634. doi: 10.1039/b918172p
- Chung, K., Rivet, C. A., Kemp, M. L., & Lu, H. (2011). Imaging single-cell signaling dynamics with a deterministic high-density single-cell trap array. *Analytical Chemistry*, 83(18), 7044-7052. doi: 10.1021/ac2011153
- Del Campo, A., & Greiner, C. (2007). SU-8: a photoresist for high-aspect-ratio and 3d submicron lithography. *Micromechanics and Microengineering*, 17(6), R81-R95. doi: doi:10.1088/0960-1317/17/6/R01
- Di Carlo, D., Aghdam, N., & Lee, L. P. (2006). Single-cell enzyme concentrations, kinetics, and inhibition analysis using high-density hydrodynamic cell isolation arrays. *Analytical chemistry*, 78(14), 4925-4930. doi:10.1021/ac060541s
- Di Carlo, D., Wu, Y. L., & Lee, P. L (2006). Dynamic single cell culture array. *Lab on a Chip*, 6(11), 1445-1449. doi:10.1039/B605937F
- Dimmeler, S., Haendeler, J., Rippmann, V., Nehls, M., & Zeiher, A. M. (1996). Shear stress inhibits apoptosis of human endothelial cells. *FEBS Letters*, 399(1-2), 71-74. doi: 10.1016/S0014-5793(96)01289-6
- Frimat, J. P., Becker, M., Ching, Y. Y., Marggraf, U., Janasek, D., Hengstler, J. G., Franzke, J., & West, J. (2010). A microfluidic array with cellular valving for single cell co-culture. *Lab on a Chip*, 11(2), 231-237. doi: 10.1039/C0LC00172D
- Ge, J., Guo, L., Wang, S., Zhang, Y., Cai, T., Zhao, R. C. H., & Wu, Y. (2014). The size of mesenchymal stem cells is a significant cause of vascular obstructions and strokes. *Stem Cell Reviews and Reports*, 10(2), 295-303. doi:10.1007/s12015-013-9492-x
- Graf, N.J., & Bowser, M.T. (2008). A soft-polymer piezoelectric bimorph cantilever-actuated peristaltic micropump. *Lab on a Chip*, 8(2008), 1664-1670. doi:10.1039/b805252b
- Hsu, T. R., (2002). *Mems and microsystems: Design and manufacture*. New York, NY:McGraw-Hill
- Huebner, A., Bratton, D., Whyte, G., Yang, M., deMello, A.J., Abell, C., & Hollfelder Florian. (2008). Static microdroplet arrays: a microfluidic device for droplet trapping, incubation and release for enzymatic and cell-base assays. *Lab on a Chip*, 9(2009), 692-698. doi:10.1039/b813709a

- Huh, D., Mills, K.L., Zhu, X., Burns, M.A., Thouless, M.D., & Takayama, S. (2007). Tuneable elastomeric nanochannels for nanofluidic manipulation. *Nature Materials*, 6(2007), 424-428. doi:10.1038/nmat1907
- Jin, D., Deng, B., Li, J. X., Cai, W., Tu, L., Chen, J., Wu, Q., & Wang, W. H. (2015). A microfluidic device enabling high-efficiency single cell trapping. *Biomicrofluidics*, 9(1), 014101. doi: 10.1063/1.4905428
- Johnston, I. D., McCluskey, D. K., Tan, C. K. L., & Tracey, M. C. (2014). Mechanical characterization of bulk sylgard 184 for microfluidics and microengineering. *Micromechanics and Microengineering*, 24(3), 035017 (7). doi: 10.1088/0960-1317/24/3/035017
- Khanafer, K., Duprey, A., Schlicht, M., & Berguer R. (2009). Effects of strain rate, mixing ratio, and stress-strain definition on the mechanical behavior of the polydimethylsiloxane (PDMS) material as related to its biological applications. *Biomedical Microdevices*, 11(2), 503-508. doi: 10.1007/s10544-008-9256-6
- Kim, M. C., Wang, Z, Lam, R. H. W., & Thorsen, T. (2008). Building a better cell trap: applying lagrangian modeling to the design of microfluidic devices for cell biology. *Applied Physics*, 103(4), 1-6. doi: 10.1063/1.2840059
- Kim, S. H., Lee, G. H., & Park, J. Y. (2013). Microwell fabrication methods and applications for cellular studies. *Biomedical Engineering Letters*, 3(3), 131-137. doi: 10.1007/s13534-013-0105-z
- Kim, S. M., Lee, S. H., & Suh, K. Y. (2008). Cell research with physically modified microfluidic channels: A review. *Lab on a Chip*, 8(7), 1015-1023. doi: 10.1039/b800835c
- Kobel, S., Valero, A., Latt, J., Renaud, P., & Lutolf, M. (2010). Optimization of microfluidic single cell trapping for long-term on-chip culture. *Lab on a Chip*, 10(7), 857-863. doi: 10.1039/B918055A
- Lawrenz, A., Nason, F., & Cooper-White, J. J. (2012). Geometrical effects in microfluidic-based microarrays for rapid, efficient single-cell capture of mammalian stem cells and plant cells. *Biomicrofluidics*, 6(2), 1-17. Retrieved from <http://scitation.aip.org.cyber.usask.ca/content/aip/journal/bmf/6/2/10.1063/1.4704521>
- Lee, G. H., Kim, S. H., Kang, A. R., Takayama, S., Lee, S. H., & Park, J. Y. (2015). Deformable L-shaped microwell array for trapping pairs of heterogeneous cells. *Micromechanics and Microengineering*, 25(3), 035005 (11). doi:10.1088/0960-1317/25/3/035005
- Lee, W. C., Rigante, S., Pisano, A. P., & Kuypers, F. A. (2010). Large-scale arrays of picolitre chambers for single-cell analysis of large cell populations. *Lab on a Chip*, 10(21), 2952-2958. doi: 10.1039/c0lc00139b
- Lei, L. (2016) Modeling and optimization of the microsphere generation process. College of Graduate Studies and Research, University of Saskatchewan.
- Lin, Y., & Zhang, W.J. (2004). Towards a novel interface design framework: function-behavior-state paradigm. *Human-Computer Studies*, 61(3), 259-297. doi: 10.1016/j.ijhcs.2003.11.008



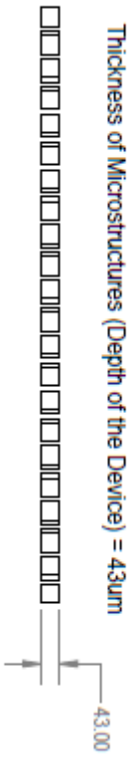
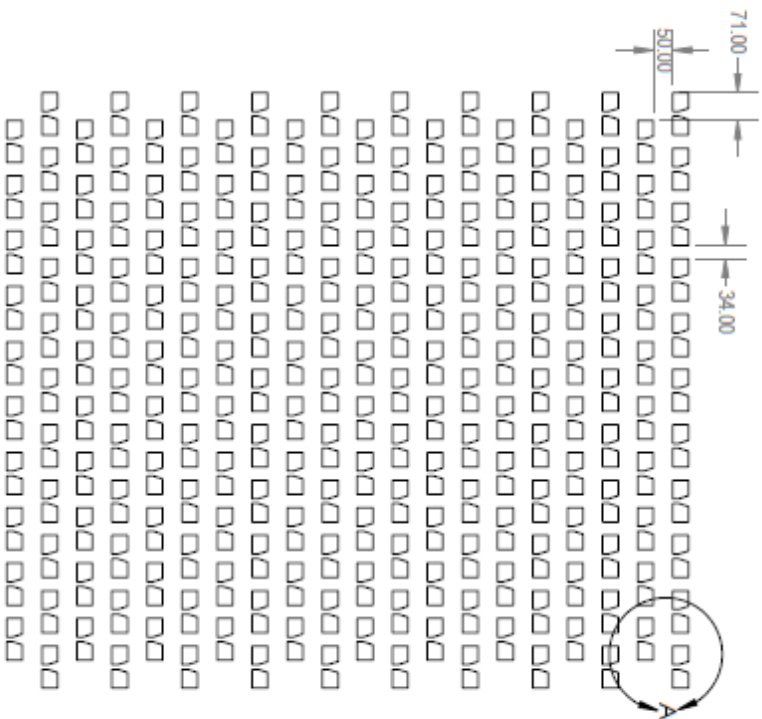
- Lindström, S., & Andersson-Svahn, H. (2010). Overview of single-cell analyses: microdevices and applications. *Lab on a Chip*, 10(2010), 3363-3372. doi:10.1039/c0lc00150c
- Liu, C., Liu, J., Gao, D., Ding, M., & Lin, J. M. (2010). Fabrication of microwell arrays based on two-dimensional ordered polystyrene microspheres for high-throughput single-cell analysis. *Analytical Chemistry*, 82(22), 9418-9424. doi: 10.1021/ac102094r
- Liu, W., Li, L., Wang, J., Tu, Q., Ren, L., Wang, Y., & Wang, J. (2012). Dynamic trapping and high-throughput patterning of cells using pneumatic microstructures in an integrated microfluidic device. *Lab on a Chip*, 12(2012), 1702-1709. doi:10.1039/c2lc00034b
- McKenna, C. (2016). Efficient cleaning of a microfluidic chip. Royal Society of Chemistry. Retrieved from <http://blogs.rsc.org/chipsandtips/2016/02/08/efficient-cleaning-of-a-microfluidic-chip/>
- McDonald, J.C., Duffy, D. C., Anderson, J. R., Chiu, D. T., Wu, H., Schueller, O. J. A., & Whitesides, G. M. (2000). Fabrication of microfluidic systems in poly(dimethylsiloxane). *Electrophoresis*, 21(1), 27-40. doi: 10.1002/(SICI)1522-2683(20000101)21:1<27::AID-ELPS27>3.0.CO;2-C
- Murray, C., McCoul, D., Sollier, E., Ruggiero, T., Niu, X., Pei, Q., & Di Carlo, D. (2013). Electro-adaptive microfluidics for active tuning of channel geometry using polymer actuators. *Microfluid Nanofluid*, 14(2013), 345-358. doi:10.1007/s10404-012-1055-y
- Nilsson, J., Evander, M., Hammarström, B., & Laurell, T. (2009). Review of cell and particle trapping in microfluidic systems. *Analytical Chimica Acta*, 649(2), 141-157. doi: 10.1016/j.aca.2009.07.017
- Pahl, G., Beitz, W., Feldhusen, J., & Grote, K. H. (2007). *Engineering design: A systematic approach*. London, UK: Springer.
- Rettig, J. R., & Folch, A. (2005). Large-scale single-cell trapping and imaging using microwell arrays. *Analytical Chemistry*, 77(17), 5628-5634. doi: 10.1021/ac0505977
- Seliger, H. (2006). Introduction: array technology-an overview. *Methods in molecular biology*, 381, 1-36. doi: 10.1007/978-1-59745-303-5\_1
- Sia, S., & Whitesides, G. M. (2003). Microfluidic devices fabricated in poly(dimethylsiloxane) for biological studies. *Electrophoresis*, 24, 3563-3576. doi: 10.1002/elps.200305584
- Sochol, R. D., Dueck, M. E., Li, S., Lee, L. P., & Lin, L. (2012). Hydrodynamic resettability for a microfluidic particulate-based arraying system. *Lab on a Chip*, 12(23), 5051-5056. doi: 10.1039/C2LC40704C
- Suh, N. P (1990). *The principle of design*. New York, NY: Oxford University.
- Tan, W. H., & Takeuchi, S. (2006). A trap-and-release integrated microfluidic system for dynamic microarray applications. *Proceedings of the National Academy of Sciences of the United States*, 104(4), 1146-1151. doi: 10.1073/pnas.0606625104
- Umenda, Y., Takeda, H., Tomiyama, T., & Yoshikawa, H. (1990). Function, behavior and structure. In Gero, J. S. (Ed.), *Applications of Artificial Intelligence in Engineering the Fifth International Conference* (pp. 177-194). Berlin, Springer-Verlag

- Wang, Y., Shah, P., Phillips, C., Sims, C. E., & Allbritton, N. L. (2011). Trapping cells on a stretchable microwell array for single-cell analysis. *Analytical and Bioanalytical Chemistry*, 402(3), 1065-1072. doi: 10.1007/s00216-011-5535-9
- Wang, Y., Tang, X., Feng, X., Liu, C., Chen, P., Chen, D., & Liu, B. F. (2014). A microfluidic digital single-cell assay for the evaluation of anticancer drugs. *Analytical and Bioanalytical Chemistry*, 407(4), 1065-1072. doi: 10.1007/s00216-014-8325-3
- Wang, Z. (2011). Polydimethylsiloxane mechanical properties measured by macroscopic compression and nanoindentation techniques. Graduate School Theses and Dissertations. Retrieved from <http://scholarcommons.usf.edu/etd/3402/>
- Wlodkowic, D., Faley, S., Zagnoni, M., Wikswo, J. P., & Cooper, J. M. (2009). Microfluidic single-cell array cytometry for the analysis of tumor apoptosis. *Analytical Chemistry*, 81(13), 5517-5523. doi: 10.1021/ac9008463
- Wolfe, D. B., Whitesides, G. M., (2005). Rapid prototyping of functional microfabricated devices by soft lithography. D. G. Bucknall (Ed.), *Nanolithography and patterning techniques in microelectronics* (pp. 76-119). Boca Raton, NW: Bucknall
- Wood, D. K., Weingeist, D. M., Bhatia, S. N., & Engelward, B. P. (2010). Single cell trapping and DNA damage analysis using microwell arrays. *PNAS*, 107(22), 10008-100013. doi: 10.1073/pnas.1004056107
- Wu, L. Y., Di Carlo, D., & Lee, L. P. (2007). Microfluidic self-assembly of tumor spheroids for anticancer drug discovery. *Biomed Microdevices*, 10(2), 197-202. doi:10.1007/s10544-007-9125-8
- Xia, Y., & Whitesides, G. M., (1998). Soft lithography. *Angewandte Chemie International Edition*, 37(5), 550-575. doi:
- Xu, X., Sarder, P., Li, Z., & Nehorai, A. (2013). Optimization of microfluidic microsphere-trap arrays. *Biomicrofluidics*, 7(014112), 1-16. doi:10.1063/1.4793713
- Yi, C., Li, C. W., Ji, S., & Yang, M. (2006). Microfluidics technology for manipulation and analysis of biological cells. *Analytical Chimica Acta*, 560(1), 1-23. doi: 10.1016/j.aca.2005.12.037
- Zhang, W.J., Lin, Y., & Sinha, N. (2005). On the function-behaviour-structure model for design. Retrieved from: <https://www.google.ca/url?sa=t&rct=j&q=&esrc=s&source=web&cd=1&cad=rja&uact=8&ved=0ahUKEwjv7OPj57TMAhWJs4MKHW2wA90QFggBMAA&url=http%3A%2F%2Flibrary.queensu.ca%2Fojs%2Findex.php%2FPCEEA%2Farticle%2Fdownload%2F3884%2F3987&usg=AFQjCNFhAE1GfyAK2nbDz2NWdrbmBqG82A&sig2=iMI7sj8Q3PSaW56NVp6BVA&bvm=bv.121070826,d.amc>
- Zheng, S., Lin, H., Liu, J. Q., Balic, M., Datar, R., Cote, R. J., & Tai, Y. C. (2007). Membrane microfilter device for selective capture, electrolysis and genomics analysis of human circulating tumor cells. *Journal of Chromatography*, 1162(2), 154-161. doi: 10.1016/j.chroma.2007.05.064
- Zhu, J., Shang, J., Olsen, T., Liu, K., Brenner, D., & Lin, Q. (2013). A mechanically tunable microfluidic cell-trapping device. *Sensors and Actuators*, In press. Retrieved from <http://www.sciencedirect.com/science/article/pii/S0924424713005219>

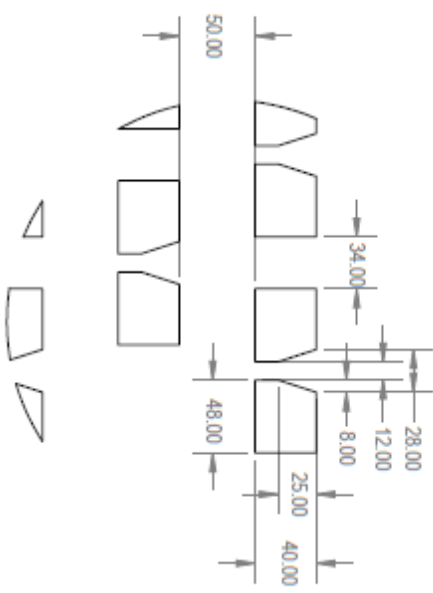
## APPENDIX A: CAD DRAWINGS OF THE NEW MICROFLUIDIC SINGLE CELL TRAPPING DEVICE

This section includes the drawings with specific dimensions used in the fabrication of the new device for experiments; the drawings of the stretching apparatus are also included.

Array of 210 Traps:  
 10 rows of 11 traps alternated with 10 rows of 10 traps.  
 Each trap consists of 2 microstructures.

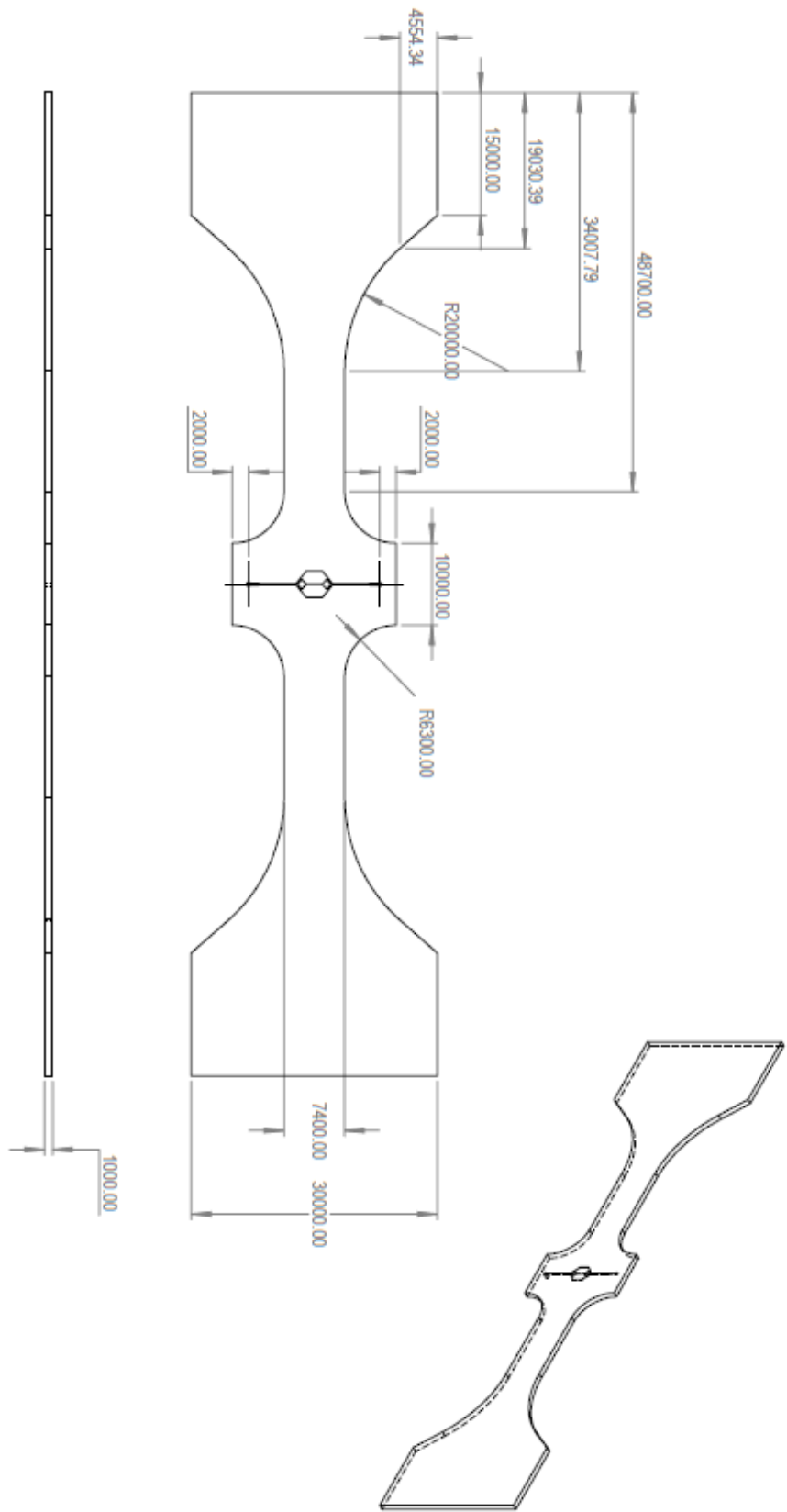


Trap's Dimensions:

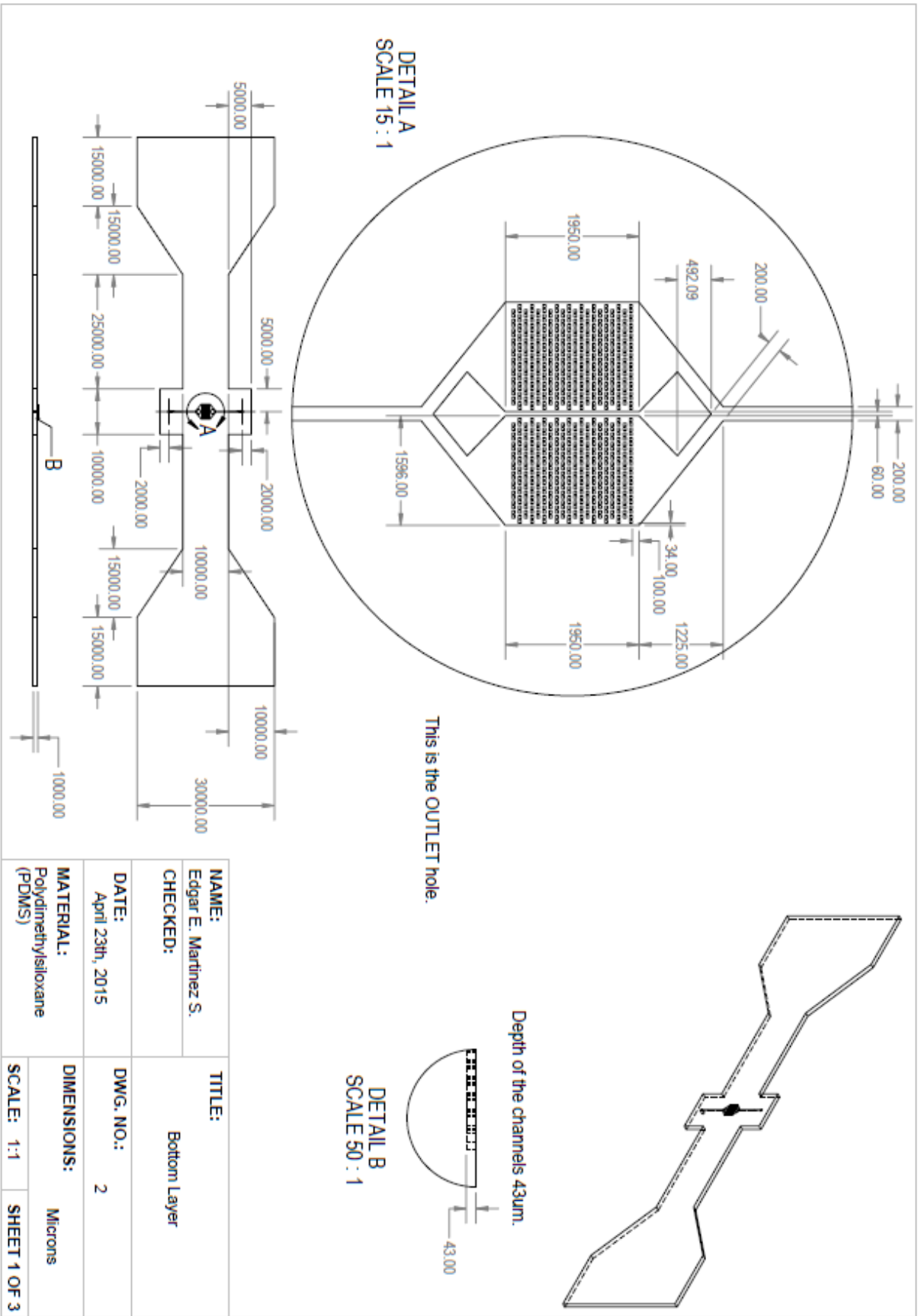


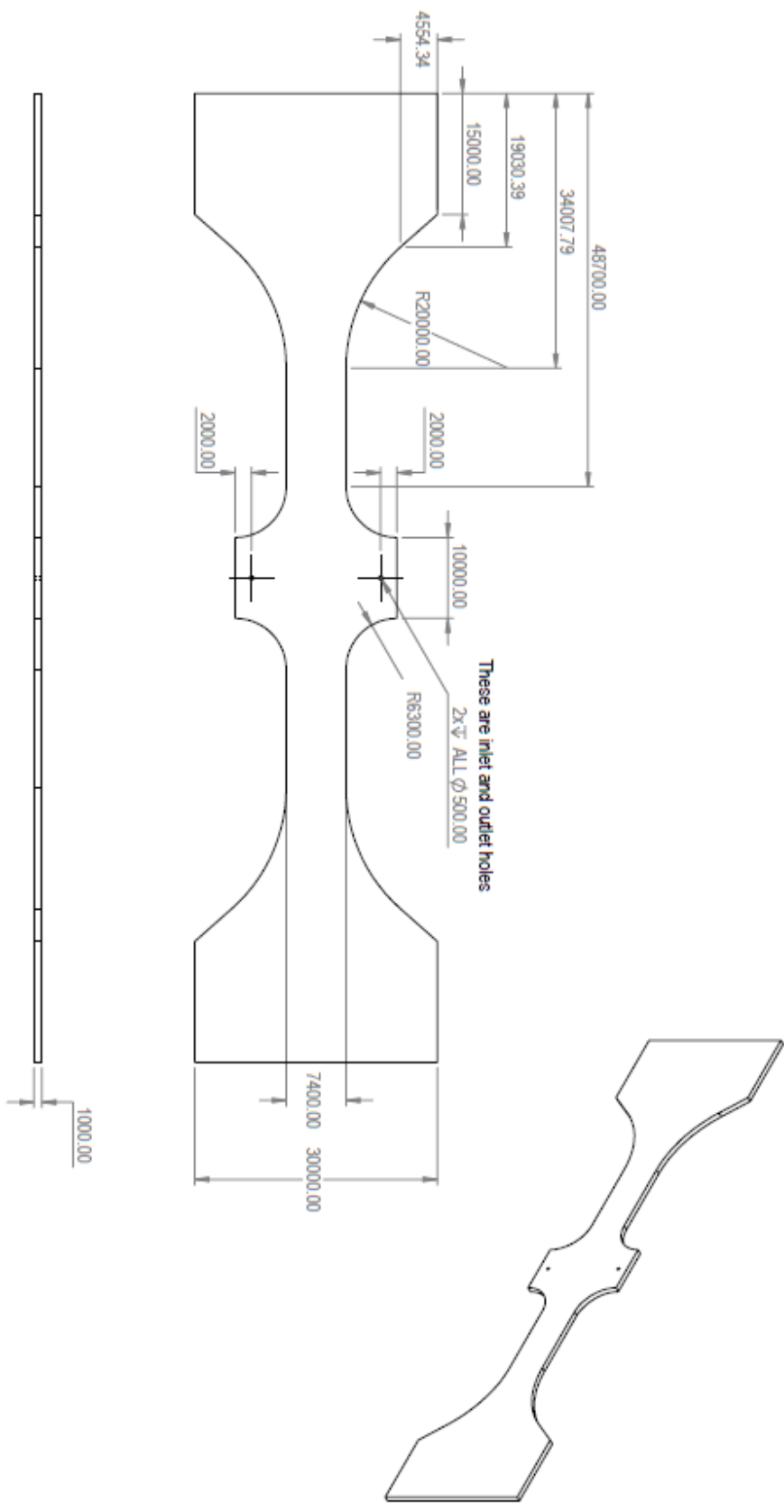
DETAIL A  
 SCALE 250 : 1

<b>NAME:</b> Edgar E. Martinez S.	<b>TITLE:</b> Cell-Traps (microstructures)
<b>CHECKED:</b>	
<b>DATE:</b> April 23th, 2015	<b>DWG. NO.:</b> 1
<b>MATERIAL:</b> Polydimethylsiloxane (PDMS)	<b>DIMENSIONS:</b> Microns
	<b>SCALE:</b> 64:1
	<b>SHEET 1 OF 3</b>

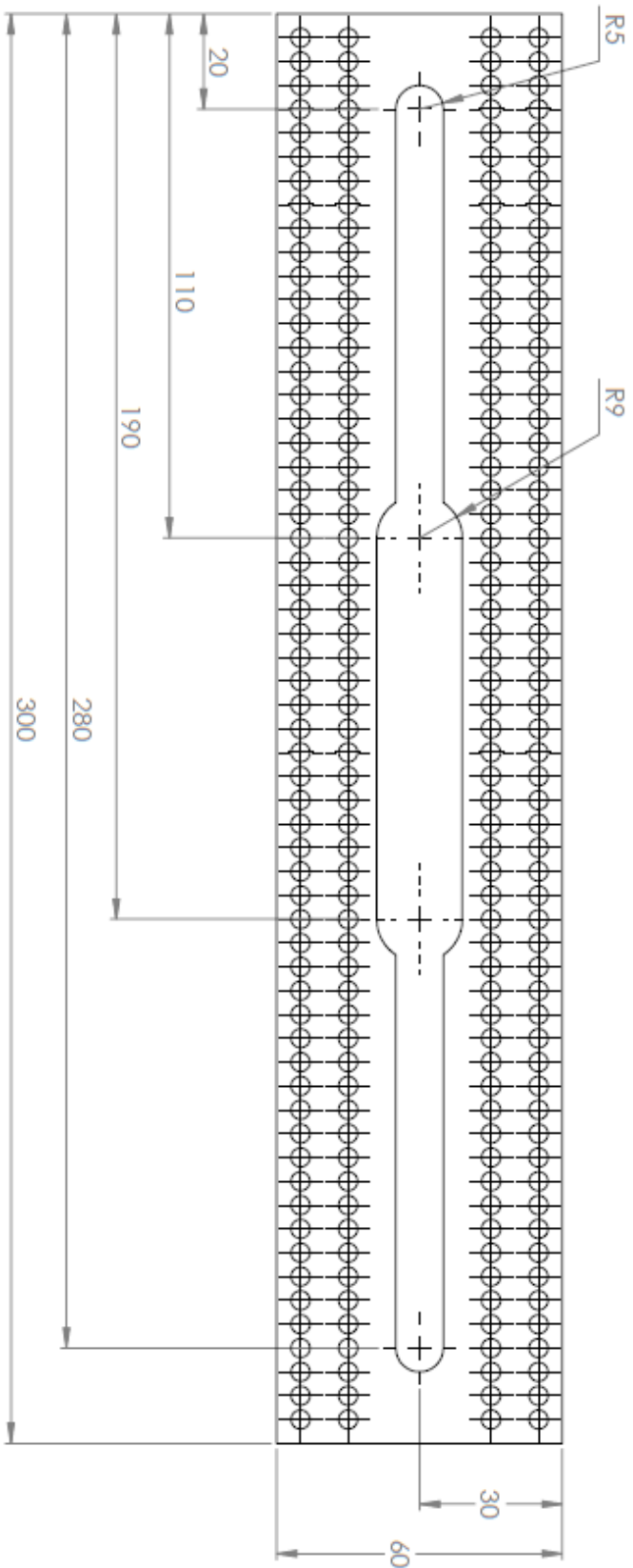


<b>NAME:</b> Edgar E. Martinez S.	<b>TITLE:</b> Bottom Layer
<b>CHECKED:</b>	
<b>DATE:</b> July 16th, 2015	<b>DWG. NO.:</b> 1
<b>MATERIAL:</b> Polydimethylsiloxane (PDMS)	<b>DIMENSIONS:</b> Microns
<b>SCALE:</b> 1.5:1	<b>SHEET 1 OF 2</b>



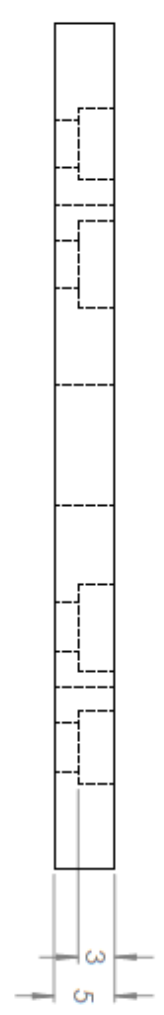
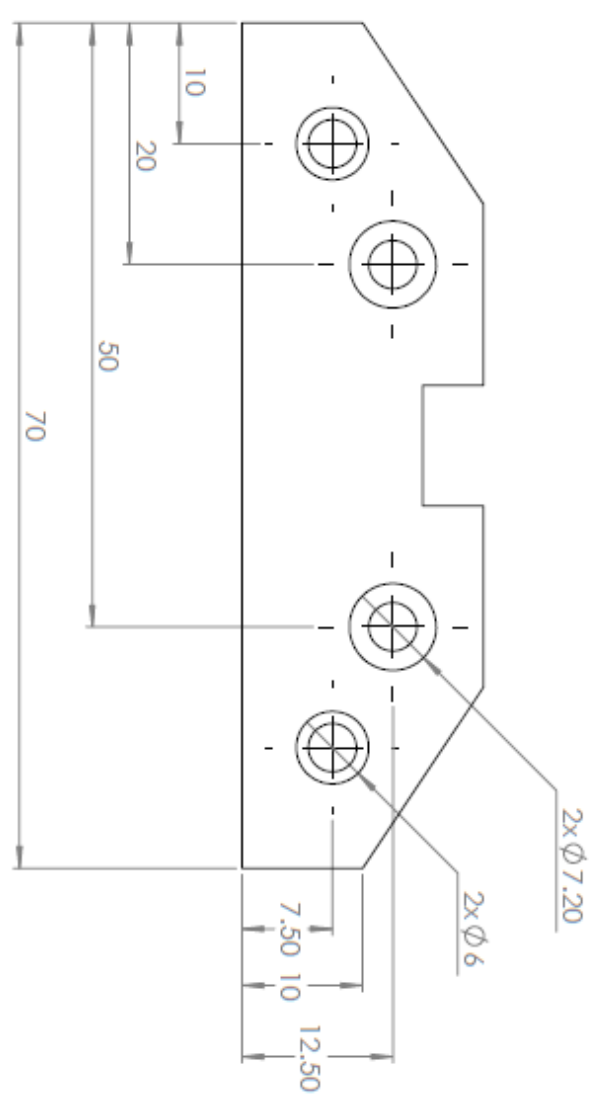
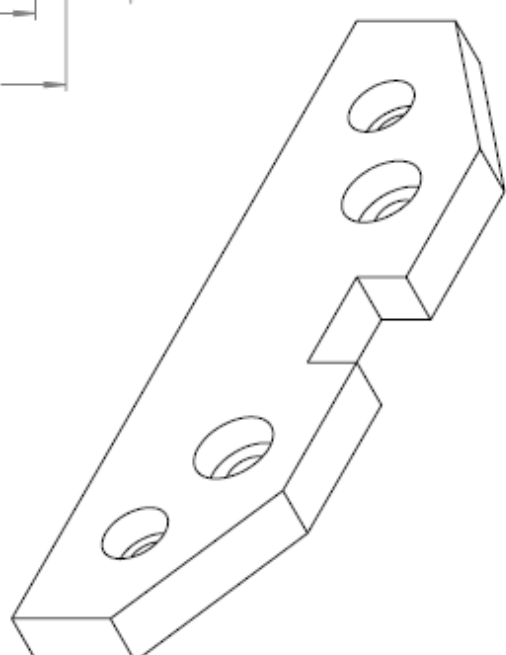


<b>NAME:</b> Edgar E. Martinez S.	<b>TITLE:</b> Top Layer
<b>CHECKED:</b>	
<b>DATE:</b> July 16th, 2015	<b>DWG. NO.:</b> 2
<b>MATERIAL:</b> Polydimethylsiloxane (PDMS)	<b>DIMENSIONS:</b> Microns
	<b>SCALE:</b> 1.5:1
	<b>SHEET 1 OF 2</b>



<b>NAME:</b> Edgar E. Martinez S.	<b>TITLE:</b> Motherboard
<b>CHECKED:</b>	<b>DWG. NO.:</b> 1
<b>DATE:</b> December 1st, 2015	<b>DIMENSIONS:</b> mm
<b>MATERIAL:</b> Acrylic	<b>SCALE:</b>
	<b>SHEET 1 OF 3</b>



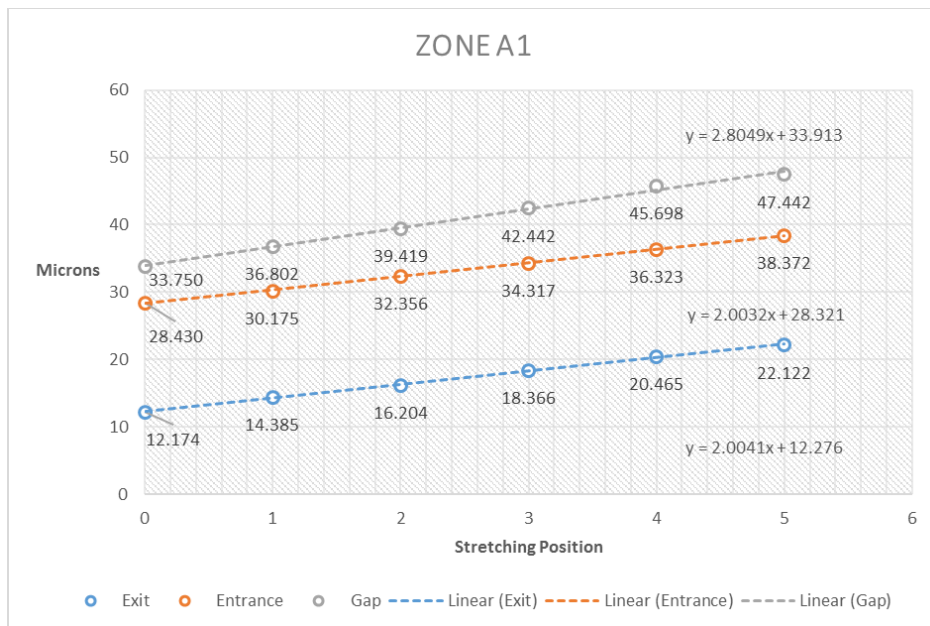


<b>NAME:</b> Edgar E. Martinez S.		<b>TITLE:</b> Holder	
<b>CHECKED:</b>		<b>DWG. NO.:</b> 1	
<b>DATE:</b> December 1st, 2015		<b>DIMENSIONS:</b> mm	
<b>MATERIAL:</b> Acrylic		<b>SCALE:</b>	
		<b>SHEET 1 OF 3</b>	

## APPENDIX B: CHARTS OF THE SIZE INCRMENT OF THE TRAPS

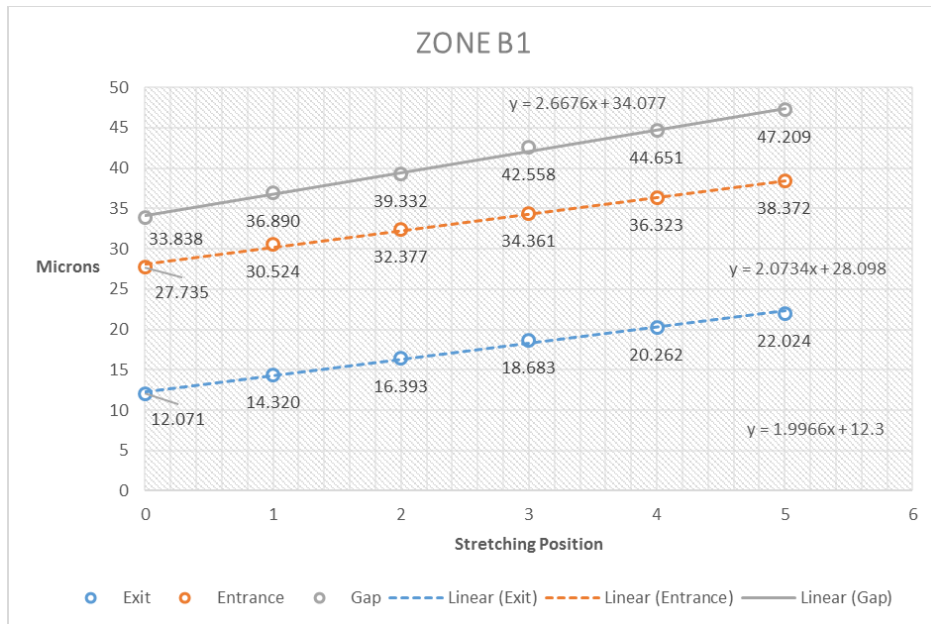
This section presents the charts which show graphically the size increment resulted on the traps after the application of different strains. In section 6.4.2, where the uniform deformation of the traps was discussed, charts corresponding to the array A1 were presented. Here the same charts are present in a larger size for the reader to have a better appreciation of the data, and the charts of the array A2 are included. Therefore, this section concludes with the discussion of the uniform deformation of the traps showing that the deformation produced in the microfluidic device is in fact uniform through all the traps in both arrays.

The following figures correspond to the deformation observed and measured on the array A1:

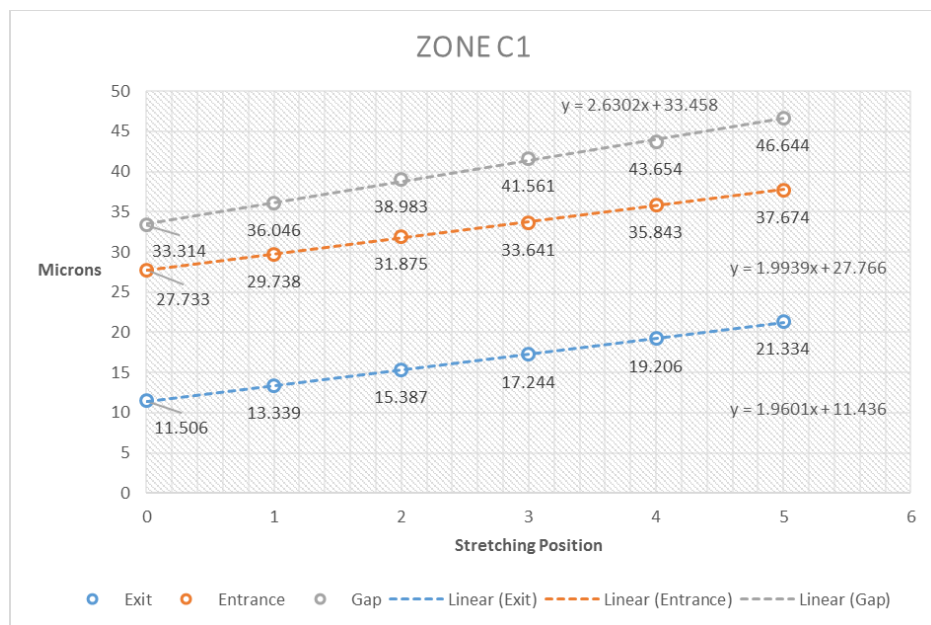


**Fig. B.1** Average magnitudes recorded for the exit (blue dots), the entrance (orange dots), and the gap between traps (grey dots) for the traps measured in the region A of the array A1, when the device is stretched progressively from hole 0 to hole 5. In the chart the x-axis is the stretching position (hole) and the y-axis is the trap dimension expressed in microns. In addition to the scattered dots, a trend line has been included with its corresponding equation for each

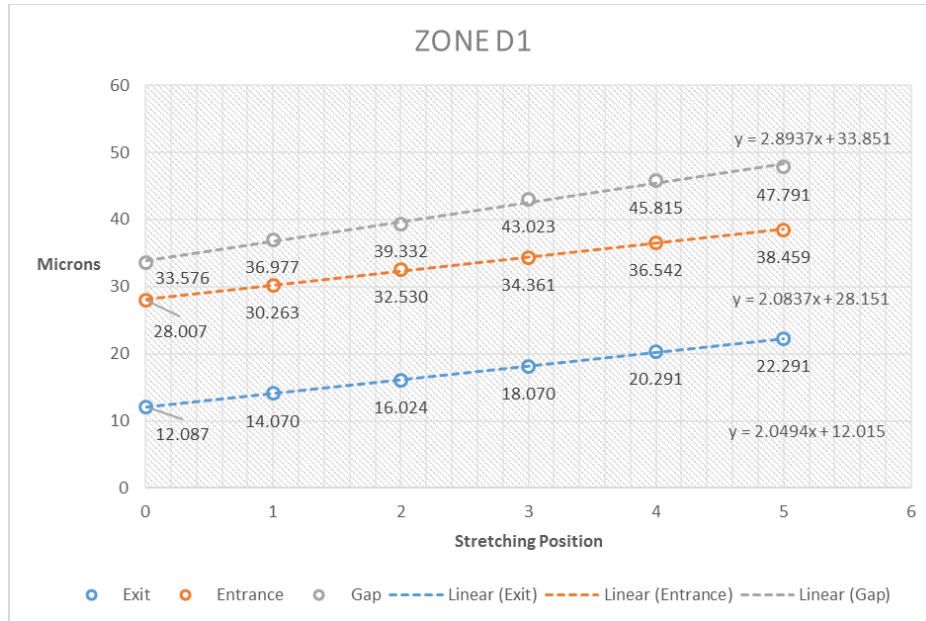
series in order to show that the deformation of the traps follows a linear and constant tendency, which can be represented by a linear equation of first order.



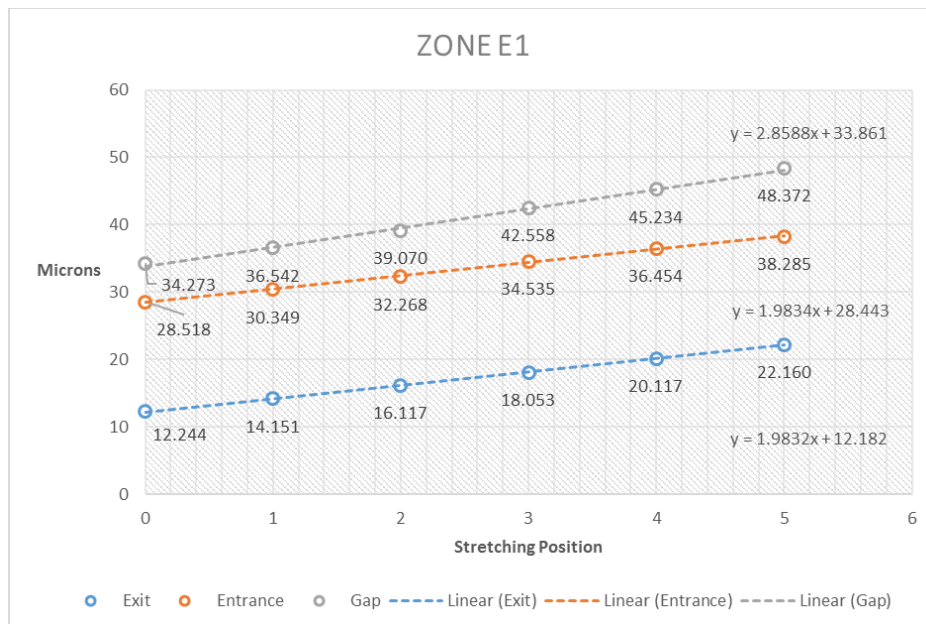
**Fig. B.2** Average magnitudes recorded for the exit (blue dots), the entrance (orange dots), and the gap between traps (grey dots) for the traps measured in the region B of the array A1, when the device is stretched progressively from hole 0 to hole 5.



**Fig. B.3** Average magnitudes recorded for the exit (blue dots), the entrance (orange dots), and the gap between traps (grey dots) for the traps measured in the region C of the array A1, when the device is stretched progressively from hole 0 to hole 5.

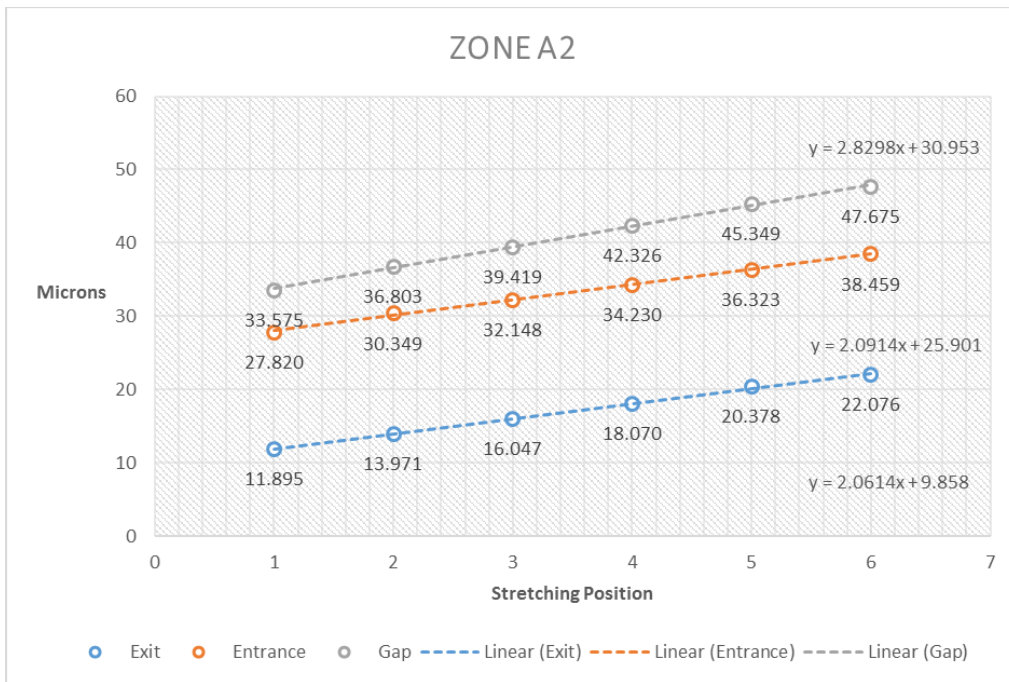


**Fig. B.4** Average magnitudes recorded for the exit (blue dots), the entrance (orange dots), and the gap between traps (grey dots) for the traps measured in the region D of the array A1, when the device is stretched progressively from hole 0 to hole 5.



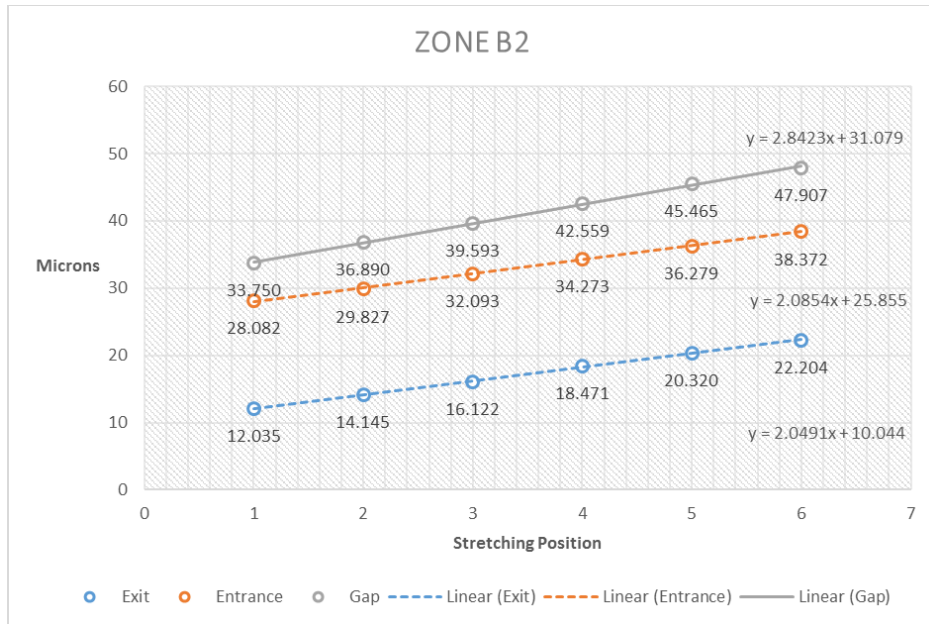
**Fig. B.5** Average magnitudes recorded for the exit (blue dots), the entrance (orange dots), and the gap between traps (grey dots) for the traps measured in the region E of the array A1, when the device is stretched progressively from hole 0 to hole 5.

The following figures correspond to the deformation observed and measured on the array A1:

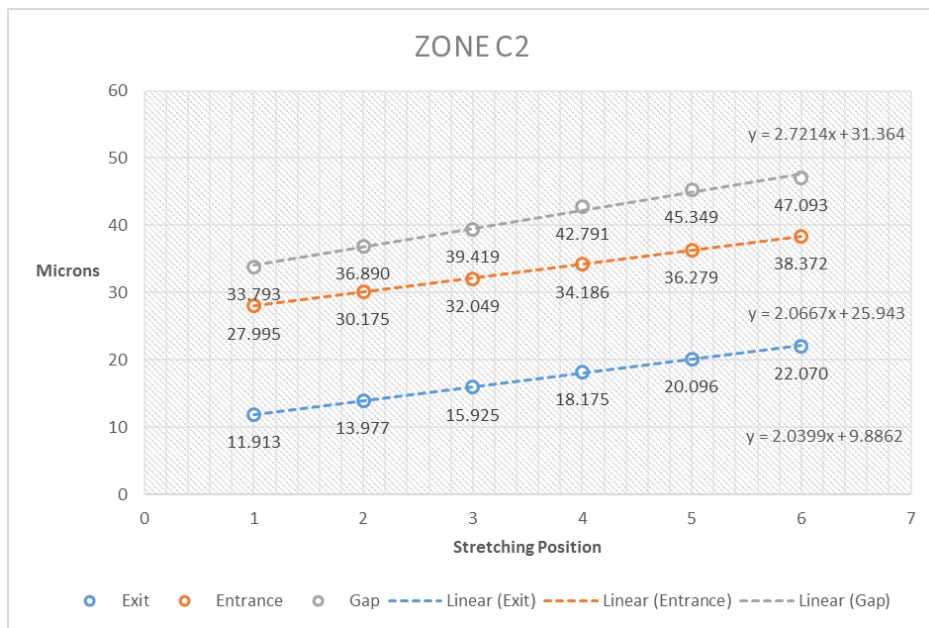


**Fig. B.6** Average magnitudes recorded for the exit (blue dots), the entrance (orange dots), and the gap between traps (grey dots) for the traps measured in the region A of the array A2, when the device is stretched progressively from hole 0 to hole 5.

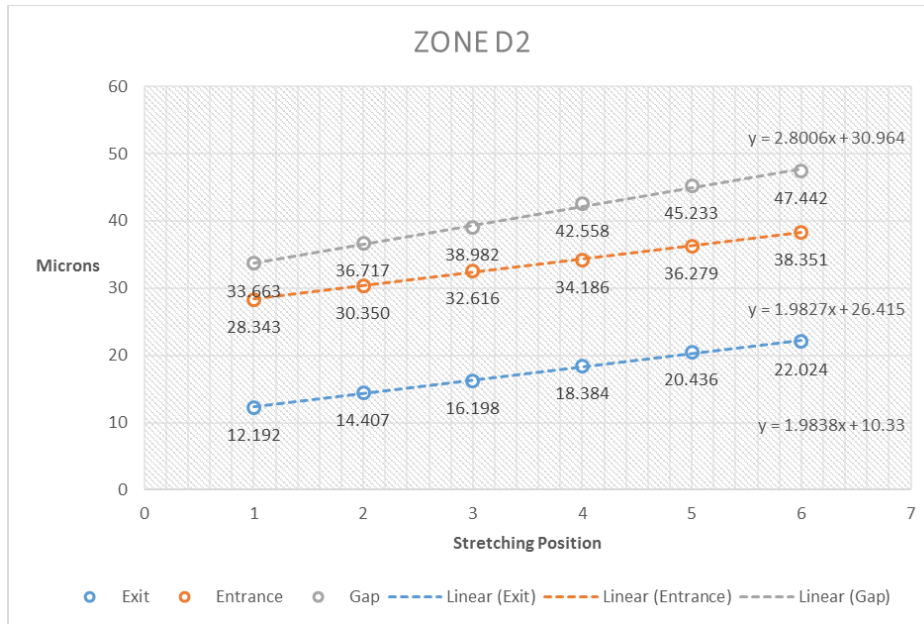




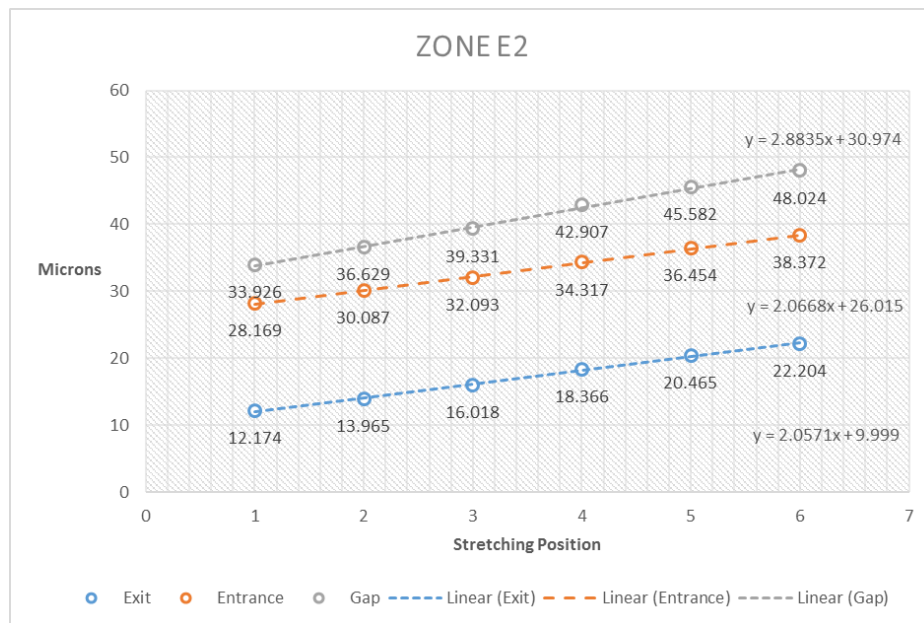
**Fig. B.7** Average magnitudes recorded for the exit (blue dots), the entrance (orange dots), and the gap between traps (grey dots) for the traps measured in the region B of the array A2, when the device is stretched progressively from hole 0 to hole 5.



**Fig. B.8** Average magnitudes recorded for the exit (blue dots), the entrance (orange dots), and the gap between traps (grey dots) for the traps measured in the region C of the array A2, when the device is stretched progressively from hole 0 to hole 5.



**Fig. B.9** Average magnitudes recorded for the exit (blue dots), the entrance (orange dots), and the gap between traps (grey dots) for the traps measured in the region D of the array A2, when the device is stretched progressively from hole 0 to hole 5.



**Fig. B.10** Average magnitudes recorded for the exit (blue dots), the entrance (orange dots), and the gap between traps (grey dots) for the traps measured in the region E of the array A2, when the device is stretched progressively from hole 0 to hole 5.

As stated on section 6.4.2, if a uniform deformation was achieved in all the traps, all the above charts must be if not identical very similar. Looking at the figures we concluded that the deformation of the traps is indeed uniform among all the traps of the device, and such deformation can be characterized as a linear deformation as shown by the linear equations obtained for each feature of the traps measured (entrance, exit, and inter-traps gap).